Iterative Joint Detection in Coordinated Network Coding for Next Generation of Communication Systems

Nazli Ahmad Khan Beigi

A Thesis
In the Department
of
Electrical and Computer Engineering

Presented in Partial Fulfillment of the Requirements
For the Degree of
Doctor of Philosophy Electrical and Computer Engineering at
Concordia University
Montreal, Quebec, Canada

November 2020

CONCORDIA UNIVERSITY
SCHOOL OF GRADUATE STUDIES

This is to certify that the thesis prepared

By: **Nazli Ahmad Khan Beigi**

Entitled: **Iterative Joint Detection in Coordinated Network Coding for Next Generation of Communication Systems**

and submitted in partial fulfillment of the requirements for the degree of

DOCTOR OF PHILOSOPHY (Electrical and Computer Engineering)

complies with the regulations of the University and meets the accepted standards with respect to originality and quality.

Signed by the final examining committee:

---------- Chair
Dr. Liangzhu Wang

---------- External Examiner
Dr. M. Salehi

---------- External to Program
Dr. H. Harutyunyan

---------- Examiner
Dr. W. Hamouda

---------- Examiner
Dr. Y. R. Shayan

---------- Thesis Supervisor
Dr. M.R. Soleymani

Approved by ----------
Dr. R. Selmic, Graduate Program Director

December 2020----------
Dr. M. Debbabi, Dean
Faculty of Engineering and Computer Science

Abstract

Iterative Joint Detection in Coordinated Network Coding for Next Generation of Communication Systems

Nazli Ahmad Khan Beigi, Ph.D.
Concordia University, 2020

The ubiquitous wireless networks in the next generation of communication systems have motivated advanced techniques with diverse ranges of connectivity, coverage, reliability, and throughput. The massive connectivity in the context of the heterogenous networks has conveyed to different sorts of challenges including inter-cell and intra-cell originated interferences. The complications aggravate due to the sporadic nature of the traffic generated by large-scale and low-powered networks over limited spectrum resources.

In this thesis, different techniques in enhancing the reliability, as well as spectral and power efficiency in the future generations of the multi-point communication networks have been investigated. Our proposed schemes are based on the coordination of the transmitters in sharing the source information followed by the joint transmission and the iterative detection. in the context of the cooperative source and channel coding. The Non-Orthogonal Multiple Access (NOMA), Coordinated Multi-Point (CoMP) transmission and the Iterative Joint Detection and Decoding (IJDD) receivers are the frameworks that we have used to validate our proposed improvements.

We have initially investigated the cooperative NOMA as the physical layer network coding scheme in the downlink of wireless communication systems. It is proposed to benefit from the so-called interference received from adjacent cells instead of ignoring or cancelling them, as in the state-of-the-art systems. The application of cooperative NOMA is evaluated in a system-level information theoretic framework to optimize the user-pairing strategy. The results show the cell edges with the strongest interference are the optimal vicinity for the NOMA applications.

Further, we have evaluated the NOMA for the uplink in the dense Internet of Things (IoT) systems, where the sensor elements observe the correlated sources. Realizing that the separation of source coding from channel coding in NOMA systems with correlated sources is suboptimal, we propose our scheme based on the cooperative source and channel coding. The transmitters are assumed to be privy to the whole data through a high-rate and low-latency background connection.

The cooperative source coding is then followed by the transmission over the non-orthogonal multiple access (NOMA) channel.

As the transmit signals experience different delay-spreads through the channel, the data streams are received asynchronously, resulting in inter-symbol interference (ISI) at the receiver. We show that the correlated nature of the asynchronous channels can be exploited as the extra source of information, provided that a proper detection technique is adopted. The capacity region is developed, where the sum-rate exceeds that of the synchronous NOMA. The potency of the successive interference cancellation (SIC) receivers, as the main block in NOMA receivers, is investigated. By applying water-filling and geometric power allocation, we show that the NOMA performance degradation in asynchronous channels is caused by the nature of SIC. We have proposed our iterative joint detection and decoding (IJDD) receiver that outperforms SIC in asynchronous NOMA receivers.

Moreover, we have addressed two key challenges in Coordinated Multi-point (CoMP) networks. The asynchronous downlink and imperfect channel state information (CSI) are jointly considered in an information theoretical framework. We assume delays from the Transmission and Reception Points (TRP) to the target user, in general, may exceed cyclic prefix (CP) length, causing symbol-asynchronous reception at the receiver. We characterize an accurate mathematical model for the asynchronous Rayleigh fading channel with imperfect CSI for multi-TRP schemes. We have derived the capacity region for asynchronous CoMP systems and have generalized it to the multi-TRP schemes. We propose a low-complexity iterative detection scheme targeting minimizing the mean square error (MMSE) in our asynchronous fading channel model.

Finally, we have associated the coordinated multi-point transmission with NOMA methodology. We have considered the downlink CoMP in a Single-Frequency Network (SFN) of Digital Terrestrial Television (DTT) broadcasting network. The coordinated transmit signals are assumed to have embedded Layered-Division Multiplexing (LDM) to enhance the coverage, reliability, and spectral efficiency in multi-content broadcasting. We have extended the MMSE-IJDD receiver to higher order modulation formats and have evaluated the order of the computational complexity for our proposed receiver to be in a decent range.

Our extensive simulations validate the proposed scheme providing a considerable boost in the channel reliability, while enhancing the spectral and power efficiency, even as the number of TRPs increases.

To my parents Jaleh and Morteza
for their unconditional love and support

To my husband Abbas
for his faith in me

And to our wonderful children Anahita and Arad,
whose overwhelming love embraces me everyday

Acknowledgements

First and foremost, I would like to express my gratitude to my supervisor, Professor M. Reza Soleymani, for giving me the great opportunity to work in his group and for all his support and kind considerations throughout my research. Without his knowledgeable guidance and instruction, I would have not been able to complete this research.

I would like to thank all members of my Ph.D. defense committee: Prof. Yousef R. Shayan, Prof. Walla Hamouda, and Prof. Hovhannes A. Harutyunyan. I appreciate their support and valuable comments and all the time they spent in all steps of my graduate studies. My especial thanks go to the external examiner, Prof. Masoud Salehi, of Northeastern University, for his time and technical insight. In addition, I wish to thank PERSWADE as well as InterDigital Canada Ltd.

I would like to thank my dear parents, Jaleh and Morteza. I would not be where I am today without their love, support, and encouragement. I also wish to thank my dear husband, Abbas, who has no limit for his ambitions. I am so grateful and proud of my daughter, Anahita, and my son, Arad, whose smiles are the sweetest and give me the energy I need every day. My thanks also go to my beloved brother, Pooya, for his warm heart and support.

Contents

List of Figures

List of Tables

List of Abbreviations

ACM	Adaptive Coding and Modulation (ACM)
ARQ	Automatic Repeat reQuest
ATSC	Advanced Television Systems Committee
BLER	Block Error Rate
BS	Base Station
CCI	Co-Channel Interference
CFO	Carrier Frequency Offset
CIR	Carrier to interference Ratio
CoMP	Coordinated Multi-Point
CP	Cyclic Prefix
CSI	Channel State Information
DTT	Digital Terrestrial Television
DVB-S2	Digital Video Broadcasting - Satellite - Second Generation
EGC	Equal-Gain Combining
FER	Frame Error Rate
GI	Guard Interval
IAN	Interference As Noise
IC	Interference Cancellation
ICToNOMA	Identical Content Transfer over NOMA
IJDD	Iterative Joint Detection & Decoding

IID	Independent and Identically Distributed
IoT	Internet of Things
IRC	Interference Rejection Combining
ISI	Inter-Symbol Interference
LLR	Log-Likelihood Ratio
MAC	Multiple Access Channel
MGC	Maximal-Gain Combining
MMSE	Minimum Mean Square Error
MODCOD	Modulation and Coding
MTRP	Multi-TRP
NCJT	Non-Coherent Joint Transmission
NOMA	Non-Orthogonal Multiple Access
NR	New Radio
OFDM	Orthogonal Frequency Division Multiplexing
OMA	Orthogonal Multiple Access
PIC	Parallel Interference Cancellation
PSD	Power Spectral Density
SC	Sources' Correlation
SE	Spectral Efficiency
SIC	Successive Interference Cancellation
SINR	Signal to Interference plus Noise Ratio
SNR	Signal to Noise Ratio
TBS	Transport Block Size
TRP	Transmission Reception Points
TSN	Time Sensitive Network
UE	User Equipment
URLLC	Ultra-Reliable Low Latency Communications

List of Symbols

$\boldsymbol{A}_n(i)$	The diagonal magnitude matrix at instance i from TRP n
α	LDM injection level
$\boldsymbol{b}_n(i)$	Transmitted code-bit vector at instance i from TRP n
β	Power normalizer coefficient in LDM
e_{CSI}	CSI error variance (dB)
$g(t), h(\mathrm{t})$	Channel's impulse response
$g(w), h(w)$	Square of magnitude of channel transfer function over the noise PSD
$G(w), H(w)$	Channel's transfer function
γ	Sources' correlation
$\gamma_i^l(w)$	SINR at *i*-th channel per layer *l*
$\lambda_1[b_n(i)]$	Joint detector's extrinsic information of TRP n and code-bit i
$\lambda_2[b_n(i)]$	SISO decoder's extrinsic information of TRP n and code-bit i
$\mu_{ij}(w)$	Asynchronous channel duo cross-correlations
h_i	Channel Coefficients from *i*-th TRP
$\boldsymbol{H}_A$	Extended Asynchronous Channel Matrix
$N(w)$	Noise spectral efficiency
P_T	Total Power
P_{uv}	Inter-Terminal Connection Power
$P_{C,B}, P_{E,B}$	Core and enhanced-layer power received from the broadcaster B
Π	Interleaver

^{p}	the *a priori* information
ρ_{ij}	Asynchronous channels' cross-correlation
$\rho(w)$	Asynchronous channels correlation
R_i^l	Data Rate at *i*-th channel per layer *l*
$\boldsymbol{R}$	Channel's correlation matrix
$\boldsymbol{R}_A$	Asynchronous representation of matrix $\boldsymbol{R}$
σ_n^2	Noise variance
$x_i(w)$	User i's coded-modulated signal
$S_i(w)$	Signal i's PSD
S_C, S_E	Data streams corresponding to core-layer, enhanced-layer
T_s	symbol time
τ_i	User i signal time delay
W_i	User i total power
$\boldsymbol{w}_n$	Minimum Mean Square Filter
χ	Degradation Factor
$z_n(i)$	Extrinsic information delivered by the soft MMSE filter

Chapter 1

Introduction

1.1. Problem Statement

The demand for ubiquitous mobile communications has motivated many advanced techniques with distinct ranges of coverage, reliability, and throughput. Such immense diversity has however conveyed to different sorts of inter-cell and intra-cell originated interferences [72][73].

The applications with massive uplink connectivity are expected to emerge along with the deployment of the Internet-of-Things (IoT) in the next generations of the communication systems [108]. This is the case in smart traffic, smart city, smart homes, smart health care, and many other use-cases. The massive IoT applications bring about many challenges concerning the reliability, latency, as well as spectral and energy efficiency. The complications aggravate due to the sporadic nature of the traffic generated by such large-scale and low-powered networks over limited spectrum resources. The massive access in IoT schemes gives rise to the massive multiple access channels (MAC), for which the traditional orthogonal multiple access (OMA) schemes are insufficient [5]. In OMA, separate channels are allocated to different devices, which results in serving only a limited number of access devices.

In an example, the video traffic captured in search-and-rescue or detection and localization applications in a multi-sensing network could pose an extensive load on the wireless connections due to data rate demands of up to tens of Gb/s [106]. In such networks, relying on the legacy video compression techniques and orthogonal channel multiplexing systems only translates into a high-

latency, and low power and spectral efficiency systems that cannot be reliable in real-time applications.

Realizing that the sensing elements in multi-sensor networks may observe and report the overlapping information, this can be addressed in a distributed source-coding of the correlated sources and based on the Slepian and Wolf theorem [29]. However, separating the source coding, i.e. compression of the source information, and the channel coding, i.e. channel multiplexing and coding techniques, is proved to be suboptimal in transmission of the correlated sources over multiple-access channels [38]. Hence, instead of dealing with the source coding and channel coding separately, the correlation of sources should be taken into consideration in a joint source and channel coding approach.

Moreover, with the increase in the scale of the radio access networks and the realization of the small cells and heterogeneous networks, the key demands for the user equipment (UE) at the cell edge or with unfavorable link conditions should be addressed including the enhanced connectivity, increased data throughput, reliability, and latency. The state-of-the-art systems are based on avoiding the interference as much as possible by using orthogonal channel multiplexing systems. The current methods to mitigate the remaining interference include ignoring the interference, as in Interference as Noise (IAN), or cancelling the interference, as in Multi-User Detection (MUD) techniques [40].

In an example, the legacy Single Frequency Networks (SFN) used in broadcasting systems has been constantly suffering from the narrow gaps at the edges of the coverage areas due to receivers experiencing the two-path zero-dB echo. The state-of-the-art SFN networks rely on ignoring the interference as in IAN and employing directional antennas to cancel the effect of interference [99].

Non-Orthogonal multiple access (NOMA) is the approach which is recently proposed in channel multiplexing [3]-[8]. NOMA outperforms OMA through sharing of the resources of time, frequency, space, and code with multiple Transmission-Reception Points (TRP). In NOMA, the resource sharing provides sufficient scalability to serve large connectivity as well as cell-edge connections in mobile networks. The cooperative NOMA has been recently proposed as a network coding method, where the involved nodes could be accompanied in a cooperative transmission [4]. However, NOMA is vulnerable to asynchronous reception of data, and at least a rough synchronization to reduce the complexity of the receiver is required [9]. The coordination of the

TRPs in a cooperative NOMA scheme translates into unfavorable overhead for synchronization and control functions, as such the control information signaling could be comparable to the data size.

Coordinated multipoint (CoMP) which was primarily supported in LTE has been proposed recently as a key candidate technique in the next generation of communication systems [75]. In CoMP, the interference between multiple TRPs is mitigated by having the joint transmission (JT) of data from the TRPs. The received data streams would then be combined at the receiver for a potential spatial diversity and power gain [76]. Despite the great achievements by CoMP, the proposed cooperative schemes assume strict synchronization requiring great deal of overhead to be achieved [84][89].

The successive interference cancellation (SIC), parallel interference cancellation (PIC), and interference rejection combining (IRC) are some of the baseband processing techniques currently used in the state-of-the-art receivers [79][93]. The methodology in the two former receivers is to detect the interference and cancel its contribution from the received signal; whereas the latter receiver relies on spatial projecting of the desired signals to prevent the interference. In this thesis, we show that the Inter-Symbol Interference (ISI) imposed by the asynchronous reception of the data streams makes interference cancellation (IC) a suboptimal receiver. Therefore, the receiver to jointly detect the data streams and benefit from their correlations is ought to be used in such schemes. We propose that by iterative joint detection and decoding (IJDD) of the data streams, the spectral efficiency gain could be achieved.

The impressive features in the cooperative source and channel coding schemes, as well as coordinated network coding has motivated us in this thesis. We consider the sharing of the information through high-rate and low-latency communication among the transmitters to be jointly transmitted. We propose a new scheme in mitigating the interference caused by asynchronous reception even with imperfect knowledge of the channel. We develop an accurate mathematical channel model for the asynchronous coordinated multi-point channels and derive the associated capacity region. adopt the iterative joint detection at the receiver to take advantage of the resulting cross-correlations, instead of cancelling it. The observations from theoretical and simulation perspectives show that despite the asynchronous channel with imperfect CSI, the reliability as well

as spectral and power efficiencies would exceed that of the non-cooperative non-iterative benchmark systems, even as the number of TRPs increases.

1.2. Literature Review

1.2.1. Non-Orthogonal Multiple Access Channels (NOMA)

NOMA has recently received considerable attention as an efficient technique for sharing the limited available resources of time, frequency, and code, not only to increase the spectral efficiency, but also to support the massive number of users in the networks [2][3][4]. The conventional multiple access channels (MAC) are based on interference avoidance by transmitting over orthogonal multiple access (OMA) channels.

NOMA and its major concepts such as MAC, SIC, and superposition coding have been studied in information theory for long time [25][26]; however, it has not been yet implemented in practice [27]. The conventional multiple access systems are all based on maintaining the orthogonality, i.e. OMA, between the resources of time, frequency, or signature codes. NOMA proposes the means of sharing the available resources, compatible with conventional multiple access systems, which achieves high spectral efficiency in comparison to OMA in enabling wireless communication networks to allocate more users to the available limited resources.

In [5], it is proven that NOMA outperforms OMA with just a slight increase in complexity. NOMA can be implemented in power-domain [6][7], as well as code-domain. In Power-domain NOMA, the users are served at the same time, frequency band and code, while they are assigned to different power levels. The power-domain NOMA is very suitable for systems with diverse Quality of Service (QoS) requirements [47]; however, it needs a very precise user-pairing and it does not gain the expected performance in schemes with almost equal power levels [48]. Code-domain NOMA can be implemented by assigning different spreading [8][9], non-spreading [10], interleaving [11], delay, scrambling, or codebook signatures [12] to different users. The receivers proposed in NOMA include Massage Passing Algorithm (MPA), Expectation Propagation Algorithm (EPA), Successive Interference Cancellation (SIC), MPA-SIC, and Parallel Interference Cancellation (PIC). These receivers come along with the linear MUD receivers such as MMSE and Elementary Signal Estimator (ESE) [12]. Currently, most NOMA systems rely on using SIC at their receivers.

NOMA has been proposed in many aspects of the future generations of wireless communication, which outperforms the corresponding OMA state-of-the-art systems. Some of these schemes are provided as follows.

Layered-Division Multiplexing (LDM). LDM is a form of power-domain Non-Orthogonal Multiple Access (NOMA), which is based on the constellation superposition technology. Advanced Television Systems Committee (ATSC) 3.0 standard has recently introduced several new features including LDM that is implemented along with a wide range of modulation formats and error correcting code rates.

There exists abundant literature on LDM and its different functionalities [95]-[102]. The LDM in ATSC 3.0 is investigated in [95], where its performance is compared with TDM. It is observed that LDM achieves 4dB and 2.5dB gain compared to TDM in mobile and fixed services, respectively. The seamless broadcasting coverage using LDM is addressed in [96], where the EL is used to deliver mobile-HD and 4k-UHD location targeted services, and CL is considered to provide wider coverage with HD quality services. The co-channel interference from other broadcasters is ignored in [96] and the receiver tunes to the stronger signal.

In a similar approach, the coverage in ATSC 3.0 equipped with LDM is investigated in [99] and [101]. In [99], the co-channel assignment in SFN is investigated, where the coverage and performance in ATSC 3.0 is compared with ATSC 1.0. As for the gaps in the midway of the two broadcasters, using directional antennas is considered. In order to mitigate the interference at the edge of the coverage areas, the MISO beamforming is proposed in [101]. The work in [97] considers the effect of GI on the overhead and proposes the zero-guard terminology for ATSC 3.0 SFN. Relying on the robust transmission modes, they compare the zero-guard OFDM with very low rates with GI-OFDM and it is shown that the benefits in performance cannot compensate the overhead penalties. It is worth to mention that the coverage enhancement in mentioned references mostly address the CL, and the enhanced layer has been mainly considered in local content insertion or location targeted advertising services.

In an interesting approach, the authors in [102] have investigated the LDM in ATSC 3.0 from the memory use aspect. Employing multiple physical layer pipes (PLP), the feasibility of time or frequency-layered division multiplexing along with the different injection levels and interleaver modes are studied.

Cooperative NOMA Network Coding. Wireless network coding has brought about new opportunities, since the wireless means of communication makes the cooperation of the nodes possible [39]. Authors in [27] have provided a comprehensive survey on the use-cases of NOMA in 5G networks, based on cooperation of nodes and relay channels.

Due to sharing of the resources in NOMA, the involved nodes could be accompanied in a cooperative transmission. Employing cooperative NOMA in improving downlink spectral efficiency has been investigated in [4] and [30]. In cooperative NOMA network coding, the user terminal with better channel condition acts as a relay by recovering both its and the other user's data and re-transmitting the data through a relay channel to that user. In another form, the same concept is used with dedicated relays that employ idol users as relays, which not only improves the spectral efficiency and the system coverage, but also minimizes the total outage probability [27][31].

However, it is stated in [4] that despite the great achievements, it is not possible to have all nodes to cooperate due to the augmented complexity. Hence, user pairing should be considered. Different user-pairing methods are proposed in [49], which includes the max-min and the two-stage relay selection. The max-min user pairing method is the optimal strategy employed in conventional cooperative networks, where the two-stage scheme creates a subset of nodes based on QoS requirements first, and then selects the nodes so that the spectral efficiency and the overall outage probability is optimized.

In this thesis, we are approaching this concept from a new aspect for the first time, which is considering the correlation of sources as the user pairing metric.

Internet of Things (IoT). Considering today's dense networks of users, there is still considerable challenge in allocation of the limited radio access resources. NOMA has been identified as a key technique in this regard [17][3]. In [17], it is shown how NOMA increases the connectivity capability in the demanding Internet of Things (IoT) systems. Also, NOMA is analyzed in [3] regarding the reliability and the outage probability and it is shown how NOMA outperforms OMA. As a subset of IoT networks, the Machine-to-Machine (M2M) communication requires a low latency connection. As investigated in [18], NOMA is the best candidate for such systems to support the massive number of nodes, as well as eliminating the Random Access (RA) procedures to reduce the access delays and signaling overheads.

NOMA-MIMO. Based on the spatial properties of MIMO, it provides a perfect foundation to implement NOMA. One aspect is to order the beams based on their path-loss corresponding to their assigned users, which can be used as user-pairing criteria to enhance the performance [50]. Also, with the recent progress in beamforming and multi-user MIMO (MU-MIMO) schemes in 3GPP standards, the spectral efficiency could be improved by employing NOMA along with MU-MIMO [51]. Moreover, as a means of providing low-latency communication schemes, MIMO-NOMA is presented in [52] to be used in time-limited scenarios.

Others. mmWave Communication [53], Simultaneous Wireless Information and Power Transfer (SWIPT) [54], and satellite networks [10][55], are other systems where NOMA is proved to be outperforming OMA. The NOMA practices are not limited to the mentioned above applications and there are new aspects emerging with the new generations of wireless communications.

1.2.2. Channel Estimation Errors and Imperfect CSI

The cooperative NOMA is based on SIC, and the system gain is in successive decoding and recovery of all the data streams. In practice the access to the exact channel properties is not possible and the user terminals have merely an estimation of the channel coefficients. This uncertainty could result in overestimation of the actual channel, which introduces the increased outage probabilities [61]. Due to the nature of SIC, the output of each level is fed as input to the next level, and so the decoding error rate will grow resulting in even more errors and data frame discards.

Data-aided and non-data aided channel estimation have been extensively studied, both in forward and return multibeam satellite systems [56][57][58]. Also, in [59], the effect of channel estimation error in 3GPP LTE NOMA with intra-beam superposition coding and SIC is investigated, and the corresponding transmission rate back-off algorithm is proposed.

Moreover, the performance in wireless communications highly relies on the accuracy of the channel knowledge at the transmitters. As the channel can be measured at the receiver, the efficient quantization and feedback of CSI with a decent payload could be challenging.

The impact of imperfect knowledge of CSI on channel capacity has been investigated in an information theoretic framework in [86]. It is shown that the loss in mutual information due to

imperfect CSI is relative to the rate of time variations through the channel. In [87], the outage performance due to imperfect CSI in Rayleigh flat-fading channels is investigated, where a modified water-filling scheme is employed over the spatial (antenna) and temporal (fading) domains. The multi-TRP transmission in the presence of CSI uncertainties is addressed in [88], where the BSs cooperatively mitigate their intercell interference. In this spirit, several schemes in multi-TRP with imperfect CSI have been also investigated, e.g., constrained backhaul [72], other-cell interference [89], and joint clustering scheduling [90].

1.2.3. Multi-User Detection

In order to accommodate NOMA, the Multi-User Detection (MUD) techniques would be used. The MUD techniques devised in practice are a combination of suboptimal linear detectors such as decorrelator or Minimum Mean Square Error (MMSE), and suboptimal nonlinear successive interference cancellation (SIC) detectors [40].

Due to the radiation pattern in multibeam satellite systems and the severe interference caused by the adjacent beams, there have been vast studies on employing MUD in satellite communications. These techniques mostly involve in interference mitigation for the return link and use of centralized processors at the gateways [41][42][43]. Previous works on forward link interference mitigation in multibeam satellite systems are scarce but do exist in the related literature. For two beams two users models, this aspect has been investigated in [44][45][46]. The authors in [44] have benefited from the Adaptive Coding and Modulation (ACM) properties of DVB-S2x in addition to their receiver that includes a joint detector followed by the SIC module. In [45], the power unbalance and phase shift between the received signals is taken into account, where the information theoretic results show that MUD is more effective at low SNR values and for stronger interferences. Also, the authors in [46] have proposed a joint multiuser detector/ decoder based on the EXtrinsic Information Transfer (EXIT) charts.

1.2.4. Asynchronous Multi-Access Channels

Despite the great achievements in NOMA, synchronous reception of the data streams has been taken for granted. Considering the fact that the overhead for synchronization and other control functions could be comparable to the data size, this assumption would not be practical, especially

in the low-latency grant-free URLLC systems. So, obtaining synchronicity could be a challenging problem in the dense sensor networks [18].

Previous works on asynchronous NOMA are scarce but do exist in the related literature. In [19], an interference cancellation (IC) method is proposed where a triangular pattern is followed in the IC of all interfering users for the sake of the desired user. In [20] and [21], the effort is to use symbol asynchronism to reduce the mutual interference between users. Authors in [22] use cyclic prefix in addition to a phase compensation technique to reduce the effect of asynchronism. Clearly, these research are all based on proposing compensation techniques to improve the SIC performance.

In contrast to much of the existing work, we have focused on a correlated signal model. In the following chapters, we show that the asynchronous reception of data streams changes the channel's attributes, making it a channel with memory that degrades SIC's functionality. The spectral efficiency degradation caused by the SIC has been investigated in detail in multi-access channels with inter-symbol interference (ISI) in [33], whose results could be applied to asynchronous multiple access channels. By relying on the cooperative NOMA, we show that the correlation caused by channel's asynchronism actually leads to higher throughputs that can be realized using our proposed IJDD receiver. Investigations on IJDD to improve the performance gain exist in the literature in multiple access schemes [35], as well as NOMA [36]. However, to the extent of our knowledge, employing IJDD in asynchronous channels has not been previously studied.

1.2.5. Distributed Source Coding with Correlated Sources in NOMA

In single user point-to-point connections, any correlation of the sources and channels are considered as impairment and so are discarded. Slepian and Wolf [29] showed that distributed source coding of the correlated sources is possible with the compression sum-rate equal to the mutual entropy of the sources instead of summation of their individual entropies.

There exist abundant research studies in the literature on sensor networks with correlated sources, with main focus on the distributed compression of the correlated sources. In [14] for instance, a rate-compatible LDPC code design is proposed that achieves every arbitrary coding rate in the distributed source coding rate region. This concept is also studied in [15] using trellis and lattice codes. The source coding methodology is out of scope of this thesis and we just provide a brief on the corresponding investigations.

Despite its great achievements, relying solely on the distributed source coding is proven to be suboptimal in multiple access channels with correlated sources [38]. The authors in [38] show that cooperative source and channel coding is optimal in multiple access channels (MAC) with correlated sources.

In this thesis, a significant contribution of our proposed system relies on our focus on the cooperation of the transmitters with correlated sources. A similar approach has been taken in [16], whose authors have considered cooperative sharing of the correlated data content between the transmitters and configuring the neighboring nodes as virtual antennas to perform beam forming toward the receiver. Their results show that cooperative transmission of the nodes outperforms the systems with separate optimization of source and channel coding; however, they have assumed full synchronicity in their studies.

1.2.6. Iterative Joint Detection and Decoding Receivers (IJDD)

The Multi-User Detection (MUD) was discussed in previous sections. In general, the joint processing in MUD techniques is followed by the channel decoders at the receiver, relying on successfully recovery of data. However, the MUD performance could be enhanced by iteratively processing of the information derived at the output of the decoders.

The Iterative Joint Detection and Decoding (IJDD) receivers is proposed in [35] for decoding the multiuser information in turbo coded multi-path CDMA systems with binary phase shift keying (BPSK) modulated signals. In the proposed IJDD, the soft output of the decoders is used as *a-priori* input information to the joint detector in an iterative scheme. First, the synchronous CDMA channel is analyzed, assuming the received signals from different users to be symbol synchronous. The IJDD is then investigated in asynchronous CDMA where the sliding-window processing is used. In the sliding window processing, it is assumed that if the window size is selected optimally, the effects of the signals outside the processing window on the decisions are negligible [120]. Hence, the effect of asynchronous reception is cancelled.

In this thesis, we have adopted the proposed IJDD receiver to be used in asynchronous channels, where we have replaced the channel matrix with our proposed asynchronous channel matrix. As such, the IJDD takes advantage of the asynchronous channels' cross-correlations, instead of cancelling them.

Most of the previous work on IJDD focused on the described methodology, where different applications have been investigated in synchronous multi-user channels [121]-[123]. In [121] the implementation of IJDD in uplink NOMA is investigated. The performance is compared with MUD, where the link-level evaluations show 4.5 dB and 9.8 dB performance improvements at block error rate equal to 10^{-2}, for QPSK and 16QAM modulations, respectively. In the accomplished simulations, the strict synchronization is assumed. The IJDD is proposed in Multiple-Input Multiple-Output (MIMO) systems in [122], wherein the Quadrature Amplitude Modulation (QAM) constellation, LDPC coding, and synchronous channel is assumed. The Dynamic-List Detector (DLD) is considered as the detection module, where the detector's list is dynamically adjusted in each iteration according to the channel's noise and fading.

The IJDD is proposed in [123] for the channels with Gaussian and non-Gaussian impulsive noise, where turbo-coded synchronous CDMA is considered. The Multiple-Access Interference (MAI) is modelled as Gaussian noise and the Parallel Interference Cancellation (PIC) is considered to recover the convolutional channel code to reduce the computational complexity.

1.2.7. Coordinated Multi-Point (CoMP) Transmission

Coordinated multi-point (CoMP) was primarily supported in LTE and it is currently being considered as a primary candidate technique in 5G NR [75]. In CoMP, the interference between multi-TRPs is mitigated by having the joint transmission (JT) of data from the TRPs, contributing to potential spatial diversity and power gain [76]. The realization of CoMP is subject to resolving the challenges of synchronization in time, non-ideal backhaul, and imperfect channel state information (CSI) in mobile networks, while keeping the control signaling overhead in a decent range [84][89].

The multi-TRP or CoMP is a promising candidate in wireless networks due to improving the reliability and spectral efficiency without relying on data repetition. In multi-TRP, the spatial diversity and multiplexing is achieved by joint transmission of the same transport block (TB) of data from multiple TRPs at the same time-frequency resources [75]. Compared to the TB repetition from a single TRP, CoMP achieves higher reliability, lower latency, and enhanced power and spectral efficiency. In [72], CoMP is evaluated in practical schemes with non-ideal backhaul and imperfect CSI. The BSs are presumed to be connected by a mesh of error-free out-of-band backhaul links, where perfect synchronization in time and frequency is considered. Uplink is

addressed and a number of cooperation schemes at the base stations are investigated. Their simulation results show that the trade-off between backhaul payload and CoMP performance may be considerable depending on the BS cooperative schemes.

Backhaul traffic, synchronization and feedback design are the issues addressed in [73]. In addition to the system-level simulations, the results of field trials from the outdoor testbeds in the EASY-C project are provided addressing both uplink and downlink. Time synchronicity is assumed which limits the areas where CoMP may be applicable, signifying the need to find a solution for asynchronous reception from multi-TRPs.

Several multi-cell coordination schemes are investigated in [74], with CoMP as one of the schemes. Being opposed to inter-cell and intra-cell interferences, the fully/ partially usage of both interferences is addressed in designing the precoder in the presence of imperfect or statistical CSI. Though not feasible, strict inter-cell synchronization is assumed. The results denote the trade-off between the reliability, power consumption, processing time, and signaling overhead.

CoMP specifically contributes in 5G ultra-reliable and low-latency communication (URLLC), where multi-TRPs are used to improve the spatial diversity, reliability, and capacity. Several CoMP options are described and compared in [75], namely: coherent joint transmission in multi-user and single-user schemes, as well as the non-coherent joint transmission (NCJT). Further, a system is proposed that allows CoMP as part of a time-sensitive network (TSN) with schemes with mobility considered as future work.

CoMP is considered from another perspective in [76], in which the transmitted signals from the different TRPs are jointly precoded, assuming prior phase alignment and strict synchronization. Yet, considering the dynamic changes in channel, such coordination may need to allocate a huge share of the bandwidth to the control signaling transmission.

Motivated by the challenges in accurate estimation of the channel in dynamic environments, in this thesis, we have investigated the scheme that could be applied in CoMP despite the imperfect channel knowledge and asynchronous timings, with the least amount of control signaling overhead.

Non-coherent joint transmission (NCJT) is an approach in CoMP which relies merely on static channel knowledge for the precoding [75]. The performance of NCJT is investigated in [79], where

three schemes are compared, namely fully overlapped NCJT (F-NCJT), non-fully overlapped NCJT (NF-NCJT), and dynamic point selection (DPS). The simulation results show that NF-NCJT achieves a higher throughput which is mainly due to lower control signaling and scheduling overhead. Also, different models of cooperation of the TRPs in NCJT are investigated in [80] followed by [81], where different sizes and models of clustering and the inter-cluster cooperation are considered, and the optimal solutions are provided.

NCJT and its open issues are currently under development in 5G NR and further standardization enhancements are expected. Yet, so far, most of the research on CoMP and NCJT consider strict synchronicity at the receiver. This may not be feasible in mobile platforms with dynamic channel conditions.

Relatively few methods have been proposed for CoMP with asynchronous interference [77][78]. In [77], amplify-and-forward (AF) relays are used to address the asynchronous reception in CoMP systems. First, the delays between users and BSs are optimized to reduce the variations of the delays. Then, the precoding matrix is optimized to reduce the effects of asynchronous paths through beamforming. Since the beamforming performance relies strictly on the accuracy of the channel estimation, they have assumed full knowledge of CSI at the relays and BSs, which might not be possible in practice. In [78], the interference cancellation in asynchronous CoMP with equal-gain combining (EGC) and maximal-gain combining (MGC) receivers are investigated. It is observed in [78] that with imperfect CSI, the performance in the proposed method degrades as the number of BSs increases. In this thesis, we prove that degradation is due to the interference cancellation at the receiver and our simulation results show that by employing the iterative joint detection at the receiver, the performance elevates even as the number of BS increases.

1.3. Thesis Contributions

In this thesis, we are interested in the applications with multiple distributed TRPs who cooperatively share their information and jointly transmit the same transmit block. Due to the distributed nature of such systems it would be challenging to attain a good trade-off between constructive exploitation of the interference and keep the synchronization and CSI control signaling overhead in a decent extent.

We consider the potential reception of the data streams with different time delay attributes, for which we have developed the capacity region. We have considered the system model to be close to practical schemes by assuming imperfect CSI. Our extensive simulation results show that the reliability and spectral efficiency can exceed that of the non-cooperative transmissions, provided that the proper receiver is employed. We propose our receiver based on iterative joint detection and decoding, by which the performance elevates even as the number of TRPs increases.

Our main contributions are described as follows:

1. **Joint Source and Channel Coding.** We have investigated the association of the source-coding and NOMA in a jointly cooperative framework. The distributed source coding as well as the exact expression for the channel capacity are provided for the two-user asynchronous uplink system model.

2. **Asynchronous Channel Model.** We have realized an accurate mathematical model for the asynchronous channels in coordinated multipoint schemes, which we have extended to the multiple number of TRPs. The asynchronous received signals from the multi-points are modelled in a channel with memory, where the cross-correlations between the asynchronous channels are included along with the channel coefficients in the extended asynchronous channel matrix.

3. **Asynchronous CoMP Capacity Region**. We have developed the exact expression for the capacity region and inner bound for the sum-rate in the asynchronous multi-TRP schemes. It is based on our proposed asynchronous channel model, where the asynchronous channels' cross-correlations are used as extra sources of information instead of being cancelled, as in current state-of-the-art systems. The evaluated capacity is different from memoryless MAC capacity. There is a supplementary term in the sum-rate due to the asynchronous channel's cross-correlation, which has a linear effect on the sum-rate.

4. **Receiver Implementation.** We have provided an iterative joint detection and decoding receiver to be used in asynchronous multi-TRP schemes. We have further developed a low-complexity MMSE-based iterative joint detection and decoding receiver, which is generalized to multiple number of TRPs. Our simulation results show that the association of our proposed asynchronous channel's model in iterative joint detection

and decoding receiver, can outperform the state-of-the-art non-iterative schemes significantly, even as the number of TRPs increases.

5. **Association of NOMA and CoMP.** We have considered the association of the CoMP and NOMA in a symbol asynchronous CoMP channel with embedded LDM. We have evaluated the channel model, channel capacity and coverage. The simulation results show a boost in coverage as well as the spectral and power efficiency.
6. **Imperfect CSI.** We have considered reasonably complex models in the simulations, reflecting interference scenarios such as imperfect CSI.

1.4. Thesis Outline

This thesis is organized as follows. In Chapter 2, the background on the main topics are provided that are referenced throughout the thesis. Chapters 3 presents the main concept of cooperative NOMA. The optimized user pairing and the effect of channel estimation errors on the downlink cooperative NOMA schemes are investigated in this chapter, followed by the corresponding evaluation and simulation results. In Chapter 4, our proposed scheme on cooperative source and channel coding in Asynchronous NOMA is provided. We demonstrate the tradeoffs that are faced in achieving the optimal spectral efficiency and their optimization, followed by investigating our proposed receiver. In Chapter 5, the Coordinated Multi-Point (CoMP) transmission is considered where two key challenges of asynchronous reception and imperfect knowledge of channel are investigated. Finally, the association of the CoMP and NOMA are investigated in Chapter 6, where we have extended our proposed IJDD receiver to higher modulation formats and have evaluated the receiver's order of complexity. The theoretical findings throughput the thesis is all supported and confirmed by simulations comparing several scenarios. The conclusion and future work are provided in Chapter 7 that concludes the thesis.

Chapter 2

Background

Introduction

In this chapter, an analysis on the fundamental topics in this thesis are provided. The concepts investigated in this chapter are the principal basis for the following chapters. The Non-Orthogonal Multiple Access channel is investigated as the basic block in the distributed channel coding scheme. Considering the cooperative correlated sources, the distributed source coding is studied next. The impairment due to the inter-symbol interference is then investigated in multiple access channels. As a special case of inter-symbol interference, the multiple access channels with symbol-asynchronous reception are explored. Finally, the iterative joint detection and decoding receivers are investigated.

2.1. Non-Orthogonal Multiple Access (NOMA)

NOMA is one of the key essential technologies to accommodate the high demand for ubiquitous mobile wireless communications. Considering the distinct ranges of coverage, reliability, and throughput, NOMA enables the allocation of the resources fairly and efficiently resulting in enhanced spectral efficiency. In this section the information theoretic basics as well as technical aspects of NOMA are provided.

Information Network Theory

The systems with multiple points of transmission and reception are investigated within the domain of network information theory, where networks of connected points are addressed. As one of the main network configurations, the Multiple-Access Channel (MAC) is identified in the network information theory as the channel with multiple transmitters and a single receiver. The Uplink (UL) channels in wireless communication are usually modeled as the MAC with the several scheduled User Equipment (UE) transmitting their data to the Base Station (BS) or the Access Point (AP). The associated channel modeling the Downlink (DL) is the Broadcasting Channel (BC), which implies the network with single transmitter and multiple receivers.

Duality of Broadcast Channel and Multiple Access Channel.

The information theoretic investigations on the capacity region, the sum-rate, the inner, and the outer bounds for MAC, can be used in the associated broadcast channels. This is due to the duality of the capacity regions in broadcast and multiple access channels. It is proved in [62] that the capacity region of the MAC could be equal to the union of BC capacity regions. Hence, this leaves us with the same capacity bounds.

Information Theoretic Analysis.

In general, the capacity region of the two-source memoryless Gaussian MAC can be written as

$$R_1 \leq I(x_1; y|x_2) = \frac{1}{4\pi}\int_{-\pi}^{\pi} \log[1 + \frac{S_1(w)}{\sigma^2}]dw \tag{2-1}$$

$$R_2 \leq I(x_2; y|x_1) = \frac{1}{4\pi}\int_{-\pi}^{\pi} \log[1 + \frac{S_2(w)}{\sigma^2}]dw \tag{2-2}$$

$$R_1 + R_2 \leq I(x_1, x_2; y) = \frac{1}{4\pi}\int_{-\pi}^{\pi} \log[1 + \frac{S_1(w)+S_2(w)}{\sigma^2}]dw \tag{2-3}$$

where, $\{S_{\mathrm{i}}(w), w \in [-\pi, \pi]\}$ is the power spectral density corresponding to transmitter i, and σ^2 is the variance of the Additive White Gaussian Noise (AWGN) power, i.e. $N(0, \sigma^2)$.

Non-Orthogonal Multiple Access Methodology.

The legacy multiple access systems are based on maintaining the orthogonality, i.e. Orthogonal Multiple Access (OMA), between the resources. Time Division Multiple Access (TDMA), Frequency Division Multiple Access (FDMA), Code Division Multiple Access (CDMA), and

Orthogonal Frequency Division Multiple Access (OFDMA) are the most distinguished multiple access schemes which are based on orthogonal sources of time, frequency, code, and subcarrier signals, respectively. Hence, only one user is served at each orthogonal resource block in OMA.

NOMA proposes the means of sharing the available resources, which achieves high spectral efficiencies in comparison to OMA in enabling wireless communication networks to allocate more users to the available limited resources. NOMA is compatible with the conventional orthogonal resource blocks, as NOMA is fundamentally overlaid over the conventional orthogonal channels.

The sharing of the resources in NOMA can be addresses in two techniques,

- Power-domain NOMA
- Code-domain NOMA

Power-Domain NOMA.

In this scheme, different users are allocated to the same resource, and the multiple access is realized by assigning different power levels to different users. The power allocation is based on the users' channel condition. So, more power is allocated to the user with the worse channel condition. The receiver in power-domain NOMA is based on SIC, where the signal received from user with more power will be decoded first. The performance in power-NOMA is based on the received power differences and achieves its best performance for users with high power differences [27].

Code-Domain NOMA.

In this scheme, different spreading, non-spreading, interleaving, delay, scrambling, or codebook signatures [12] are assigned to the users who are transmitting on the same resource. The code domain NOMA is basically built upon the concept of superposition coding, using different means of implementation. As an instance, in the spreading technique, short length spreading code-words are used, where their design is desirable to support the Welch bound [28] with equality that minimizes the cross correlation of the spreading code-words. Also, in the non-spreading code-domain, different users' data are coded with different rates, to be recovered through SIC at the receiver.

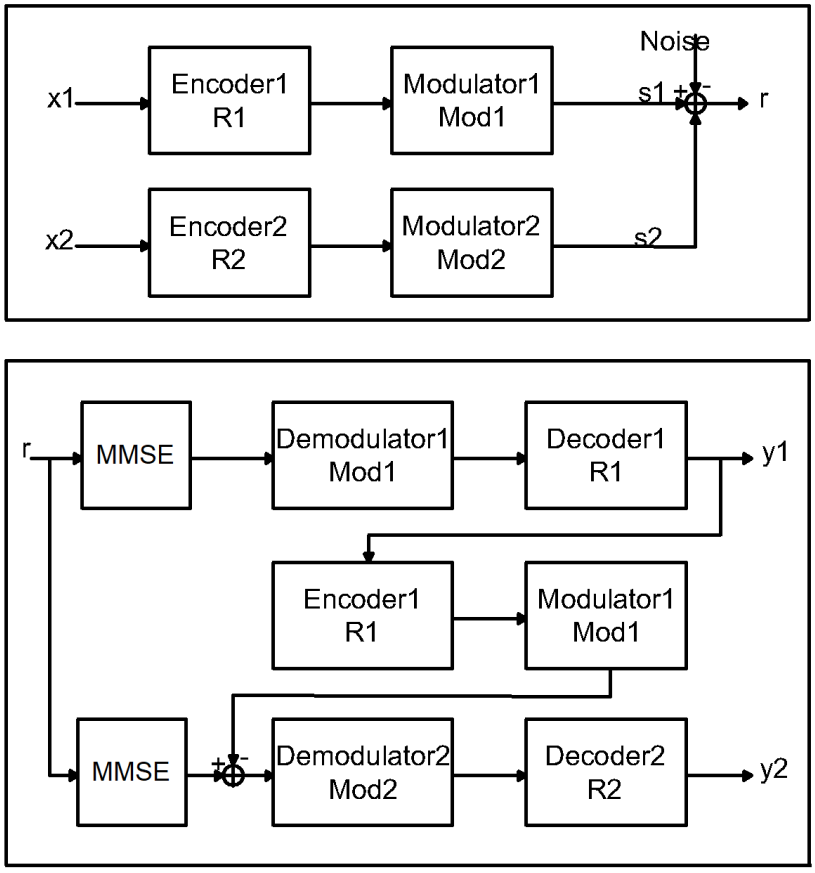

Figure 2.1: Typical Transmitter and MMSE-SIC Receiver in Code-Domain NOMA

NOMA Transmitter and Receiver

At the transmitter, the input data go through the prerequisite operations that are defined based on the power-domain or the code-domain NOMA techniques. As for the channel, the N transmitted signals add together with the channel noise after going through different fading channels. At the receiver, at least N sequences of detection and decoding are accomplished, where the information of the transmitters will be recovered successively.

In this thesis we are interested in non-spreading code-domain NOMA, where the different levels of robustness are allocated to different transmit data. The robustness is based on the Modulation format and Coding rate (MODCOD), where the user with poor reception and worst channel condition has the highest robustness and the other users with better reception have higher MODCOD rates. The transmitter and receiver for the two-transmitter scheme is typically provided in Figure 2.1, where the MMSE-SIC receiver is considered. Without loss of generality, we have

assumed that the first data stream is the one with more robust coding. At the receiver, r is the aggregated received signal that goes through the Minimum Mean Square Error (MMSE) filter followed by the demodulator and decoder corresponding to the first data stream. If the decoding is successful, the results from previous step will be reconstructed to be subtracted from the aggregate received signal. The recovered data stream once again will be encoded and modulated based on first transmit data's MODCOD. The reconstructed data will be subtracted and cancelled from the aggregate received signal. The remaining signal will go through the MMSE filter followed by the demodulator and the decoder, to recover the second data stream.

Layered Division Multiplexing (LDM)

NOMA has been proposed in ATSC 3.0 standard in Digital Terrestrial Television (DTT) in the context of LDM. LDM is a form of power-domain NOMA. LDM is a constellation superposition technology which is implemented based on the physical layer pipes (PLP) concept in ATSC 3.0. LDM employs the flexible physical layer in ATSC 3.0 with versatile coding rates and modulation formats. As such, multiple broadcasting services with different robustness demands such as mobile, indoor, or stationary, could be implemented in a single radio frequency (RF) channel.

In LDM transmitter, the different content is assigned to different layers. Each layer undergoes a different Bit Interleaved and Coded Modulation (BICM) chain. The different layers are then injected with different power levels. At the receiver, the most robust layer known as Core Layer (CL) is first decoded, considering the other layers as interference. Using the interference cancellation (IC), the core layer is then removed from the received signal. Thus, the Enhanced Layer (EL) could then be decoded as if there was no CL [100].

2.2. Multiple-Access Channel with Correlated Sources

Based on Slepian and Wolf theorem [29], for two arbitrary correlated sources U and V, the rate region could be shown as

$$R_u \geq H(U|V), R_v \geq H(V|U),$$
$$R_u + R_v \geq H(U,V) = \mathrm{H(U)} + \mathrm{H(V|U)} \tag{2-4}$$

Hence, instead of sending the correlated sources independently, i.e. $R_u + R_v = \mathrm{H(U)} + \mathrm{H(V)}$, we need less bits in total by using the Slepian-Wolf encoding. There are many researches on the

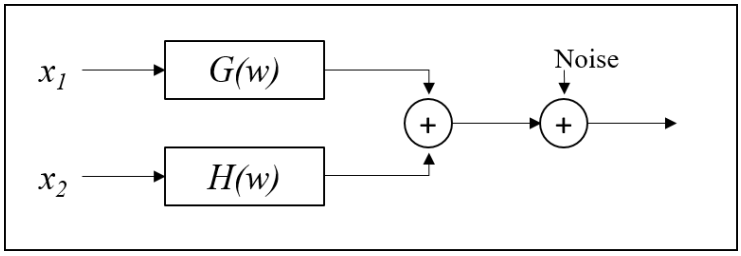

Figure 2.2: Gaussian two-user multiple access channel model

coding techniques in distributed source coding based on LDPC or Turbo codes, as well as sending syndrome or parity bits [14].

The authors in [38] have investigated the remarkable twist in the Slepian and Wolf theorem, for the frameworks where the correlated sources are transmitted in a multiple access channel (MAC). They have investigated the Slepian and Wolf data compression theorem along with multiple access channels' capacity regions and have proved that both theorems are the special approaches to a single theorem. They have studied the special case where both channel inputs have access to the same source and have shown that a cooperative MAC capacity can be found for this case that outperforms the separate source and channel coding schemes. Moreover, the Salehi-Cover-El Gamal theorem proves multiple access channels with correlated sources can use the dependence of the sources to associate the channel coding in a cooperative approach.

2.3. Gaussian Multi-Access Channels with ISI

The Gaussian MAC with Inter-Symbol Interference (ISI) is studied in detail in [33] where the capacity region is achieved through a multiuser water-filling scheme that we briefly present the results here. The sequel can also be used in Gaussian MAC with asynchronous channel, as the asynchronous reception shows in the form of ISI in multiple-access channels.

The channel model for the two-user Gaussian MAC with ISI is shown in Figure 2.2, where $G(w)$ and $H(w)$ are the channels' transfer functions. We denote $g(w) = |G(w)|^2/N(w)$ and $h(w) = |H(w)|^2/N(w)$, as the square of magnitude of channel transfer function over the noise PSD, i.e. $N(w)$.

As the capacity of memoryless Gaussian multiple access channels are well known, the tactic to evaluate the capacity region of NOMA with ISI would be to decompose the channel into parallel memoryless channels. This is not as straight forward as single user channels, as the two channels'

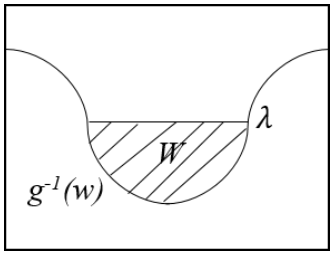

Figure 2.3: Single user water-filling scheme

affect each other. As such a water-filling scheme could be used to show graphically the optimal total PSD over frequency domain. Thus, the successive cancellation is modelled graphically on the water-filling scheme to find the optimal PSD of each user over the bandwidth. As follows, the two-user multiple access channel with similar and dissimilar transfer functions are investigated. The case with similar transfer functions is provided for clarification, where the one with dissimilarity is our case of interest.

Two-User Channel with $\boldsymbol{H(w) = G(w)}$.

For a single user channel, the water-filling scheme is shown in Figure 2.3, where W is the total power. The $g^{-1}(w)$ is the bottom of the water-filling container and the fixed amount of water (power), W, is poured into the container. Based on water-filling scheme, the optimal PSD, i.e. $S(w)$, as it is shaded in Figure 2.3 is the solution to below equations:

$$S(w) = [\lambda - g^{-1}(w)]^{+} \tag{2-5}$$

$$W = \frac{1}{\pi}\int_0^{\pi} S(w)dw \tag{2-6}$$

Where the '+' sign indicates that $S(W) \geq 0$. The same aspect can be followed for finding optimal PSD of two-user channel when the transfer functions are analogous. $q^{-1}(w) = g^{-1}(w) = h^{-1}(w)$ will be used as the bottom of the containers for $S_1(w)$, $S_2(w)$, and $S_1(w) + S_2(w)$ water-filling diagrams separately, while satisfying the following equations

$$S_1(w) + S_2(w) = [\lambda_{12} - q^{-1}(w)]^{+} \tag{2-7}$$

$$W_1 + W_2 = \frac{1}{\pi}\int_0^{\pi} S_1(w) + S_2(w)dw \tag{2-8}$$

$$S_i(w) = [\lambda_i - q^{-1}(w)]^{+} \tag{2-9}$$

$$W_i = \frac{1}{\pi}\int_0^{\pi} S_i(w)dw \tag{2-10}$$

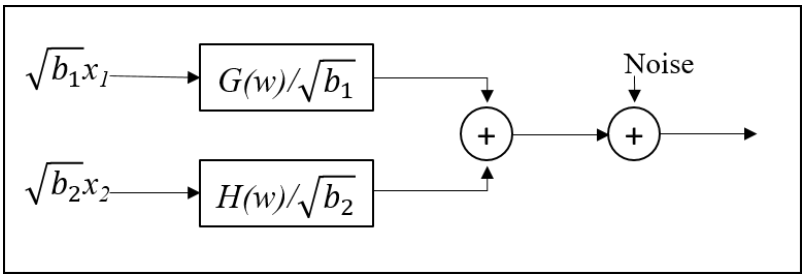

Figure 2.4: Equivalent Gaussian two-user multiple access channel model

Two-User Channel with $H(w) \neq G(w)$.

In this case, the goal is to find the optimal PSD for the two users that maximizes a weighted sum rate as

$$\alpha R_1 + (1-\alpha)R_2, \qquad \alpha \in [0,1]$$

The optimal PSD of the two users cannot be found in two separate water-filling diagrams as they cause interference on each other. In order to overcome this problem, an equivalent channel is required to combine both $g^{-1}(w)$ and $h^{-1}(w)$. Using this equivalent channel allows us to find the optimal sum of the PSDs as well as individual PSDs.

The equivalent channel is shown in Figure 2.4. The idea behind this channel is to use a scaled version of the original channels to be able to combine both in one water-filling diagram. The optimal PSD for the equivalent channel that maximizes the weighted sum rate is the solution to the following equations

$$C = \{(R_1, R_2) \in R^2 : \alpha R_1 + (1-\alpha)R_2 \leq C(\alpha)\} \tag{2-11}$$

where, $C(\alpha)$ is defined as

$$C(\alpha) = \begin{cases} \alpha F(S_1, S_2) + (1-2\alpha)F(0, S_2), & \text{if } \alpha \in [0,1/2] \\ (1-\alpha)F(S_1, S_2) + (2\alpha-1)F(S_1, 0), & \text{if } \alpha \in [1/2,1] \end{cases} \tag{2-12}$$

where, $F(Z_1, Z_2)$ can be written as

$$F(Z_1, Z_2) = \frac{1}{2\pi}\int_0^{\pi} \log[1 + Z_1(w)g(w) + Z_2(w)h(w)]\, dw \tag{2-13}$$

The intuition behind above equations is exactly based on the SIC methodology that defines how to split the equivalent combined water-filling diagram. The user with worse channel condition is

considered lower priority and is decoded first, considering the second user's signal as noise. Then the first user's signal is reconstructed and subtracted from the aggregate signal to decode the second user's signal with no effect from the first user. As an instance, for $\alpha \in [0,1/2]$, since User1 is considered as the low priority, the corresponding data is recovered while having the signal from User2 as interference, i.e. $\alpha F(S_1, S_2)$; whereas, User2 as the one with high priority would recover its data as if there was no User1, i.e. $(1-\alpha)F(0, S_2)$. It is similar for the cases with $\alpha \in [1/2,1]$. Also, for $\alpha = 1/2$ with equal priority, the sum rate will be divided between users based on their channel conditions.

Without loss of generality, we have shown a typical water-filling diagram for $\alpha \in [0,1/2]$ in Figure 2.5. With the fixed water level equal to 1, the minimum of the two curves is considered as the bottom of the container, i.e.

$$\arg \min_{w,b_1,b_2} (b_1 g^{-1}(w) + (1-\alpha), b_2 h^{-1}(w) + \alpha) \tag{2-14}$$

The parameters b_1 and b_2 are adjusted so that the total amount of water (power) is equal to $b_1 W_1 + b_2 W_2$. Then the two shaded areas define the optimal PSD for the two users.

Optimal Water-Filling Algorithm for a Gaussian MAC with ISI.

In order to find the optimal scales, i.e. b_1, b_2, that maximize the sum rate, we have adopted the procedure in [34], which is based on a geometrical water-filling method. The methodology is based on maximizing the weighted sum-rate of the two users, as in (2-11), subject to each user's power constraints.

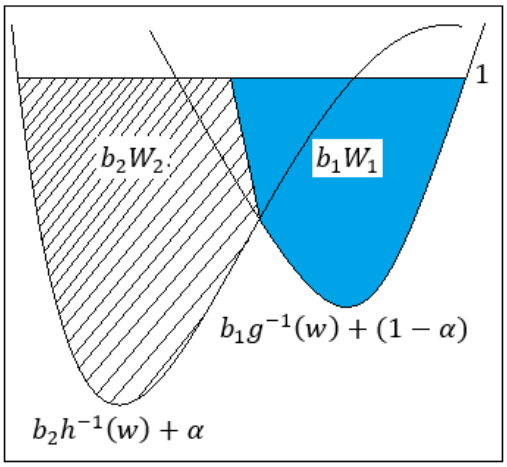

Figure 2.5: Two-user water-filling scheme with $H(w) \neq G(w)$

By iteratively changing the value of the α, the water-filling diagram Figure 2.5 and equation (2-14) change accordingly. Thus, based on the channel transfer function and the PSD of each user, all options of the scaling parameters will be calculated. As such, the optimum scales of b_1, b_2 will be selected as the ones that maximize the weighted sum-rate.

In a two-user MAC, for each value of the priority factor α a rectangular region is assumed in the two-dimensional coordinates. This is to calculate the (b_1, b_2) pairs relative to each other. The outer boundary of the specified region is defined based on single-user detection and ignoring the other user, which results in $b_{1,\max}$ and $b_{2,\max}$, that can be written as

$$\sum_w \left[b_{1,\max} g^{-1}(w) + (1-\alpha)\right]^+ - b_{1,\max} W_1 = 0 \tag{2-15}$$

$$\sum_w \left[b_{2,\max} h^{-1}(w) + \alpha\right]^+ - b_{2,\max} W_2 = 0 \tag{2-16}$$

In order to find the optimal (b_1, b_2) pair, an iterative algorithm is proposed. The (b_1, b_2) pair is first initiated with the corresponding maximum threshold $(b_{1,max}, b_{2,max})$ pair. In each iteration the pair is changed until the both the single and aggregate power constraints are satisfied,

$$\sum_w S_1(w) - b_1 W_1 = 0 \tag{2-17}$$

$$\sum_w S_2(w) - b_2 W_2 = 0 \tag{2-18}$$

$$\sum_w (S_1(w) + S_2(w)) - (b_1 W_1 + b_1 W_1) = 0 \tag{2-19}$$

Thus, as the priority factor α sweeps from 0 to 1, the different points in the sum-rate capacity is calculated, where the final capacity region could be found by association of all the resulting points.

Information Theoretic Evaluation Results.

Due to the channel having ISI, the capacity region is no more pentagon. So, we had to calculate the optimal PSD for every boundary point, and not just the corner points. Also, at each point, we had to take into consideration the effect of the signals from both users, as they appear as noise for each other.

As an instance, we evaluated two-user multiple access channel with transfer functions as follows for multiple values of $\alpha \in [0,1]$.

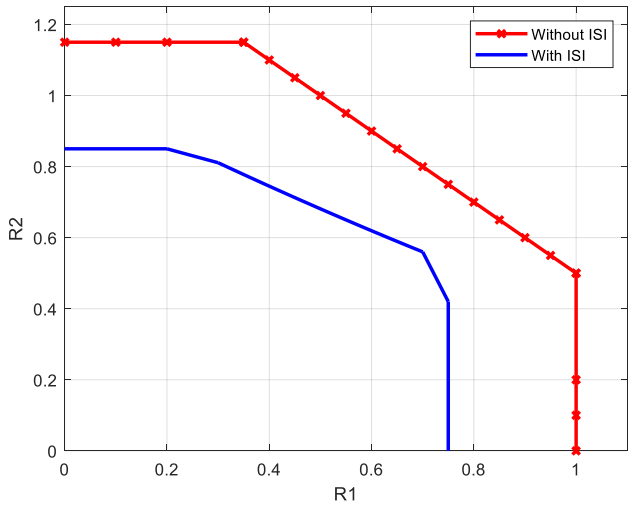

Figure 2.6: Two-user MAC with SIC at the receiver, Capacity region with or without ISI

$$H(w) = \left(1 + 0.1e^{-j\omega}\right)/1.005 \tag{2-20}$$

$$G(w) = \left(1 + 0.3e^{-j\omega}\right)/1.044 \tag{2-21}$$

We have assumed $W_1 = 3$, $W_2 = 4$, and noise variance of one. The transfer functions are normalized to have unit energy. The capacity region is shown in Figure 2.6 with the solid line; where, the capacity region of the channel without ISI, i.e. $h(t) = g(t) = \delta(t)$[1], is provided as starred line. As expected, the ISI between the two channels degrades the single-user as well as the sum-rate capacities. Also, the capacity region is no more pentagonal, and it is curved at the boundary corner points.

In this thesis, we have used the above arguments to prove that the SIC receivers are suboptimal in multiple access channels with asynchronous reception. The cross-correlations between asynchronous channels are regarded as interference in SIC and are discarded. In next chapters we show that there is the coding information available through the cross-correlations that can be used for the benefit of the spectral efficiency. This is succedent of the Salehi, Cover and ElGamal theorem in [38], wherein taking advantage of the partial information of the sources about the others can lead to an error-free transmission. Thus, we employ the unwanted coding provided by the asynchronous channel's cross-correlations as extra information instead of discarding it.

[1] $\delta(t)$ is the Dirac delta function

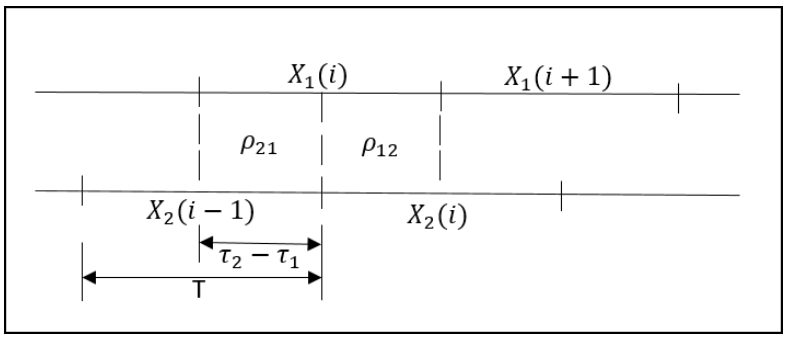

Figure 2.7 Symbol asynchronism and cross correlations

2.4. Symbol-Asynchronous Gaussian Multiple-Access-Channels

In general, two types of synchronism could be considered in multiple-access channels. Frame synchronism takes place when the transmitters cooperate to adjust their transmission time in order to transmit at the same time. Symbol synchronism is when the symbols received from different transmitters are totally aligned at the receivers. In this section, the study and the results on the capacity region in symbol-asynchronous MAC are provided, which were primarily investigated in [32] for two user MAC in the Gaussian channel with no fading.

Figure 2.7 shows the symbol asynchronous channel model. The asynchronous channel is parameterized by the channels' cross correlations, which depend on the signals' time offset. Without loss of generality, assuming $\tau_1 \leq \tau_2$ in Figure 2.7, the cross correlations can be shown as

$$\rho_{12} = \int_0^{T_s} x_1(t)x_2(t+\tau_1-\tau_2)\,dt \tag{2-22}$$

$$\rho_{21} = \int_0^{T_s} x_1(t)x_2(t+T_s+\tau_1-\tau_2)\,dt \tag{2-23}$$

This leads to the channel's correlation matrix as

$$\begin{bmatrix} 1 & \rho_{12}+\rho_{21}e^{-jw} \\ \rho_{12}+\rho_{21}e^{jw} & 1 \end{bmatrix} \tag{2-24}$$

for which the determinant is defined as $(1-\rho^2(w))$. This gives the definition for asynchronous channel's cross-correlation (SCCC) as below

$$\rho(w) \triangleq \sqrt{\rho_{12}^2+\rho_{21}^2+2\rho_{12}\rho_{21}\cos(w)}\,, |\rho| \in [0,1] \tag{2-25}$$

In this thesis, as cooperating transmitters are assumed, so we consider just slight symbol misalignments and consequently $|\rho|$ to be very close to one.

Based on the discussion on the multiple-access channels with SIC at the receiver, the asynchronism is traditionally believed to degrade the channel capacity due to the ISI caused by adding memory and correlation. As follows, we show that by benefiting the added correlation, the capacity region could be improved.

The capacity region for asynchronous Gaussian MAC is studied in detail in [32] that we briefly present the results here. Due to the symbol asynchronism, each transmitted symbol will overlap with the preceding and succeeding symbols of the other transmitters. For the two-user Gaussian MAC, the received signal at the base station is the sum of contributions from both users plus noise,

$$y(t) = x_1(t-\tau_1) + x_2(t-\tau_2) + n(t) \tag{2-26}$$

Where, X_i are the transmitted signal vectors, and $n(t)$ is the complex AWGN, $n \sim N(0, \sigma_n^2)$. The transmit signals are delayed with an independent delay, $0 \le \tau_i \le T_s$, during the transmission, where T_s is the symbol time. The discrete-time projection of $y(t)$ can be written as

$$\boldsymbol{Y}[i] = \boldsymbol{H}(-1)\boldsymbol{X}[i-1] + \boldsymbol{H}(0)\boldsymbol{X}[i] + \boldsymbol{H}(1)\boldsymbol{X}[i+1] + \boldsymbol{N}[i] \tag{2-27}$$

where, $\boldsymbol{Y}[i] = [Y_1(i)\ Y_2(i)]^T$, $\boldsymbol{X}[i] = [X_1(i)\ X_2(i)]^T$, and the matrices are as

$$\boldsymbol{H}(0) = \begin{bmatrix} 1 & \rho_{12} \\ \rho_{12} & 1 \end{bmatrix},\ \boldsymbol{H}(-1) = \boldsymbol{H}^T(1) = \begin{bmatrix} 0 & \rho_{21} \\ 0 & 0 \end{bmatrix} \tag{2-28}$$

The modeled channel has memory and the inputs from different coordinates interfere with each other. In (2-28), even noise vector is affected by the channel's memory and $\boldsymbol{N}[i] = [N_1(i)\ N_2(i)]^T$ is the Gaussian random process with zero mean and covariance matrix as

$$\mathrm{cov}(\boldsymbol{N}) = \mathrm{E}\left[\begin{bmatrix} N_1(i) \\ N_2(i) \end{bmatrix} [N_1(j) \quad N_2(j)]\right] = \sigma^2 \boldsymbol{H}(i-j) \tag{2-29}$$

where, $\boldsymbol{H}(i) = 0$ for $|i| > 1$.

It is proved in [32] that the sum rate of the asynchronous channel where the transmitters are aware of their time offset can be written as

$$C = \bigcup \begin{Bmatrix} (R_1, R_2), 0 \le R_i \le \frac{1}{4\pi}\int_{-\pi}^{\pi} \log\left(1 + \frac{S_i(w)}{\sigma^2}\right) dw \\ R_1 + R_2 \le \frac{1}{4\pi}\int_{-\pi}^{\pi} \log[1 + \frac{S_1(w)}{\sigma^2} + \frac{S_2(w)}{\sigma^2} + \frac{S_1(w)S_2(w)}{\sigma^4}\left(1 - \rho^2(w)\right)]dw \end{Bmatrix} \tag{2-30}$$

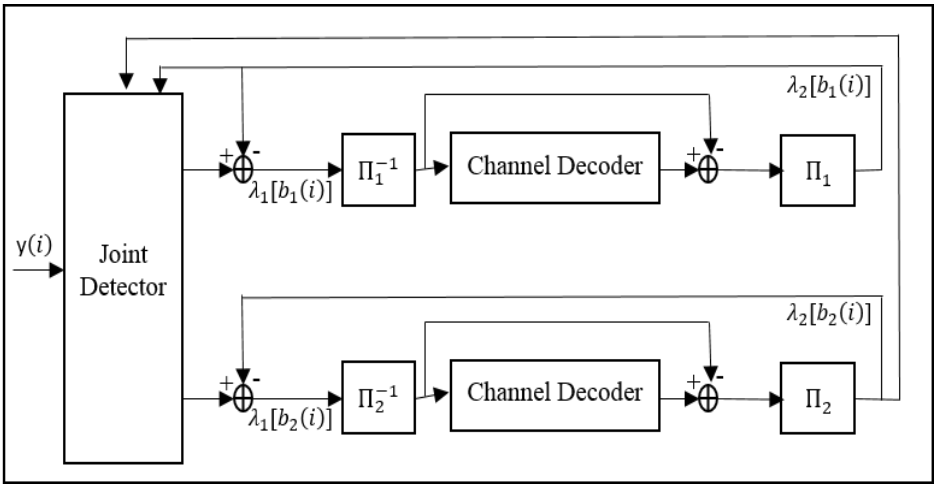

Figure 2.8 Iterative joint detection and decoding in the i-th iteration

where, $\{S_{\mathrm{i}}(w), w \in [-\pi, \pi]\}$ is the power spectral density corresponding to transmitter i. The proof is based on applying singular-value decomposition (SVD) theorem to the asynchronous channel to decomposes the channel into two independent parallel ones without interference on each other. Then the capacity for this channel is evaluated based on weighted capacity maximization.

The capacity in (2-30) is different from memoryless MAC capacity in (2-3). Though the single user capacity is the same as the synchronous channel, there is an extra term $(\frac{S_1(w)S_2(w)}{\sigma^4}\left(1-\rho^2(w)\right)$ in the sum-rate. This is due to the asynchronous channel's cross-correlation, where the maximum rate is attained for $\tau = \tau_2 - \tau_1 = 0.5T_s$. This extra term results in a bigger capacity region than a synchronous NOMA. This is in contrary with results provided in previous section, which emphasizes on the fact that SIC is not the appropriate receiver in a NOMA channel with symbol asynchronous reception.

2.5. Iterative Joint Detection and Decoding Receivers (IJDD)

The iterative joint detection and decoding (IJDD) receiver is investigated in detail by Wang and Poor in [35], who have considered their channel to be strictly synchronous. The proposed IJDD to recover the information in a two-user system is provided typically in Figure 2.8 , where Π_i denotes the interleaver at data stream i.

At the transmit side, information bits are encoded, interleaved, and modulated. The receiver is based on an iterative scheme including a joint detector with separate decoders. At each iteration, extrinsic information collected from joint detector and the decoders is used as a priori information in the next iteration.

The received signal from the channel is the input to the IJDD, that can be written as

$$\boldsymbol{Y}[i] = \boldsymbol{RAb}[i] + \sigma \boldsymbol{N}[i] \tag{2-31}$$

where, $\boldsymbol{R}$ presents the channel coefficient matrix, $\boldsymbol{A}$ is the diagonal magnitude matrix, and $\boldsymbol{b}[i]$ is the code-bits. At the receiver, the multi-user data are detected at the joint detection soft-input soft-output module. The extrinsic information delivered by the joint detector is calculated based on the channel value of the desired user as well as the other users' channel value, and the *a-priori* information extracted from the decoders. The soft extrinsic information delivered by the joint detector $\lambda_1[b_k(i)]$ is the log-likelihood ratio (LLR) corresponding to *i*-th code-bit of the *k*-th user, defined as

$$\lambda_1[b_k(i)] = \frac{2A_k y_k(i)}{\sigma^2} + \log \frac{\sum_{\boldsymbol{b}\in\beta_k^+}\left\{\exp\left(-\frac{\boldsymbol{b}^T\boldsymbol{ARAb}}{2\sigma^2}\right)\prod_{j\neq k}\left[1+b_j\tanh\left(\frac{A_j y_j(i)}{\sigma^2}\right)\right]\left[1+b_j\tanh\left(\frac{1}{2}{\lambda_2}^p[b_j(i)]\right)\right]\right\}}{\sum_{\boldsymbol{b}\in\beta_k^-}\left\{\exp\left(-\frac{\boldsymbol{b}^T\boldsymbol{ARAb}}{2\sigma^2}\right)\prod_{j\neq k}\left[1+b_j\tanh\left(\frac{A_j y_j(i)}{\sigma^2}\right)\right]\left[1+b_j\tanh\left(\frac{1}{2}{\lambda_2}^p[b_j(i)]\right)\right]\right\}} \tag{2-32}$$

As for the other terminologies, the $\boldsymbol{b}_n(i)$ is the code-bits vector from transmitter n at the i-th instance, while $b_n(i)$ is the single code-bit from transmitter n at the i-th instance. Likewise, $\boldsymbol{A}_n$ is the magnitude matrix from transmitter n, and $A_n(i)$ is the magnitude of transmitted signal from transmitter n at the i-th instance. As the transmission magnitude does not change during the transmission, the index i is omitted in equations, i.e. A_n.

The index p in ${\lambda_2}^p[b_j(i)]$ presents the a priori extrinsic information from previous iteration, and for the K user system, the terms β_k^+ and similarly β_k^- are basically described as

$$\beta_k^+ \triangleq \{(b_1, \dots, b_{k-1}, +1, b_{k+1}, \dots, b_K): b_j \in (+1, -1\}, j \neq k\}$$

$$\beta_k^- \triangleq \{(b_1, \dots, b_{k-1}, -1, b_{k+1}, \dots, b_K): b_j \in (+1, -1\}, j \neq k\}$$

The extrinsic information provided by the joint detector is then fed to the set of single-user channel decoders that are separate for each user. The decoder's extrinsic information is then fed back to the joint detector to be used at the subsequent iteration.

2.6. URLLC in IoT

With the promise of connecting everything that can be connected, Internet of things (IoT) is expanding rapidly in various applications such as smart homes, healthcare, smart cities, smart grids, process automations, etc. The IoT services can be divided into low and high data-rate, as well as short-distance and WAN communication technologies [23]. In this thesis, we are interested in low-data-rate and short distance IoT applications with massive number of nodes, with access to correlated sources. Low outage probabilities resulting in high reliability, and the efficient power consumption, are the most important aspects that we consider in our investigations. Besides, our scheme provides higher spectral efficiency by making more users share the limited available resources.

In order to accommodate the emerging services in IoT, Ultra-Reliable Low-Latency Communication (URLLC) is providing strict criteria on the reliability. Both IoT and URLLC are still under investigations toward the fifth generation (5G) standardization. Yet, based on the agreed performance metrics and simulation assumptions in 3GPP standards, the block error rate in URLLC should be lower than 10^{-5} [24], which is the target BLER in our simulations.

2.7. Digital Video Broadcasting Standards

2.7.1. DVB-S2x in Satellite Systems

The Digital Video Broadcasting - Satellite - Second Generation (DVB-S2) is the digital television broadcast standard, where DVB-S2x is the extension to be employed in forward link of satellite communication systems [60]. The DVB-S2x proposes LDPC as the error correcting codes. In addition, a variety of MODCOD is supported to include data rates ranging from very low SNRs to very high data throughputs. The Adaptive Coding and Modulation (ACM) employed in DVB-S2x enables dynamic MODCOD allocations, resulting in capacity region very close to the theoretical bounds. Due to the antenna propagation pattern and the long distances, the DVB-S2x communication channel is generally considered as AWGN. The Line-of-Sight (LOS) is assumed which is guaranteed by the ground directional roof-top antennas.

2.7.2. ATSC 3.0 in Terrestrial Television Systems

The next-generation Digital Terrestrial Television (DTT) standard, known as Advanced Television Systems Committee (ATSC) 3.0, has introduced many breakthrough technologies. As such, the networks can benefit from a higher spectral efficiency, coverage, and flexibility from user access perspective. The ATSC 3.0 physical layer is based on Orthogonal Frequency Division Multiplexing (OFDM). To accommodate the OFDM in different scenarios, it supports three FFT sizes of 8K, 16K, and 32K, with twelve guard intervals (GI) from ~27μs to ~700 μs. It has employed the LDPC coding with twelve code rates, i.e. 2/15, 3/15, …, 13/15, in two frame lengths, i.e. 16,200 and 64,800 bits. The six modulation formats are supported as well which order from QPSK to 64QAM [95].

Chapter 3

Cooperative NOMA Interference Mitigation

3.1. Introduction

In recent years, the demand for high data throughput has led to research and development efforts towards new technologies wireless communication systems. In this chapter, we employ the cooperative non-orthogonal multiple access (NOMA) in interference-limited scenarios. The proposed cooperative NOMA uses the cooperation of the strongest co-channel interference (CCI) as extra source of information, where the data intended for the target receiver is shared between the cooperating transmitters in the adjacent cells. The involved transmitters cooperate in jointly transmitting the data to the target user at the same time. Thus, the target user receives a signal that includes the aggregate of the data streams.

Modeling of the cooperative NOMA in a downlink connection, which is by nature a broadcast channel, is due to the duality of broadcast channel (BC) and the multiple access channel (MAC). It is proved in [91] that the capacity region of the MAC could be equal to the union of BC capacity regions. Hence, this leaves us with the same capacity bounds.

It is observed that by managing the interference, it is possible to remove the destructive effect of the interference, and even better, use it as an extra resource. This can be deployed in the downlink wireless communications. The transmitters in the incumbent and the interfering cells have access to both data resources and can contribute for cooperative NOMA purposes. Hence,

the transmitters in the incumbent and the interfering cells cooperate to jointly target one user at a time. At each time slot, the data for the target user is shared by cooperating transmitters that send data to target user at the same time and frequency band. Thus, the target user will receive the sum of data signals from two sources. This is the known characteristic of MAC.

In the cooperative NOMA, an interfering data stream is overlaid to the original data which will be recovered at the receiver resulting in more data throughput provided to each user. So, the proposed cooperative NOMA achieves the capacity of MAC in a cooperative scheme. The user will recover both data through Successive Interference Cancellation (SIC). Likewise, the user in the adjacent beam will be served in the remainder of the time.

In order to employ the cooperative NOMA, we propose an approach based on optimized user pairing strategies. We devise an information theoretic framework followed by simulation to compare different strategies by evaluating the aggregate data rate in a system-level evaluation.

Being based on SIC, the existence of residual errors will degrade the spectral efficiency gain in cooperative NOMA. We investigate the effect of channel signal to noise plus interference ratio (SINR) estimation errors. Finally, it is verified by simulation that these issues can be overcome, and cooperative NOMA can reach expected data throughput very close to the cases with perfect channel estimation.

In this chapter, we have assumed the system model such that we could extend the DVB-S2x links with AWGN channel in multibeam satellite system with dense frequency reuse. However, this is not a restriction of the method and the cooperative NOMA can be used in fading channels as discussed in next chapters.

3.2. System Model

3.2.1. Channel Model

The system model includes a downlink system in a wireless network with full frequency reuse, consisting of B adjacent cells, see Figure 3.1. The system model is based on DVB-S2x standard and so the channel is AWGN. All transmitters are supposed to provide service to the users in their corresponding cells, in addition to cooperating with adjacent transmitters in cooperative NOMA, if applicable. Due to the frequency reuse, each user receives the signals from the transmitters in all

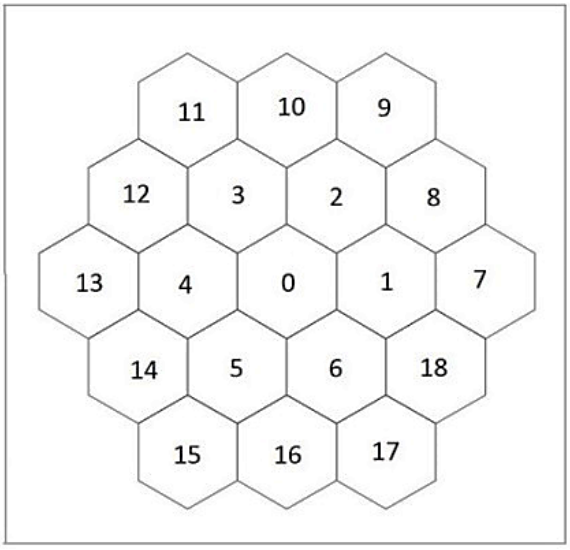

Figure 3.1 Multibeam Satellite Communication System Model, Cell Configurations

other cells. We assume the f_b as the on-board multibeam antenna gain. Uniform distribution of users in all cells in addition to equal number of users per cell (M) is assumed. In cell b, i.e. $b = 1, \dots, B$, the set of users is provided as $S = \{u(b,1), u(b,2), \dots, u(b,M)\}$. The term $u(b,k)$ stands for the k-th, i.e. $k = 1, \dots, M$, user located at cell b. At the transmitters, each $u(b,k)$-th user data stream is channel coded and modulated independently. Considering $S_{u(b,k),b\prime}$ as the coded-modulated symbol of user $u(b,k)$ from transmitter b', with average power equal to one, i.e. $E[|S_{u(b,k),b\prime}|^2 = 1$, and the transmitted power as $P_{u(b,k),b\prime}$, the transmit signal vector is dented as

$$x(t) = \sum_{b\prime=1}^{B} f_b \sum_{k=1}^{M} \sqrt{P_{u(b,k),b\prime}} S_{u(b,k),b\prime} p(t - kT). \quad (3\text{-}1)$$

So, the received signal vector at user $u(b,k)$ can be written as

$$y_{u(b,k)} = H_{u(b,k)} x + w_{u(b,k)}. \quad (3\text{-}2)$$

Where $H_{u(b,k)}$ is the $1 \times B$-dimensional channel vector between the transmitters' network and user $u(b,k)$ indicating the interference caused by other transmitters, and $w_{u(b,k)}$ is the complex Gaussian noise $N(0, n_{u(b,k)})$. We define channel parameter as $g_{u(b,k)} = \sqrt{|H_{u(b,k)} f_b|^2}$, so (3-2) could be written as:

$$y_{u(b,k)} = g_{u(b,k)} \sum_{b\prime=1}^{B} \sqrt{P_{u(b,k),b\prime}} S_{u(b,k),b\prime} + n_{u(b,k)}. \quad (3\text{-}3)$$

3.2.2. Cooperative NOMA: Overlay Coding

The cooperative NOMA investigated in this chapter is based on the overlay of the codes on the existing orthogonal resources. Hereafter, the overlay coding may be interchangeably used with the cooperative NOMA.

It is observed that the spectral efficiency is boosted if two or three adjacent transmitters with the most dominant interference cooperate in transmitting to the target user. In other words, by employing the overlay coding, not all the signals received from interfering cells degrade the system performance; whereas, the signal received from the cells with the most dominant interference is used as extra source of information. Based on the proposed overlay coding with two cells cooperation, we assume b_m to be the cell number for which the user $u(b,k)$ receives the dominant interference from, denoted as

$$h_{u(b,k),b_m} = max\left(H_{u(b,k)}\right), b_m \neq b \tag{3-4}$$

where $h_{u(b,k),v}$ is the v-th element of vector $H_{u(b,k)}$.

Based on the definition of the sum-rate in MAC as defined in network information theory, see (2-3), the SINR can be written as

$$\gamma_{u(b,k)} = \frac{g_{u(b,k),b}{}^2 P_{u(b,k),b} + g_{u(b,k),b_m}{}^2 P_{u(b,k),b_m}}{\sum_{b'=1,\neq b',\neq b_m}^{B} g_{u(b,k),b'}{}^2 P_{u(b,k),b'} + n_{u(b,k)}} \tag{3-5}$$

Where, the numerator is the sum of the received powers from the incumbent and the most dominant interfering transmitters. The denominator is the addition of channel noise and summation of all interferences, except for the cooperating most dominant interference. The sum rate is denoted as

$$R_{sum-rate-overlay} = W log_2\left(1 + \gamma_{u(b,k)}\right) \tag{3-6}$$

3.2.3. State-of-the-Art Systems: Four Color Frequency Mapping

Currently, the state-of-the-art systems are based on interference avoidance by using orthogonal channels in multibeam satellite systems. This includes mapping non-overlapping frequency bands, i.e., colors, in the adjacent cells. The analyzed system is the four-color frequency mapping. Due to frequency reuse, the whole available bandwidth is divided by four. Also, to be able to compare this scheme with full frequency reuse, as in the cooperative NOMA, the power constraints are

taken into consideration by dividing the noise by four. These are considered in evaluating the channel SINR and sum rate as

$$\gamma_{4C,u(b,k)} = \frac{{g_{u(b,k),b}}^2 P_{u(b,k),b}}{\sum_{b'=1,\neq b,if\ the\ same\ freq.}^{B} {g_{u(b,k),b'}}^2 P_{u(b,k),b'} + \frac{1}{4} n_{u(b,k)}} \tag{3-7}$$

$$R_{sum-rate-4C} = \frac{W}{4} log_2\left(1 + \gamma_{4C,u(b,k)}\right) \tag{3-8}$$

In (3-7), the interference at the denominator is the sum of received power from interfering cells, only when they use the same frequency band as in the cell of interest.

3.2.4. Classic Overlay Coding vs. State-of-the-Art Systems

The overlay coding and the four-color frequency mapping are compared numerically. The input to this evaluation is SINR values at locations spread throughout the cells. The channel is AWGN and strict synchronization is assumed. Figure 3.1 shows the typical multibeam system with 19 cells considered in this evaluation. Cell #0 at the center with the greatest interference is the beam of interest. As part of our previous research in [68], it is observed that considering the system level analysis, the overall data throughput in overlay coding may be lower than the four-color frequency model. This is due to the fact that overlay coding performs best where the interference is strong, which is at the border of the beams. Thus, employing overlay coding throughout the cells and for instance at the center of the cell is a waste of energy and time. Hence, when considering overlay coding in system level for dense multiuser, multibeam schemes, an optimized strategy should be taken into consideration.

3.2.5. Channel State Information (CSI) Estimation

In this section, we have investigated the channel estimation errors in multibeam satellite forward links. We adopt the pilot-aided technique presented by DVB-S2x standard, Annex E.4 [60] for channel estimation of our proposed cooperative NOMA in the forward link of multibeam satellite systems. Based on DVB-S2x, the pilot fields are constructed by a Walsh-Hadamard (WH) sequence of 32, resulting in a set of 32 orthogonal WH sequences. Hence, the data stream from incumbent beam in addition to 31 other beams can be completely distinguished.

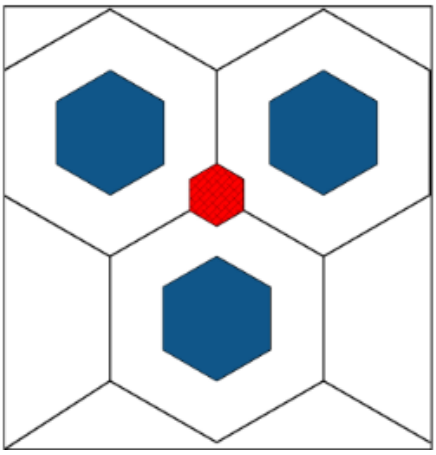

Figure 3.2 User Pairing Optimization Strategies

3.3. User-Pairing Optimization

3.3.1. Optimization Strategy

The strategy is to employ the overlay coding in cooperative NOMA scheme, based on pairing the users in a carrier to interference ratio (CIR)-wise methodology. For instance, as the CIR is higher at the center of the cells, the users will be served only by their corresponding cell. In this case, the CCI received from all other cells is treated as additive noise, as in interference as noise (IAN) model. In the contrary, at the border of the cells, CIR has lower values declining to 0 dB at the cell-edge. So, the overlay coding will be used to compensate the lower CIR by managing the interference. The blue area in the center of each cell in Figure 3.2 shows the area for which IAN will be employed.

So, the strategy to employ IAN or the overlay coding as in cooperative NOMA can be written as below, where T_D is the CIR threshold, and $CIR_D$is the dominant interference.

$$Strategy: \begin{cases} IAN & CIR_D > T_D, \\ Overlay & CIR_D < T_D. \end{cases} \tag{3-9}$$

The strategy to use the cooperative NOMA depends on the number of dominant interfering cells as well. In other words, overlay coding could benefit more in case of having the cooperation of three cells in locations where two dominant interferences exist. Such spot is shown typically as red area in the common corner of three cells in Figure 3.2 . Thus, the cooperative NOMA strategy to employ IAN, overlay coding of two adjacent cells, or overlay coding of three adjacent cells can

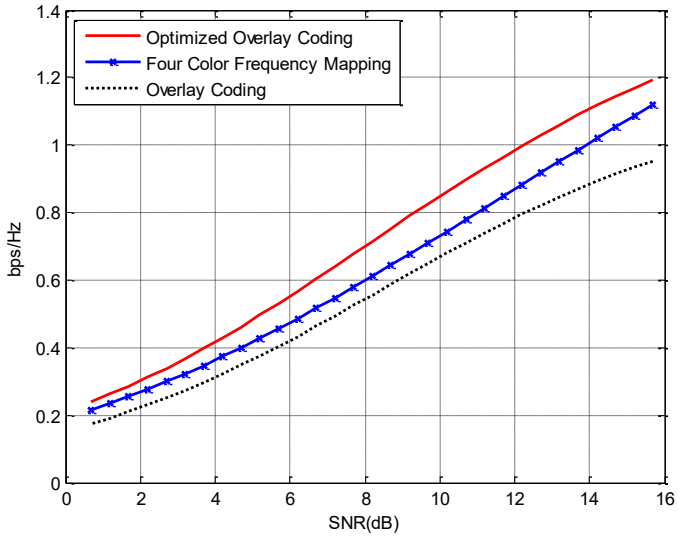

Figure 3.3 Sum Rate in the Main Beam

be summarized as below, where $T_{Di}$and CIR_{Di} are the CIR threshold and the dominant interference, respectively, and $i = 1,2$ presents the first and second dominant interferences.

$$Strategy: \begin{cases} IAN & CIR_{D1} > T_{D1}\ and\ CIR_{D2} > T_{D2}, \\ Overlay\ (2\ Beams) & CIR_{D1} < T_{D1} and CIR_{D2} > T_{D2}, \\ Overlay\ (3\ beams) & CIR_{D1} < T_{D1} and\ CIR_{D2} < T_{D2}. \end{cases} \quad (3\text{-}10)$$

3.3.2. Optimized Cooperative NOMA, Analytical Analysis

The optimized overlay coding and the four-color frequency mapping are compared numerically. Figure 3.3 shows the comparison of the achieved data throughput. For the purpose of analyses, the classic overlay coding is also provided. It is observed that the proposed optimized overlay coding in full frequency reuse, achieves almost 2dB and 3dB gain in data throughput, compared to the state-of-the-art four-color frequency mapping and the classic overlay coding, respectively.

3.4. Channel Estimation

3.4.1. Channel Estimation Analysis

Based on the SINR in (3-5) for the cooperative NOMA, the estimated SINR can be written as

$$\tilde{\gamma}_{u(b,k),b} = \frac{\tilde{g}_{u(b,k),b}{}^2 P_{u(b,k),b} + \tilde{g}_{u(b,k),b_m}{}^2 P_{u(b,k),b_m}}{\sum_{b'=1,\neq b',\neq b_m}^{B} \tilde{g}_{u(b,k),b'}{}^2 P_{u(b,k),b'} + n_{u(b,k)}} \quad (3\text{-}11)$$

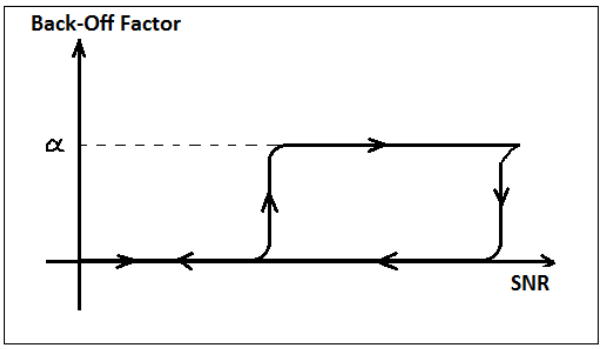

Figure 3.4 SINR back-off factor Hysteresis

Where, $\tilde{g}_{u(b,k),b}$is the estimated channel coefficient. The channel estimation error affects the actual SINR that may cause faulty rate estimations. Over-estimation of the MODCOD rates generally causes decoding error and severe degradation in the performance. We propose considering a back-off factor, i.e. α, in the estimated SINR by assuming a margin in the achievable data rate. This degrades the system performance from the ideal channel estimation; however, by decreasing SIC residual errors, it results in less decoding errors, lower packet discard, and higher actual throughput eventually. Hence, by employing SINR back-off, the aggregate data rate achieved by overlay coding in the existence of the channel estimation error could be written as below

$$\tilde{R}_{sum-rate-overlay} = W log_2\left(1 + (1-\alpha)\tilde{\gamma}_{u(b,k),b}\right) \quad (3\text{-}12)$$

3.4.2. SINR Back-Off Factor Optimization

The SINR back-off factor should have the lowest value possible in order not to degrade the channel capacity, while decreasing the frame error rate (FER) as much as possible. We have investigated the strategy to select the SINR back-off factor in this section.

Based on DVB-S2x standard [60] employed in forward link of satellite communication systems, the adaptive coding and modulation (ACM) follows a step-wise rate allocation approach based on channel SINR. At each rate-level, the SINR values in the range of that step will all have the same modulation and coding (MODCOD) rate. Hence, if for a particular SINR the estimated SINR is within that step, the rate would be still equal to the desired MODCOD. Also, if the estimated SINR is lower than the actual value, although the allocated rate will drop to the previous MODCOD rate-level, but at least the transmission would be still possible and there will not be any frame discards.

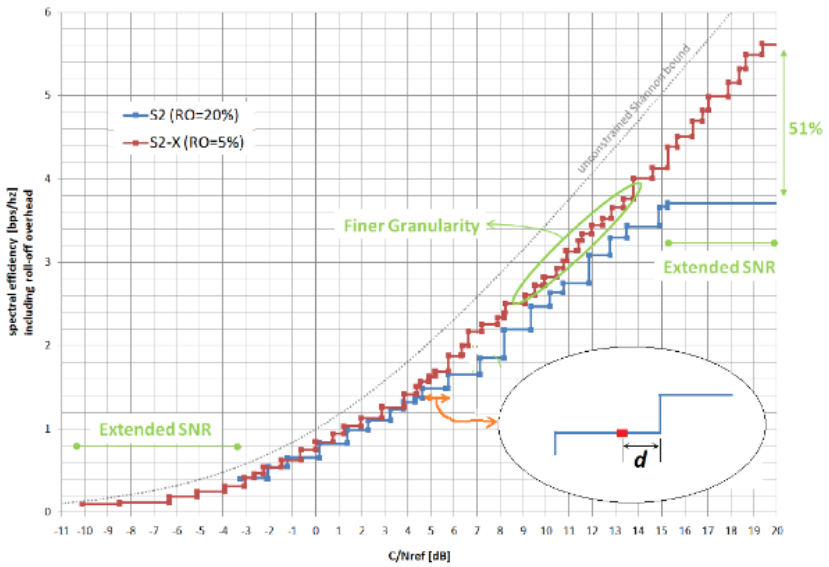

Figure 3.5 DVB-S2x Efficiency vs. C/Nref [[70], Fig. 67]

However, if the channel SINR estimation is higher than the actual SINR range of the actual rate-level, this results in overestimation of the channel rate and increases the frame discards. Hence, devising the SINR back-off factor might be of no use in most of the rate-level or while the estimation is lower than the actual SINR. So, we can only consider the back-off factor for SINR values close to the rising edge of each step to avoid jumping to next step. This can be shown as in a hysteresis as provided in Figure 3.4 .

Although the hysteresis ideally models the concept of optimizing the usage of the SINR back-off factor, still as the actual SINR is not known at the receiver, the state of the channel and whether the estimated value is more or less than the actual value cannot be determined. Hence, we have to stick to what we have which is the estimated SINR.

So far, we have proposed the SINR back-off factor to avoid the errors caused by SINR estimation. It is desired to select the back-off factor so that it prevents jumping from one rate-level to the next rate-level in the rate vs. SNR arrangement of DVB-S2x. Based on [70], Figure 3.5 shows an actual SINR value of the channel which is close to the rising edge of its corresponding rate-level with a distance of d. If the difference between estimated SINR, i.e. $SNIR_{estim}$, and the actual SINR, i.e. $SNIR_{actual}$, is less than d, it is assured that the allocated MODCOD rate will be within the acceptable range of corresponding rate-level. However, if the difference is higher than d which is caused by channel noise, this leads to higher MODCOD rate allocation and results in

increased FER. According to [71], the channel estimation error is a Gaussian random variable with zero mean and variance

$$\sigma_e^2 = \frac{1}{(ln2)^2}\sigma_m^2 \tag{3-13}$$

Where σ_m^2 is the AWGN channel noise variance.

Although $(SNIR_{estim} - SNIR_{actual}) = SNIR_{diff} > d$ is probable, by adding the SINR back-off factor $(1-\alpha)$, we could have

$$(1-\alpha)SNIR_{diff} < d \tag{3-14}$$

Which is desirable and prevents the degradations due to the overestimation. Hence, the probability of error can be written as:

$$P(err) = P\left(SNIR_{diff} > \frac{d}{(1-\alpha)}\right) = Q\left(\frac{d}{(1-\alpha)}.\rho\right) \tag{3-15}$$

Where, ρ is the channel SINR, and $Q(\alpha)$ is the q-function. To optimize the back-off factor, we differentiate $P(err)$ with respect to α and equal to zero.

$$\frac{dP(err)}{d\alpha} = \exp\left(-\frac{1}{2}.\left(\frac{d.\rho}{1-\alpha}\right)^2\right).\frac{-d.\rho}{(1-\alpha)^2} = 0 \tag{3-16}$$

This can be solved only by having $\alpha = 1$. Indeed, in next section, simulation results confirm that increasing the back-off factor results in lower FER. However, it is not possible to have $\alpha = 1$, as based on (3-12), it degrades the channel capacity to zero data rate.

Table 3-1, Simulation Parameters

Frequency reuse	Four Color Mapping	Full Frequency Reuse
Polarization	Single	Dual
Antenna Diameter	2.2 m	2.2 m
Beams Radius	140 km	140 km
TWTA Saturated Power	130 W	130 W
# of carriers per beam, in FL	1	2

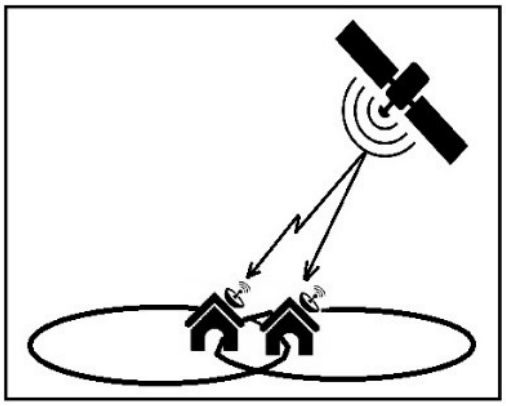

Figure 3.6 Simulation System Model

3.5. Simulation Results

We first provide the simulation results of overlay coding as the cooperative NOMA scheme assuming accurate channel estimation, followed by the simulation results of the effect of the channel estimation errors. Simulations parameters are briefly provided in Table 3-1.

3.5.1. Overlay Coding, Simulation Results

We consider the forward link of a multibeam satellite communication system. The channel is AWGN and strict synchronization is assumed. The simulation model consists of two adjacent beams, each with one user at the common border of the beams, see Figure 3.6. In this model, the power received from incumbent and the interfering cells would be almost equal, i.e. $CIR = 0\ dB$, which results in an aggressive interference. The system operates under full frequency reuse. Without loss of generality, it is assumed that the data stream #1 is the data with lower rate, i.e. stronger coding. So, QPSK and LDPC code rate of 2/9 is allocated to data stream #1, based on DVB-S2x MODCOD [60], Table 20.a]. The error performance of the second data stream versus

SNR is provided in Figure 3.7 , where modulation format of 8PSK with different LDPC coding rates are simulated. This confirms the achievability of the overlay coding in the context of multibeam satellite systems.

In addition to overlay coding, we have simulated the state-of-the-art four-color frequency mapping. Moreover, single user detection (SUD) is simulated, where no MUD technique is used in the full frequency reuse. This is to show how destructive is the interference at the point of evaluation and highlight the overlay coding gains as the cooperative NOMA scheme. We have used Mont Carlo method for the simulations. The achievability is simulated so that the channel code guarantees a FER not exceeding 10^{-4}. The physical layer frames with frame length of 64,800 symbols, in addition to DVB-S2x MODCOD are used.

Simulation results of spectral efficiency in overlay coding, four-color frequency mapping and SUD are provided in Figure 3.8 . Though the bandwidth in SUD is four times the four-color mapping, yet the system performance is degraded due to the aggressive interference imposed. However, the cooperative NOMA scheme by employing overlay coding overcomes the interference by using it as extra source of information, making benefit of the extra available bandwidth in the full frequency reuse scheme.

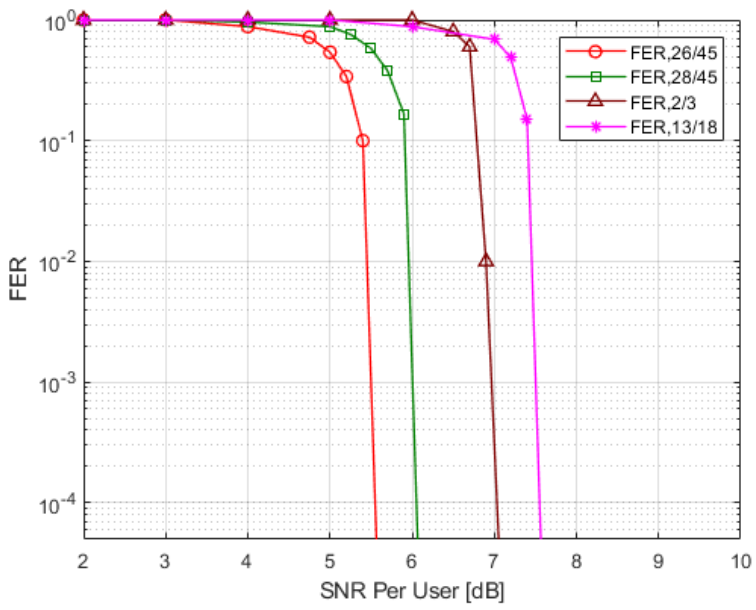

Figure 3.7 Data stream #2 error performance

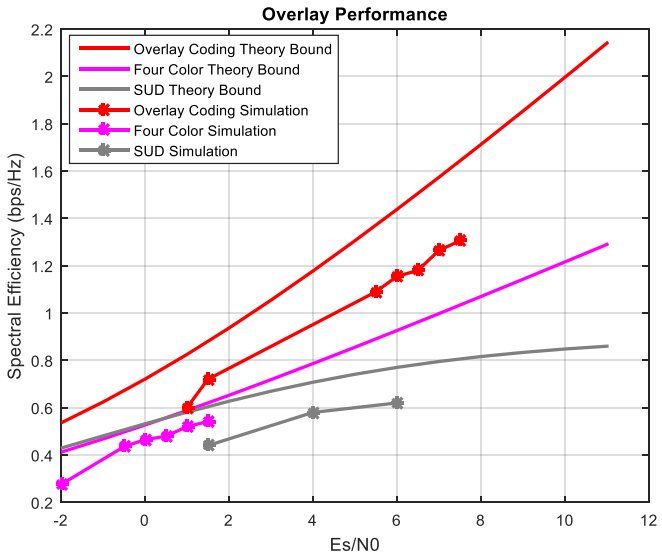

Figure 3.8 Overlay coding performance simulation results

3.5.2. Channel Estimation, Simulation results

In simulation results provided in Figure 3.8 , it is assumed that SNR and CIR values are accurately available at the user terminals; however, it is not possible in practice. Figure 3.9 shows the cumulative probability of the FER in overlay coding where the channel estimation inaccuracies are considered. The scenarios with SINR back-off ($\alpha = 0.05, 0.10$) and without SINR back-off ($\alpha = 0$) are simulated. When SINR back-off is not employed, the overlay coding performance degrades extremely as huge number of frames are discarded due to the decoding errors. However, by devising the back-off factor, the FER drops significantly which implies more reliable data transfer and increased data throughput. As expected, increasing the back-off factor reduces FER.

Figure 3.10 shows the cumulative probability of the aggregate data rate. Although the aggregate data rate is a bit less in cases with SINR back-off ($\alpha = 0.05,0.10$), it is more likely to achieve the overlay coding ultimate rate; whereas, in cases without SINR back-off ($\alpha = 0$), user terminals are more probable to experience a very low data rate. These results are in total consistency with Figure 3.9 ; as, without SINR back-off, most data frames will be discarded resulting in many user terminals experiencing unreliable connections with low data throughput. This degrades the overlay performance down to the SUD level, see Figure 3.8 . However, by employing the SINR back-off, the number of discarded frames drops, resulting in many users benefiting from the promised overlay coding reliable connections with higher data throughput.

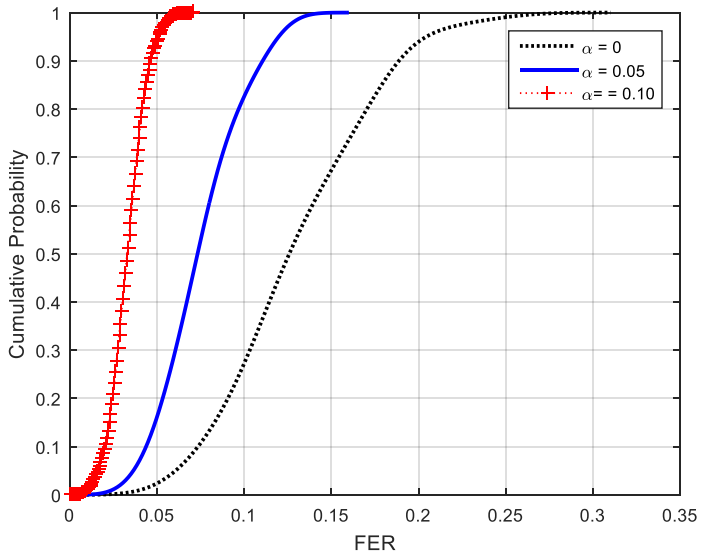

Figure 3.9 Cumulative Probability of Frame Error Rate

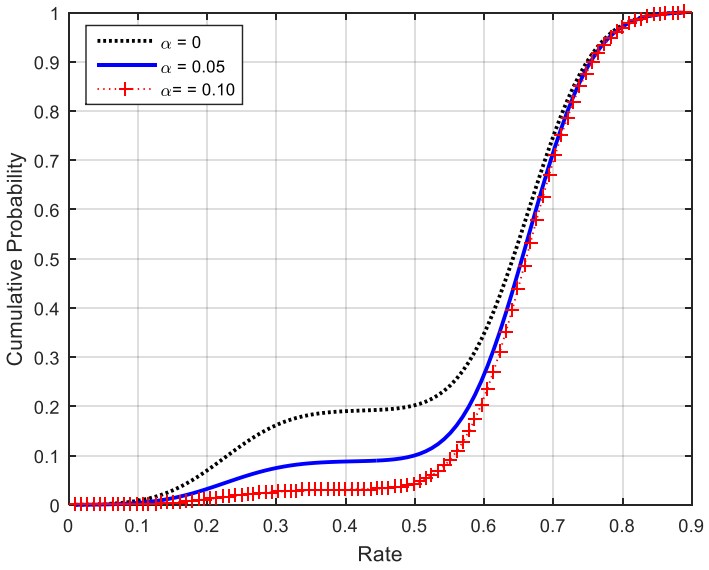

Figure 3.10 Cumulative probability of aggregate user throughput

3.6. Discussion

In this chapter, the applicability of overlay coding method as the cooperative NOMA scheme was investigated in forward link of the wireless communication systems, with an aggressive frequency reuse. The overlay coding in addition to a new optimized user-pairing approach were analyzed. Performance results were compared with the state-of-the-art, i.e. four-color mapping.

Our results show that the optimized overlay coding will considerably increase the spectral efficiency. As overlay coding is based on successive interference cancellation, the residual errors in SIC degrade the performance severely. The effect of residual errors caused by the channel estimation errors were investigated, which result in decoding errors and unreliability of the connection. We devised channel estimation algorithms and simulated the effect of possible inaccuracies in the performance of the proposed overlay coding. In this regard, we used SNIR back-off algorithm to decrease the errors in rate allocation and consequently to mitigate the impact of channel estimation errors. The simulation results show that a huge drop in FER is achieved with almost the same data throughput as the cases with perfect channel estimation.

Chapter 4

Cooperative Source and Channel Coding in Asynchronous NOMA

4.1. Introduction

The applications with massive connectivity are expected to emerge along with the deployment of the internet-of-things (IoT) in the next generations of the wireless communications. This brings about many challenges concerning the reliability, latency, as well as spectral and energy efficiency [108]. The complications aggravate due to the sporadic nature of the traffic generated by such large-scale and low-powered networks over limited spectrum resources. In these applications the overhead for synchronization and control functions is comparable to the data size, hence the control/data ratio is very unfavorable.

In this chapter, we consider the compute-and-forward technique for the transmission of the sensed data in the uplink of IoT networks. We investigate the techniques to take advantage of the fact that transmitters are privy to whole data in order to boost the spectral and power efficiency, while increasing the reliability. We consider a dense sensor IoT network, the sensor nodes observe a correlated field and transmit their observations, which are data with correlated sources. Due to the highly correlated sources, the terminals would send messages with many similarities, and so what we are proposing is arranging the messages into an agreed order. We propose that instead of assigning a separate channel to each terminal, they cooperatively share and transmit over the same

uplink channel. This approach can also be regarded as in wireless network coding where the terminals transmit as members of a cooperative network. Likewise, their a priori data is used at the receiver to recover data cooperatively.

In an example, the application of unmanned aerial vehicles (UAV)-assisted sensing networks are expected to emerge widely along with the next generations of the communication systems [107][108]. Multi-UAV networks functioning as distributed sensing platforms have been proposed in civilian applications such as multi-model sensing and traffic monitoring as part of smart city applications. Emergency communication is another use-case including search-and-rescue or detection and localization schemes in wild or out of reach areas in the disaster surveillance [109][110].

In particular, the video traffic captured by UAVs poses an extensive load on the wireless connections due to data rate demands of up to tens of Gb/s [106]. This brings about many challenges concerning the reliability, latency, as well as spectral and power efficiency in realization of the multi-UAV networks. The complications aggravate specifically when dealing with the traffic generated by large-scale swarms of limited-energy UAVs. Considering different design objectives, the challenges have been extensively investigated in the related literature. Store-carry-and-transmission [111], hover-and-fly [112], sense-and-send [113], and multi-hop device-to-device [114] are some of the proposed solutions for enhancing the data acquisition throughput, delay, and coverage.

There exists abundant literature on UAV-assisted traffic monitoring and corresponding processing systems [115][119]. Considering the UAV-to-UAV communication, the captured images and videos can be shared through a high-rate and low-latency communication, e.g., Terahertz band [19][105]. The UAVs use the shared data to create a satellite view of the surrounding traffic [106], which is then transmitted to the uplink access point to be used for real-time monitoring and localization purposes.

We propose our novel scheme based on identical content transmission over NOMA for transmitters with correlated sources, who cooperatively combine and transmit identical messages over consecutive data packets. Our proposed redundant transmission of data is not as straightforward as it seems, considering the asynchronous reception of the data streams at the receiver. Traditionally, it is believed that the substantial spectral efficiency achievements in

NOMA could be jeopardized in the asynchronous channels. In contrast to the previous works on NOMA with strict synchronous assumptions, we consider the asynchronous reception of the data streams at the receiver. We show that the NOMA channel capacity erodes rapidly due to the Inter-Symbol Interference (ISI) caused by the asynchronous channel.

Despite the performance degradation in asynchronous NOMA, we prove that by having the terminals to combine and transmit the identical content over the NOMA given that the proper receiver is employed, the spectral and power efficiency as well as reliability are improved. We investigate the potency of successive interference cancellation (SIC), as the main block in current NOMA receivers, in asynchronous channels. By applying water-filling and geometric power allocation, we show that the spectral efficiency degradation is caused by the nature of SIC.

Moreover, we demonstrate that the spectral efficiency is improved in asynchronous NOMA by managing the channel's memory and correlation instead of cancelling it. In addition, we propose our iterative joint detection and decoding (IJDD) receiver to outperform SIC in asynchronous NOMA receivers. Our extensive simulations show that our proposed scheme can outperform NOMA by providing a considerable boost in the channel reliability while increasing the spectral and power efficiency.

Our proposed scheme yields to a much higher reliability by reducing the outage probability and the block error rate (BLER). Hence, instead of sending transmitters' data independently and devising automatic repeat request (ARQ) [11] due to the packet loss, we propose avoiding the retransmission by combining and sending the same data at the transmitters with correlated data to boost the reliability even at the lower signal to noise ratios (SNR).

Regarding the energy efficiency, our simulation results show that the power conservation obtained by our proposed scheme is to the extent of one-fifth of the initial power. This implies achieving the proposed reliability and spectral efficiency at much lower SNR while compensating for the inter-terminal background cooperation. We have assumed a low-energy high-rate communication scheme for the inter-terminal cooperation, which we have optimized considering the trade-off between the allocated time and power to the inter-terminal communications.

As for the receiver, we have proposed an iterative joint detection and decoding (IJDD) receiver that achieves significant performance with average number of 1.6 iterations in a two-user system; where, there is no need for redundant coding or spreading at the transmitter. This is in contrary to

the SIC receivers, as the data streams are detected in succession and cancelled from the aggregate received signal; hence, the SIC receiver goes through at least two iterations in a two-user system, requiring spreading, coding, or power-differences in the NOMA channel to accomplish the detection. The fewer number of iterations in our proposed IJDD, in addition to no requirement for coding or spreading, results in lower latency and higher spectral efficiency.

In this chapter, we show that although NOMA performance with SIC gets degraded even with slight time misalignments at the reception, our proposed scheme has better performance by taking advantage of the asynchronous channel's extra memory and correlation.

This chapter is organized as follows. The system model is provided in Section (4.2). Extending the works studied in Sections (2.3) and (2.4), we discuss the main scenarios that are investigated in this chapter as well as our proposed scheme in Section (4.3). We demonstrate the tradeoffs that are faced in achieving the optimal spectral efficiency by our scheme and their optimization in Section (4.4), followed by Section (4.5) where we investigate our proposed receiver. Simulations compare our proposed scheme with other scenarios in section (4.6), confirming the theoretical results that are concluded in Section (4.7).

4.2. System Model

The system model includes a group of sensors involved in a measurement scheme, where they encounter a change and wish to transfer their observation to the common uplink access point. It is desired to transmit the aggregation of the huge volume of the sensed data promptly and with the least amount of power consumption. We consider the uplink channel, where single-antenna sensors and single-antenna access point are considered. Each resource is considered to be used only by two users in a NOMA framework, where the case with more users will be considered in the next chapters. It is assumed that ideal channel state is available at the receiver, where the schemes with channel estimation error are considered in the next chapter.

We have proposed our scheme for scenarios where the engaged users have correlated sources and that they are willing to cooperatively combine and send the identical content over the channel. Otherwise, if no correlation or cooperation exists between the transmitters, there is no efficiency in our proposed scheme compared to NOMA. The terminals' cooperation in combining their data

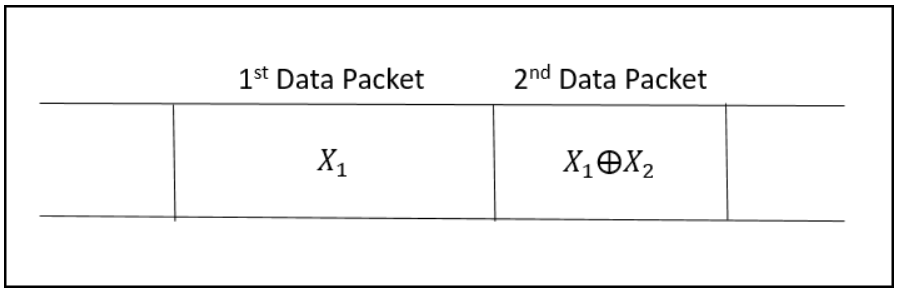

Figure 4.1 Identical transmission data packets

and transmitting identical content over the NOMA channel in a two-user model is accomplished in two successive data packets.

Based on the Slepian-Wolf theorem in (2-4), the distributed source coding rate can be written as $H(U) + H(V|U)$, where the former is the entropy of source U and the latter is the entropy of the discrepancies between sources (U, V). The transmission data packets are typically shown in Figure 4.1. Without loss of generality, X_1 is the source-coded input data corresponding to the first transmitting sensor equipment, and $X_1 \oplus X_2$ is the discrepancies between the source-coded input data corresponding to the first and second sensor equipment, where $\oplus$ denotes the XOR.

As for the effect of distributed source coding on the channel capacity, we define sources' correlation as $\{\gamma : |\gamma| \in [0,1]\}$, which is basically the rate of deviation of the conditional entropy of the sources from the common part's entropy, that can be shown as

$$\frac{H(V|U)}{H(U)} = 1 - \gamma \tag{4-1}$$

In particular, we are interested in systems with highly correlated sources, i.e. $H(V|U) \ll 1$, which implies that γ is very close to one. Considering γ as the sources' correlation rate and assuming the transmit block to be N bits long, the intuition behind Figure 4.1 is as follows. The two data packets may include: first data packet including User 1 data with N information bits, i.e. X_1; and, the second data packet including only the two users' data discrepancies, with $N(1-\gamma)$ information bits, i.e. $X_1 \oplus X_2$.

This implies that our proposed scheme uses the channel additionally to transmit the extra $N(1-\gamma)$ bits in the second data packet. This will definitely affect the channel's capacity as we transfer

$N + N(1-\gamma) = (2-\gamma)N$ total bits per transmission. So, we model the channel getting degraded with a degradation factor equal to

$$\chi = \frac{1}{2-\gamma} \tag{4-2}$$

This degradation factor is considered later in this chapter in evaluating the spectral efficiency.

Asynchronous Channel Model. We consider a main IoT terminal T_1 transmitting over uplink channel. Terminal T_2 is a close-by terminal sharing the channel with T_1, i.e. sending at the same time, frequency and coding, as in NOMA scheme.

The code-bits of both users are BPSK symbol mapped. Considering $s_i(t)$ as the coded-modulated symbol of user terminal i, with average power equal to one, i.e. $E[|s_i(t)|^2] = 1$, T_s as the symbol time, the transmitted code-word as $\{b_i(1), \dots, b_i(k)\}$, and the transmitted amplitude as A_i, the transmitted signal vector can be written as

$$x_i(t) = \sum_{k=1}^{n} b_i(k) A_i(k) s_i(t - kT_s)\,, i = 1,2 \tag{4-3}$$

The channel is modeled as an asynchronous Rayleigh-fading multiple access with additive white Gaussian noise (AWGN). Each user's signal is delayed with an independent delay, $0 \le \tau_i \le T_s$, during the transmission. Hence, for the two-user scheme, the received signal at the base station is the sum of contributions from both users plus noise, i.e.

$$y(t) = h_1 x_1(t - \tau_1) + h_2 x_2(t - \tau_2) + n(t) \tag{4-4}$$

where, h_i is the independent and identically distributed (iid) channel coefficient that is circularly symmetric complex normal with Rayleigh magnitude and uniformly distributed phase, and $n(t)$ is the complex AWGN, $n \sim N(0, \sigma_n^2)$.

4.3. Scenarios

In this section, we investigate three main scenarios in the information theoretical framework. First, we evaluate the NOMA channels with ISI based on having SIC at the receiver, where the results can be applied in the asynchronous NOMA channels. This is to emphasize that how cancelling the channel's correlation by SIC in an asynchronous channel degrades the spectral efficiency. Then, we demonstrate how the asynchronous NOMA channel's spectral efficiency is

improved by taking advantage of the channel's correlation at the receiver. Finally, we review our proposed scheme and show how its capacity sum-rate outperforms both schemes.

4.3.1. Scenario I, Asynchronous Gaussian NOMA with SIC at the Receiver

The two-user Gaussian NOMA has a capacity region in the form of a pentagon, where the points at the edges are defined by the power spectral density (PSD) of the inputs, denoted in (2-3) as

$$C = \bigcup \begin{Bmatrix} (R_1, R_2), 0 \le R_i \le \frac{1}{4\pi}\int_{-\pi}^{\pi} \log\left(1 + \frac{S_i(w)}{\sigma^2}\right) dw \\ R_1 + R_2 \le \frac{1}{4\pi}\int_{-\pi}^{\pi} \log[1 + \frac{S_1(w)+S_2(w)}{\sigma^2}] dw \end{Bmatrix} \quad (4\text{-}5)$$

In asynchronous NOMA, as the symbols are overlapped by two preceding and succeeding symbols of the other sources, the channel changes to a channel with memory; hence, the optimal PSD could merely be realized if the interference from the other users is considered.

The capacity region in Gaussian MAC with ISI is studied in [32][33] that we briefly presented in Section (2.3). The weighted sum-rate model was used to characterize the point-by-point instances on the capacity region. For each point, the PSD of the inputs were jointly optimized through an iterative greedy algorithm and over a multiuser water-filling scheme.

The capacity region of the two-user Gaussian NOMA with and without ISI is provided in Figure 2.6, where SIC is used at the receiver. The methodology of SIC is based on cancelling and removing the interferences caused by channel's cross-correlations. Hence, as expected, the ISI degrades the single-user as well as the sum-rate capacity in a NOMA with SIC, as SIC cannot benefit from the asynchronous channel's cross-correlation.

4.3.2. Scenario II, Asynchronous Gaussian NOMA Benefiting the Correlation

Based on the results from the previous section, in a NOMA channel with SIC at the receiver, the asynchronous reception degrades the channel capacity by adding memory and correlation. In this section we show that this degradation is just due to the nature of the SIC at the receiver. As SIC recovers and subtracts signals in successions, it cannot benefit from the introduced correlation and memory in the asynchronous multiple access channels.

The capacity region in asynchronous Gaussian MAC is studied in detail in [32] that we briefly presented in Section (2.4). In computing the capacity region in Gaussian symbol-asynchronous NOMA, the channel is modelled as a channel with memory. The added cross-correlations are used

as favorable properties, and as a result, the sum-rate is improved compared to synchronous NOMA. Let the capacity region be as discussed in (2-30),

$$C = \cup \begin{Bmatrix} (R_1, R_2), 0 \le R_i \le \frac{1}{4\pi}\int_{-\pi}^{\pi} \log\left(1 + \frac{S_i(w)}{\sigma^2}\right) dw \\ R_1 + R_2 \le \frac{1}{4\pi}\int_{-\pi}^{\pi} \log[1 + \frac{S_1(w)}{\sigma^2} + \frac{S_2(w)}{\sigma^2} + \frac{S_1(w)S_2(w)}{\sigma^4}\left(1 - \rho^2(w)\right)]dw \end{Bmatrix} \quad (4\text{-}6)$$

where, the maximum sum-rate can be achieved for the time-offset equal to half the symbol time, i.e. $|\rho| = 0.5$. This would not be desirable in our scheme, as we consider the cooperative source and channel coding, and expect the delay-spread of the received signals to be close.

4.3.3. Scenario III, Identical Content Transmission over NOMA (ICToNOMA)

Here we investigate the capacity region in our proposed scheme which is based on cooperation of uplink nodes with correlated sources to combine and send identical data over the NOMA channel, denoted as ICToNOMA. Despite the cooperation between the transmitters, due to the practical issues, the two data streams will be received with imperfect symbol synchronicity or symbol asynchronous. In our proposed ICToNOMA, the terminals send the same data which have cooperatively shared through a background connection. This implies that $x_1(t - \tau_1)$ and $x_2(t - \tau_2)$ in (4-4) are dependent and correlated version of each other.

To calculate the power spectral density and further the channel's output entropy, the covariance of the received signal is calculated. In general, the covariance between K variables $\boldsymbol{X} = \{X_1, X_2, \dots, X_K\}$, is a $K \times K$ matrix $\boldsymbol{D}$ with diagonal entries equal to $d_{i,i} = \mathrm{var}(X_i)$, and, the ij-th entry equal to $d_{i,j} = \mathrm{cov}(X_i, X_j)$.

Based on Cauchy–Schwarz inequality, for two correlated variables, the covariance is

$$|\mathrm{cov}(X_i, X_j)| \le \sqrt{\mathrm{var}(X_i)\mathrm{var}(X_j)}$$

Considering the Fourier transform of the channel in (2-27), the channel could be equivalently written as

$$\boldsymbol{Y}[i] = \begin{bmatrix} 1 & \rho_{12} + \rho_{21}e^{-jw} \\ \rho_{12} + \rho_{21}e^{jw} & 1 \end{bmatrix} \boldsymbol{X}[i] + \boldsymbol{N}[i]$$

Hence, the covariance matrix of the received signal can be denoted as

$\mathrm{cov}(Y) \le$

$$\begin{bmatrix} 1 & \rho_{12}+\rho_{21}e^{-jw} \\ \rho_{12}+\rho_{21}e^{jw} & 1 \end{bmatrix}\left[\sigma^2 \boldsymbol{I}_2 + \begin{bmatrix} \mathrm{var}(X_1) & \sqrt{\mathrm{var}(X_1)}\sqrt{\mathrm{var}(X_2)} \\ \sqrt{\mathrm{var}(X_1)}\sqrt{\mathrm{var}(X_2)} & \mathrm{var}(X_2) \end{bmatrix}\begin{bmatrix} 1 & \rho_{12}+\rho_{21}e^{-jw} \\ \rho_{12}+\rho_{21}e^{jw} & 1 \end{bmatrix}\right] \tag{4-7}$$

where, I_2 is the identity matrix of size two.

Based on the information theory, the entropy of the received vector $Y = (Y_1, Y_2)$ is written as

$$h(Y_1, Y_2) = \frac{1}{2}\log(2\pi e)^2 \mathrm{cov}(Y) \tag{4-8}$$

The mutual information of the Gaussian channel is given by

$$I(X_1, X_2; Y) = \frac{1}{2}\log\det[\mathrm{cov}(Y)] - \frac{1}{2}\log\det\left[\sigma^2\begin{bmatrix} 1 & \rho \\ \rho & 1 \end{bmatrix}\right] \tag{4-9}$$

where, ρ is the asynchronous channel's cross-correlation defined in (2-25), as

$$\rho(w) \triangleq \sqrt{\rho_{12}^2 + \rho_{21}^2 + 2\rho_{12}\rho_{21}\cos(w)}, |\rho| \in [0,1] \tag{4-10}$$

After extensive calculation of the above equations, the achievable capacity region in ICToNOMA can be written as

$$C_{ICToNOMA} = \bigcup_{\substack{S_i(w)\geq 0, w\in[-\pi,\pi], i=1,2 \\ W_i=\frac{1}{2\pi}\int_0^{2\pi} S_i(w)dw}} \begin{Bmatrix} (R_1, R_2), 0 \leq R_i \leq \frac{1}{4\pi}\int_{-\pi}^{\pi}\log\left(1+\frac{S_i(w)}{\sigma^2}\right)dw \\ R_1 + R_2 \leq \frac{1}{4\pi}\int_{-\pi}^{\pi}\log[1+\frac{S_1(w)}{\sigma^2}+\frac{S_2(w)}{\sigma^2}+2\rho(w)\sqrt{\frac{S_1(w)S_2(w)}{\sigma^4}}]dw \end{Bmatrix} \tag{4-11}$$

where, $\{S_{\mathrm{i}}(w), w \in [-\pi, \pi]\}$ is the input i's power spectral density.

In the provided spectral efficiency in ICToNOMA, the single-user capacity has not changed from the synchronous NOMA as described in (4-5). However, there is a linear relation with the asynchronous channel's cross-correlation in the sum-rate which is an extra term compared with synchronous NOMA. The extra term in our proposed scheme is due to the cooperative source and channel coding, which brings about sum-rates more than synchronous NOMA.

4.4. ICToNOMA Optimization

Based on the achieved sum-rate capacity for our proposed ICToNOMA scheme, in this section we investigate the effect of asynchronous channel's cross-correlation and the source's correlation on optimizing the spectral and power efficiency.

4.4.1. Asynchronous Channel's Cross-Correlation

We show that there is a trade-off between the asynchronous channel's cross-correlation and the achieved sum-rate. To evaluate ICToNOMA, we compare the sum-rate with synchronous NOMA along with the sum-rate in asynchronous NOMA as discussed in Scenario II.

The asynchronous NOMA in Scenario II is based on employing and benefiting from the asynchronous channel's cross-correlations, where non-cooperative source and channel coding is considered. The maximum sum rate is achieved for time offset $\tau = \tau_2 - \tau_1 = 0.5T_s$, i.e. $|\rho| = 0.5$. As ρ increases and gets closer to one which implies the smaller time offsets, i.e. $\tau \ll T_s$, the sum rate capacity declines as provided in (4-6). This is not desirable in applications with cooperative transmissions with small time offsets.

On the contrary, ICToNOMA achieves higher sum rates as the two data streams get their timing closer, i.e. get more correlated. In an example, though it's not applicable in practice, for $|\rho| = 1$, the sum-rate substantially increases similar to the channels with coherent reception of the two data streams which is equal to $C = R_1 + R_2 \leq \frac{1}{4\pi}\int_{-\pi}^{\pi} \log\left(1 + \frac{\left(\sqrt{S_1(w)}+\sqrt{S_2(w)}\right)^2}{\sigma^2}\right) dw$.

The impact of the channel's cross-correlation is depicted in Figure 4.2 , which shows the capacity region for asynchronous NOMA and asynchronous ICToNOMA for different values of $|\rho|$. The synchronous NOMA is also provided as the benchmark and for the comparison purposes. In Figure 4.2, the similar SNR equal to 5dB is assumed for the data streams. As $|\rho|$ gets closer to one, ICToNOMA performance gets better compared to asynchronous NOMA. In fact, asynchronous NOMA gets closer to synchronous NOMA as ρ increases.

4.4.2. Optimization of the Asynchronous Channel's Cross-Correlation

Following the analysis in the previous section, here we find the optimal asynchronous channel's cross-correlation such that the asynchronous ICToNOMA outperforms asynchronous NOMA. For comparison purposes, we assume constant cross-correlation and PSD throughout the investigated bandwidth. The sum-rates in asynchronous ICToNOMA and asynchronous NOMA are the basis of the calculations that are defined in Equations (4-11) and (4-6), respectively.

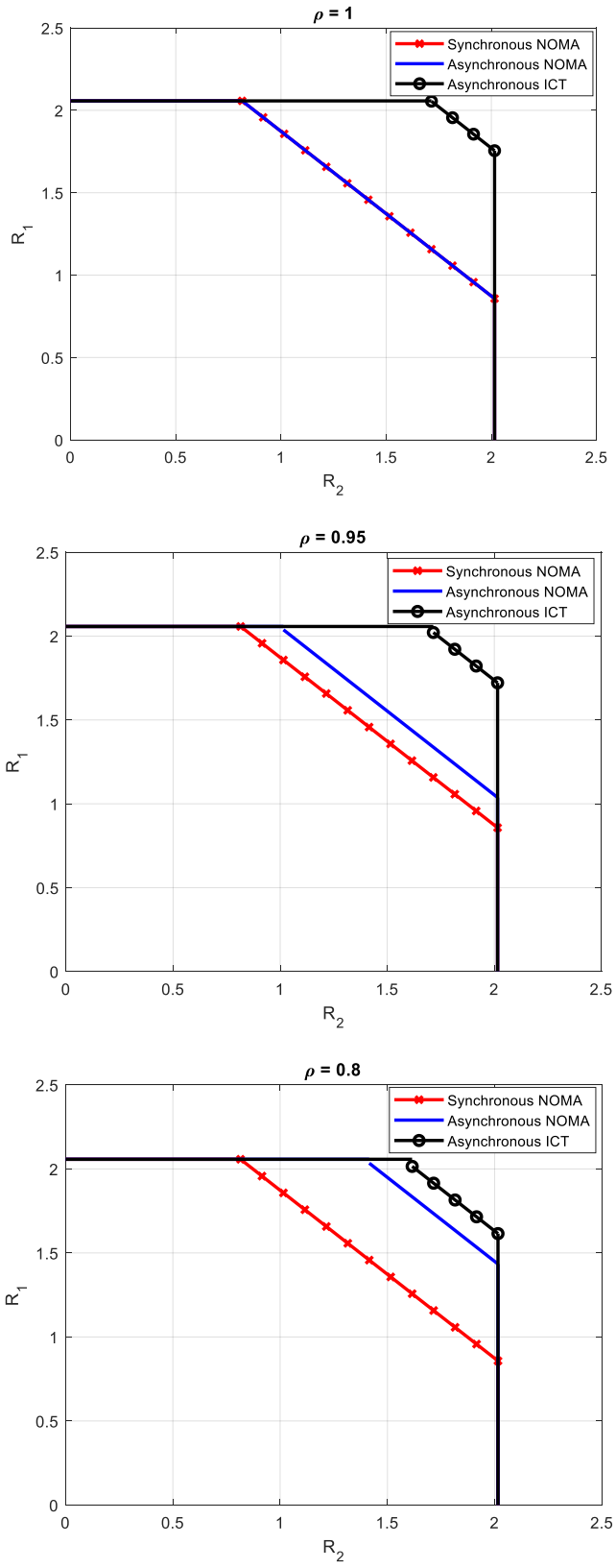

Figure 4.2 Asynchronous Gaussian multiple access channel capacity region analysis

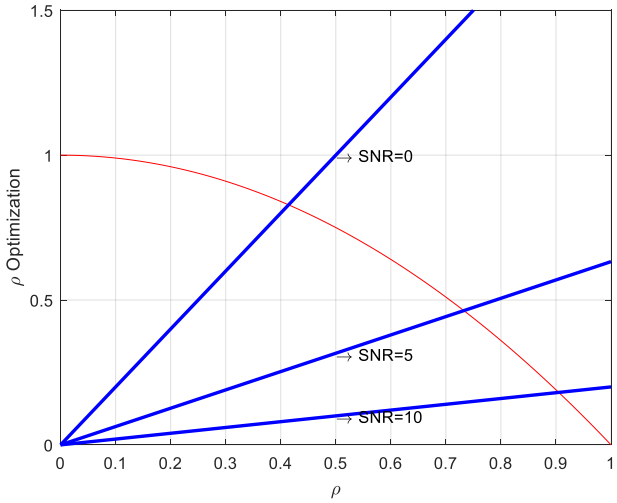

Figure 4.3 Optimal asynchronous channels' cross-correlation calculation for different SNR

With some calculations, the optimal asynchronous channel's cross-correlation for ICToNOMA can be shown as

$$\arg\max_{\rho_{opt}} C_{ICToNOMA} = \left\{ \rho_{opt} \left| \frac{2\rho_{opt}}{\sqrt{SNR_1}\sqrt{SNR_2}} \geq 1 - \rho_{opt}^2 \right. \right\} \tag{4-12}$$

Where, SNR_i is the received SNR values of the i-th data stream, defined as

$$SNR_i(w) = S_i(w)/N_i(w)$$

We have evaluated the optimal ρ_{opt} numerically, where Figure 4.3 shows some instances for different SNR values. In this figure, the received SNR of both data streams are assumed to be equal for better intuition. The lines indicate the left side of (4-12) inequality for different SNR values, where the curve shows the right side of (4-12) inequality. Hence, for each SNR we can find the optimal cross correlation for which the ICToNOMA performs better than NOMA; e.g. in SNR = 5dB for $|\rho| \geq 0.74$ ICToNOMA outperforms NOMA. Clearly, our proposed ICToNOMA achieves higher spectral efficiency compared to NOMA for asynchronous channel's cross-correlation closer to one, which is the case in our proposed system.

4.4.3. Optimization of the Correlation of the Sources

As discussed earlier, the length of the second data packet has a degrading effect on the spectral efficiency equal to the degradation factor, see (4-2). In order to find the optimized sources' correlation, we are interested in finding the correlation values for which the spectral efficiency in

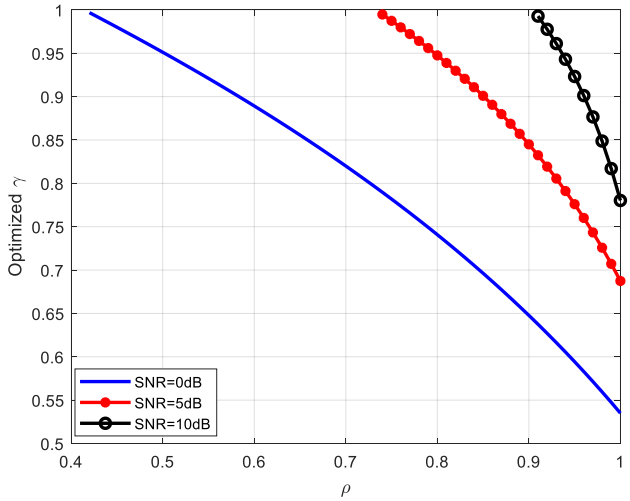

Figure 4.4 Optimized sources' correlation vs. ρ for different SNR

ICToNOMA outperforms NOMA. For comparison purposes, we assume constant asynchronous channel's cross-correlation and PSD throughout the investigation bandwidth. With some calculations, the optimal sources' correlation can be shown as

$$\arg\max_{\gamma_{opt}} C_{ICToNOMA} = \left\{ \gamma_{opt} \middle| \gamma_{opt} \geq 2 - \frac{\log\left(1+\sqrt{SNR_1}+\sqrt{SNR_2}+2\rho\sqrt{SNR_1}\sqrt{SNR_2}_1\right)}{\log\left(1+\sqrt{SNR_1}+\sqrt{SNR_2}+SNR_1SNR_2(1-\rho^2)\right)} \right\} \quad (4\text{-}13)$$

The inequality in (4-13) is relatively associated with the results in (4-12). The optimized ρ_{opt} that was already evaluated in previous section also maximizes the second term in (4-13), implying the minimum for γ_{opt}.

We have examined the γ_{opt} optimization numerically, where Figure 4.4 shows the optimized sources' correlation based on the asynchronous channel's cross-correlation for some different SNR values. In this figure, both data streams are assumed to have equal average SNR for the purpose of comparison. As a reminder from Figure 4.3, at SNR = 5dB ICToNOMA outperforms NOMA for $|\rho| \geq 0.74$. Figure 4.4 seconds this and shows that for instance if we have $|\rho| = 0.95$ at SNR = 5dB, the sources' correlations should be more than $\gamma \geq 0.78$. Clearly, ICToNOMA achieves higher spectral efficiency for sources' correlation closer to one, which is the case in our proposed system. It is confirmed in Figure 4.4 as well, as $|\gamma| > 0.5$ is achieved in all examined SNR values.

4.4.4. Inter-Terminal Communication

In this section we investigate the inter-terminal communication proposed in ICToNOMA. We assume close-by terminals in a dense IoT system. The communication is modeled in a time division scheme, in which a t_1 fraction of the time is allocated to the inter-terminal communication. It is assumed that the allocated time to the inter-terminal communication, i.e. t_1, is divided equally among the two terminals, so that when a terminal transmits, the other only listens. This background communication is performed by a low-power means of communication, and it is in parallel and simultaneous with the channel transmission so that it would not cause any burden or extra delay to the system. Regarding the power consumption, we assume each user has a constant total transmit power P_T, from which the power P_{uv} is allocated to the active user transmitting in the inter-terminal communication. Information theoretic analysis is used to evaluate the optimal values of t_1 and P_{uv}, for which we have followed the approach in [16].

Based on Slepian-Wolf theorem as depicted in (2-4), it is only required to jointly share the information corresponding to the conditional entropy of the two sources, i.e. $H(V|U)$. Considering the source-channel coding theorem, the information transfer between the terminals is achievable if the entropy corresponding to the source coding rate is lower than or equal to the channel capacity. Moreover, considering the cooperative source and channel coding for the correlated sources in a MAC, as discussed in Section 2.2, the inequality between the source-coding and channel-coding rates for the inter-terminal connection can be expressed as

$$H(V|U) \leq \left(\frac{t_1}{2}\right)\frac{1}{2}\log(1+\frac{P_{uv}}{\sigma_{uv}^2}) \tag{4-14}$$

Where, the P_{uv}/σ_{uv}^2 implies the SNR in the inter-terminal connection. The capacity in inequality (4-14) has the factor $t_1/2$ to include the time that is allocated to each terminal during the background communication. So, the power required for inter-terminal communication is

$$P_{uv} \geq \sigma_{uv}^2\left(2^{\frac{4H(V|U)}{t_1}}-1\right) \tag{4-15}$$

Furthermore, the source and channel coding inequality for the terminal-to-access point MAC channel can be written as

$$1+H(V|U) \leq \frac{1}{2}t_1\log(1+\frac{2(1+\rho)(P_T-P_{uv})}{\sigma_T^2})+\frac{1}{2}(1-t_1)\log(1+\frac{2(1+\rho)P_T}{\sigma_T^2}) \tag{4-16}$$

The right side in inequality (4-16) represents the channel capacity while allocating P_{uv} to the inter-terminal communication for a t_1 fraction of time, where P_T/σ_T^2 implies the terminal-to-access point SNR. In order to calculate the optimal t_1^* that maximizes the channel capacity, we have calculated the derivative of the inequality with respect to t_1 and equal it to zero which results in

$$\log(1-\frac{2(1+\rho)P_{uv}}{\sigma_T^2+2(1+\rho)P_T})+2^{\frac{4H(V|U)}{t_1}}\left(\frac{4\sigma_{uv}^2(1+\rho)H(V|U)}{t_1\left(\sigma_T^2+2(1+\rho)(P_{T-P_{uv}})\right)}\right)=0 \qquad (4\text{-}17)$$

We have evaluated this optimization problem numerically by substituting P_{uv} from (4-15). Based on the preceding optimization constraints, $|\rho|=0.9$, SNR = 5dB, and the sources' correlation $\gamma=0.85$ are assumed. As the two terminals are close-by, it is assumed that $\sigma_{uv}^2/\sigma_T^2 \ll 1$. So, considering $\sigma_{uv}^2/\sigma_T^2=0.1$, the numerical calculations results in $t_1^*=0.84$, $P_{uv}^* \leq 0.02P_T$.

The results imply that due to the highly correlated sources, the background inter-terminal communication can be performed with a very low fraction of the initial power, i.e. less than two percent. This is a very interesting finding that confirms the feasibility of our proposed ICToNOMA. Moreover, the performance of the system while scaling down the terminals' power is simulated, and results are provided in Section 4.6. The results indicate that ICToNOMA outperforms NOMA even with each user's power reduced to half and one-fourth of its initial power, which compensates for the power in inter-terminal communication.

4.5. Iterative Joint Detection and Decoding (IJDD) Receiver

We have already shown that the approach for the receiver based on SIC degrades the spectral efficiency in case of asynchronous uplink channel in NOMA, in the sense that SIC cannot benefit from the asynchronous channel's cross-correlation, see Section 2.3. In this section we propose our iterative joint detection and decoding (IJDD) receiver to benefit from the cross-correlation of the asynchronous channel as extra information in asynchronous uplink NOMA. The iterative joint detection and decoding (IJDD) receiver is investigated in detail by Wang and Poor in [35], that was considered for the channels that are strictly synchronous, see section 2.5.

We have revised the synchronous IJDD receiver in order to accommodate our asynchronous NOMA channel, where the LDPC is used as the error correcting code.

The joint detector is the main block in our receiver which detects the multiuser data based on the correlated received signal. Based on the transmit signal definition in (4-3), the received signal can be equivalently written in discrete time as

$$\boldsymbol{Y}[i] = \boldsymbol{RAb}[i] + \sigma \boldsymbol{N}[i] \tag{4-18}$$

where, $\boldsymbol{R}$ presents the channel matrix, $\boldsymbol{A}$ is the diagonal magnitude matrix, $\boldsymbol{b}[i]$ is vector of the code-bits, where the code-bits are assumed to be BPSK symbol mapped. $\boldsymbol{N}[i]$ is the noise vector. Though the vectors and matrices in (4-18) are supposed to have an order of two for a two-user multiple access channel, this is not the same in the asynchronous mode.

In our proposed IJDD, due to the channel having memory, each symbol at the output as well as the vectors and matrices, have the dimension four, denoted as

$$\begin{bmatrix} y_1(i) \\ y_2(i) \\ y_1(i+1) \\ y_2(i+1) \end{bmatrix} = \boldsymbol{R}_A . \begin{bmatrix} A_1 & 0 & 0 & 0 \\ 0 & A_2 & 0 & 0 \\ 0 & 0 & A_1 & 0 \\ 0 & 0 & 0 & A_2 \end{bmatrix} \begin{bmatrix} b_1(i) \\ b_2(i) \\ b_1(i+1) \\ b_2(i+1) \end{bmatrix} + \begin{bmatrix} n_1(i) \\ n_2(i) \\ n_1(i+1) \\ n_2(i+1) \end{bmatrix} \tag{4-19}$$

We have defined $\boldsymbol{R}_A$ to denote the asynchronous representation of matrix $\boldsymbol{R}$ as

$$\boldsymbol{R}_A \triangleq \begin{bmatrix} [\boldsymbol{R}]_{11}(i) & [\boldsymbol{R}]_{12}(i).\rho_{12} & 0 & 0 \\ [\boldsymbol{R}]_{21}(i).\rho_{12} & [\boldsymbol{R}]_{22}(i) & [\boldsymbol{R}]_{21}(i+1).\rho_{21} & 0 \\ 0 & [\boldsymbol{R}]_{12}(i).\rho_{21} & [\boldsymbol{R}]_{11}(i+1) & [\boldsymbol{R}]_{12}(i+1).\rho_{12} \\ 0 & 0 & [\boldsymbol{R}]_{21}(i+1).\rho_{12} & [\boldsymbol{R}]_{22}(i+1) \end{bmatrix} \tag{4-20}$$

In our proposed asynchronous channel matrix, not only the channel matrix is extended, but also the asynchronous channels' correlations, i.e. ρ_{ij}, along with the synchronous channel coefficients, i.e. $[\boldsymbol{R}]_{ij}$, are included.

It is worth mentioning that the proposed IJDD receiver has a complexity of order $O(2^K)$ with large number of users, K. The study on a simpler receiver is accomplished in next chapter.

Table 4-1, Simulation Assumptions

Channel Model	Rayleigh Fading
Modulation Format	BPSK
Error Control Coding	LDPC rate 1/6
Transport Block Size (BPS)	120-Bytes
Antenna Configuration	SISO, 1Tx, 1 Rx
Average Receiver SNR	Equal average SNR
Target BLER	10^{-5}
Receiver Type	IJDD in our proposed scheme SIC for the state-of-the-art systems

4.6. Simulation Results

In this section, the simulation results are provided. The two-user uplink NOMA with BPSK modulation, LDPC code with irregular lower-triangular parity check matrix with rate 1/6 and 120-Byte transport block size (TBS) are considered. The users are assumed to have the equal average SNR, which is the worst-case scenario as they cause the highest interference on each other. The channel is modeled as an asynchronous Rayleigh-fading multiple access channel with AWGN. We have simulated the three scenarios discussed in Section 4.3. In our simulations, no spreading or extra coding is used in the proposed NOMA scenarios, which we denote as uncoded.

The simulation results are provided for both synchronous, i.e. $\tau = 0$, and asynchronous receptions, i.e. $\tau = \alpha T_s$ for $\alpha \in (0,1)$. The asynchronous channel's cross-correlation can be defined based on the delay offset as $|\rho| = (T_s - \tau)/T_s$

Moreover, the trade-off between asynchronous channel's cross-correlation and sources' correlation with the spectral efficiency in ICToNOMA are investigated. The Monte Carlo method is used in simulations. The achievability is simulated so that the channel guarantees a Block Error Rate (BLER) not exceeding 10^{-5}, which is the target BLER based on 3GPP standard [24]. The simulation assumptions are briefly provided in Table 4-1.

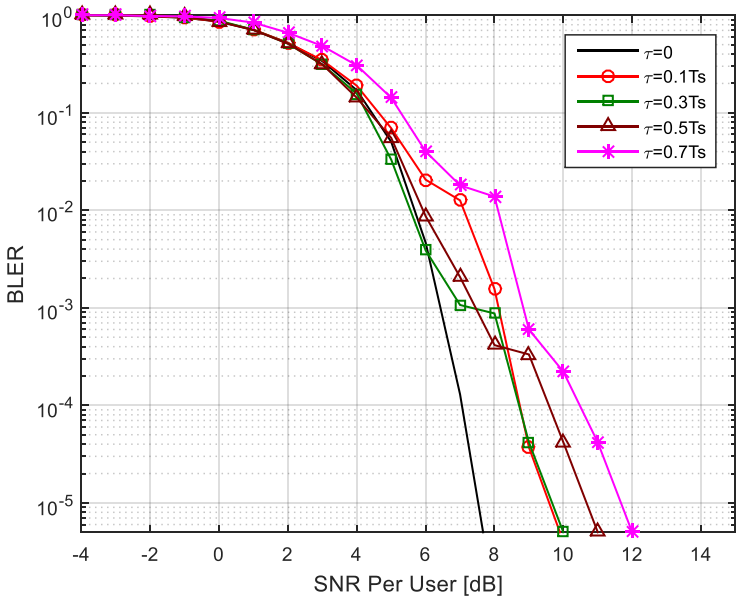

Figure 4.5 Performance of asynchronous NOMA with SIC at the receiver

4.6.1. Asynchronous NOMA with SIC Receiver (NOMA-SIC)

We have investigated the performance of NOMA with SIC at the receiver. The performance is expected to degrade as the asynchronous channel acts as the channel with memory for the SIC receiver. The SIC receiver cannot process the added correlation as it recovers and cancels off the decoded data streams one at a time. In Figure 4.5 , it is shown that as the delay increases, the performance is degraded more, where at the BLER=10^{-5}, there is more than 4dB degradation for the reception with $0.7T_s$ delay compared to synchronous reception.

Moreover, it is observed that except for the synchronous reception, the result plots of the different delay values have a knee in the corresponding BLER performance. This is due to the fact that the ISI caused by the asynchronous reception of the data streams grows slower than the power and that results in the knee in the diagram.

4.6.2. Asynchronous NOMA with IJDD Receiver (NOMA-IJDD)

Figure 4.6 shows the simulation results for the NOMA with IJDD at the receiver. As expected, as the delay gets closer to $0.5T_s$, the IJDD performance improves. It is a great achievement; yet, it is not beneficial in our proposed scheme, as we assume the data streams to be received with just slight time differences.

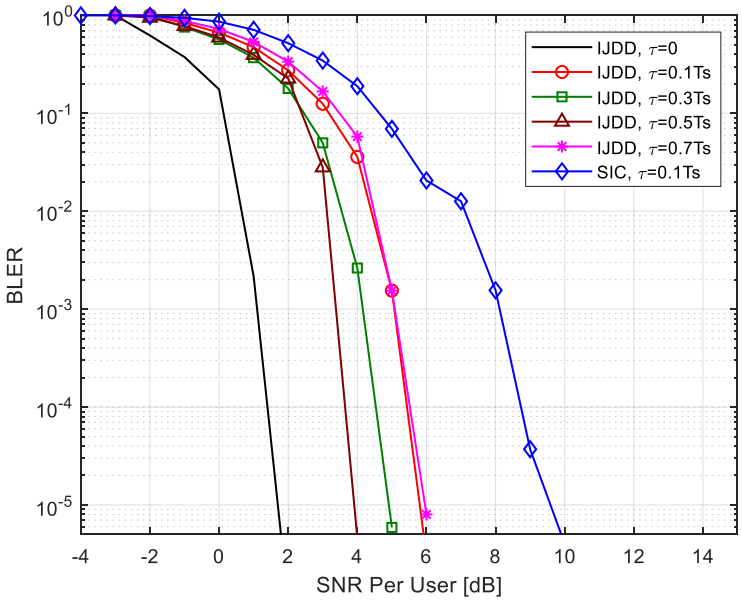

Figure 4.6 Performance of asynchronous NOMA with IJDD at the receiver

For comparison purposes, the BLER for NOMA-SIC at $\tau = 0.1T_s$ is also provided. It is observed that an almost 4dB performance is achieved by NOMA-IJDD, at $\tau = 0.1T_s$ and BLER = 10^{-5}. This shows the effectiveness of our proposed IJDD receiver in asynchronous channels.

In this scenario, another interesting outcome is the synchronous performance that is significantly improved compared to the similar system with the SIC at the receiver. The reason for the more than 6dB improvement at BLER=10^{-5} is the fact that no spreading or coding scheme is used in the proposed scenarios. Also, since the equal average SNR is assumed for the two data streams, the two signals are severely correlated even in the synchronous reception. This correlation degrades the SIC receiver drastically, while serving the IJDD receiver as supplementary source of information. So, the iterative joint detection and decoding at the receiver is outperforming the SIC receiver even without any needs to coding/signature redundancy or power differences as proposed in code and power-domain NOMA, respectively.

4.6.3. Asynchronous ICToNOMA Performance

We investigate the performance of our proposed ICToNOMA in the existence of asynchronous reception with IJDD at the receiver. The simulation results for both synchronous and asynchronous receptions are provided in Figure 4.7 . Although our proposition is optimal for the cooperative

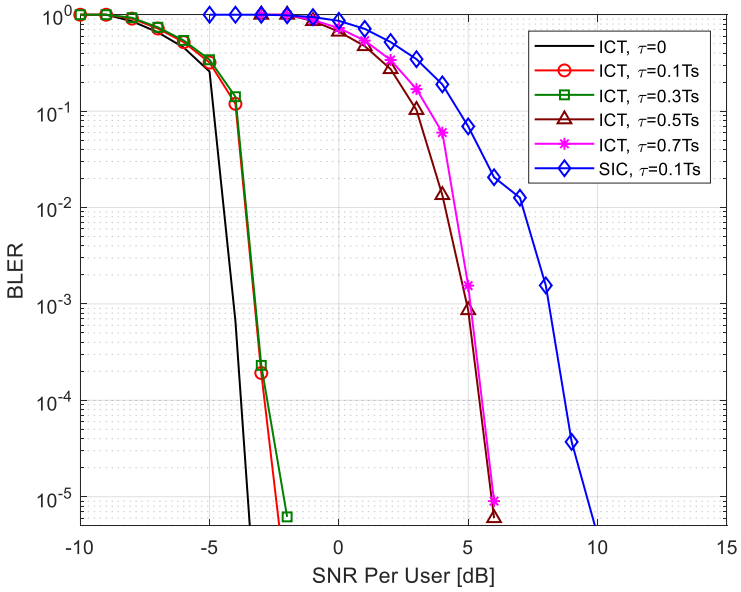

Figure 4.7 Performance of asynchronous ICToNOMA with IJDD at the receiver

uplink NOMA with slight time offsets at the receiver, we have simulated different values of delay for the comparison purposes. Also, for better contrast, the NOMA-SIC result at $\tau = 0.1T_s$ is provided.

For $0 < \tau < 0.5T_s$, more than 12dB and 8dB performance at BLER=10^{-5} is achieved in comparison with asynchronous NOMA-SIC and NOMA-IJDD, respectively. This is more obvious in Figure 4.8 which includes all proposed scenarios in synchronous and asynchronous channels with delay $\tau = 0.1T_s$ and $0.3T_s$. The great performance is due to sending identical content from the transmitters, that augments the channel's correlation or in other words feeds the IJDD receiver with supplementary information. Also, as the two signals are added through the channel, this improves the received power that allows the ICToNOMA's better performance even in lower SNRs.

As for $\tau \geq 0.5T_s$, i.e. $\rho \leq 0.5$, as shown in Figure 4.7, the ICToNOMA has no advantage over NOMA-IJDD and shows the same results. This is confirmed by the BLER performance in Figure 4.7 , as the performance is almost the same as in NOMA-IJDD for $\tau > 0.5T_s$.

For the synchronous reception of both signals, i.e. $\tau = 0$, a performance gain of more than 4dB in comparison with NOMA-IJDD is observed. This is in compliance with the theory, as the coherent addition of the two signals improves the performance for at least 3dB.

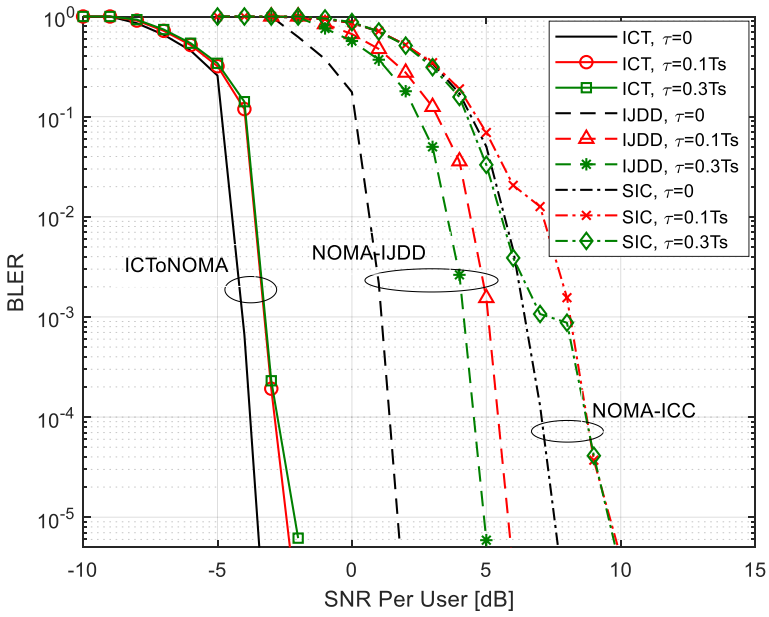

Figure 4.8 Performance of ICToNOMA vs. NOMA-IJDD vs. NOMA-SIC

It is worth to mention that based on the simulation results, the average iteration at BLER=10^{-5} is 1.6 times in ICToNOMA, which means that the joint detection block in the IJDD can detect a good ratio of the signals even at the first iteration. This is another improved aspect of ICToNOMA regarding the low latency communications compared to SIC which has to perform at least two iterations in the two-user NOMA successive decoding.

4.6.4. Asynchronous ICToNOMA: Power Compensation

We have proposed using a low power means of transmission for the inter-terminal background communications. As it was investigated in Section 4.4.4, the cooperation consumes extra power that should be taken into considerations.

In this section, we evaluate the ICToNOMA, while lowering each user's power to half and one-fourth of its initial power. This conserves enough margin to compensate for the inter-terminal communications. The simulation results are provided in Figure 4.9, which shows that the performance is still almost 7dB and 2dB better than the NOMA-IJDD at $\tau = 0.1T_s$, even with reducing the users' power to half and one-fourth, respectively.

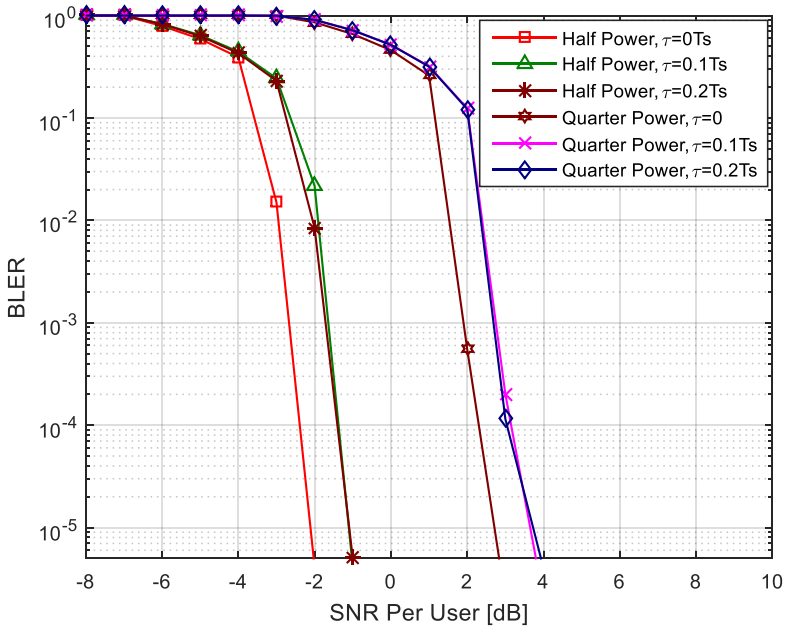

Figure 4.9 Performance of ICToNOMA with power reduced to half and one-fourth

4.6.5. Asynchronous ICToNOMA: Spectral Efficiency

Based on the simulation results till now, the reliability in ICToNOMA outperforms NOMA-SIC as well as NOMA-IJDD, even in low SNR values. However, as discussed earlier, the effect of the correlation between the sources should be considered in studying the spectral efficiency. In this section, we use the degradation factor evaluated earlier in (4-2), as we simulate the achieved spectral efficiency for ICToNOMA.

Due to the huge power saving in the ICToNOMA compared to NOMA-IJDD, a fair comparison is not quite possible. Considering similar modulation and coding schemes, at $\tau = 0.1T_s$, the NOMA-IJDD achieves the target BLER at SNR=+6dB; whereas, it is at SNR=-2dB with ICToNOMA. So, we considered lowering the users' initial power to make the comparison possible. The simulation results led to the optimized power to be one-fifth of the initial power, to have a fair comparison of the spectral efficiency of the two scenarios.

Hence, we assumed that the transmit power in ICToNOMA is decreased to one-fifth of the initial value. We simulated both NOMA-IJDD and ICToNOMA with delay of $\tau = 0.1T_s$ at SNR=2dB. The reason for this selection was the fact that with these assumptions and at the sources' correlation rate equal to $\gamma = 0.75$, the average spectral efficiency of both scenarios was

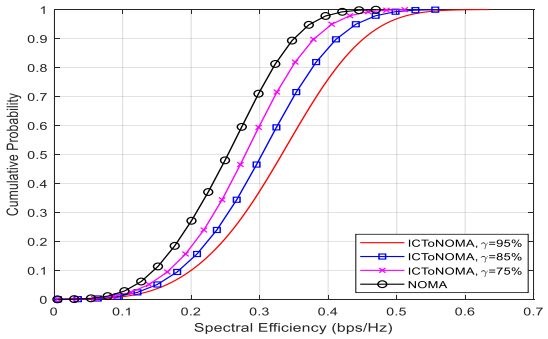

(a)

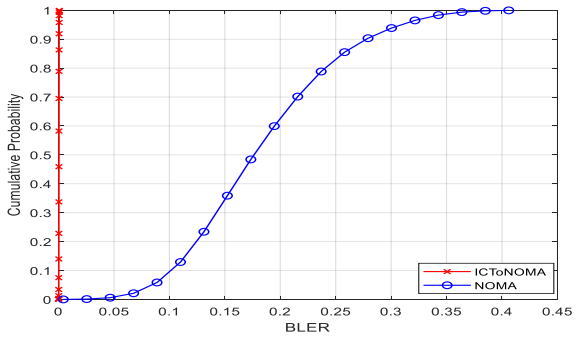

(b)

Figure 4.10 SNR = 2 dB, $\tau = 0.1T_s$, ICToNOMA power reduced to $\frac{1}{4}$th (a) Cumulative probability of spectral efficiency (b) Cumulative probability of BLER

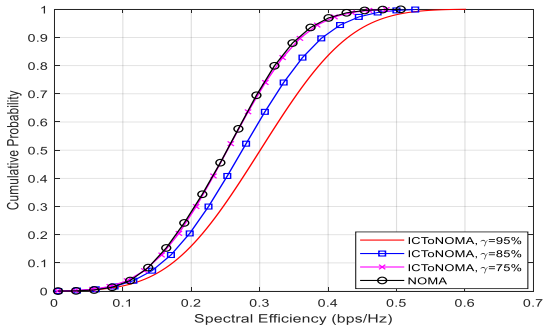

(a)

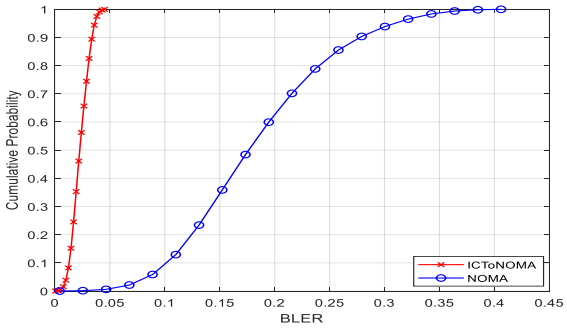

(b)

Figure 4.11 SNR = 2 dB, $\tau = 0.1T_s$, ICToNOMA power reduced to $\frac{1}{5}$th (a) Cumulative probability of spectral efficiency (b) Cumulative probability of BLER

almost the same. Figure 4.10 and Figure 4.11 show the cumulative probability of the spectral efficiency and BLER for power reduced to one-fourth and one-fifth, respectively. In Figure 4.10a, the cumulative probability of sum-rate spectral efficiency for NOMA-IJDD and ICToNOMA, for different values of sources' correlation is provided. It is observed that ICToNOMA outperforms NOMA-IJDD for $\gamma \geq 0.75$, even with users' power reduced to one-fourth of its initial power. Moreover, this efficiency is achieved with huge increase in reliability as shown in Figure 4.10b. As for power reduction to one-fifth of its initial value, as shown in Figure 4.11a, the NOMA-IJDD's average spectral efficiency is almost equal to ICToNOMA for $\gamma = 0.75$; whereas, ICToNOMA achieves more than eight times more reliability than NOMA-IJDD, see Figure 4.11b.

It is worth to mention that our proposed ICToNOMA system is optimal for sources with high correlation rates, which obviously outperforms NOMA even with power reduced to one-fourth and one-fifth.

4.7. Discussion

In this chapter, we proposed our system that achieves considerable boost in reliability and spectral efficiency for very low SNR values in URLLC IoT networks. Our scheme is based on the cooperation of users with correlated sources in uplink of IoT systems, who combine their data and transmit identical content over NOMA (ICToNOMA). Although, the redundant transmission is a well-studied concept, it is known to be vulnerable to the asynchronous reception of the data streams at the receiver; yet, we show how we can use this in favor of our system. We propose taking advantage of the added correlation due to the asynchronicity rather than combating it. NOMA with SIC receivers gets severely degraded in case of asynchronous channel, and so we have proposed our version of iterative joint detection and decoding (IJDD) to be used at the receiver of the asynchronous channel to take advantage of the channel's correlation as extra source of information. The theoretic findings were confirmed by the simulation results, where more spectral efficiency was achieved with impressively increased reliability, even after decreasing the users' power to one-fourth of their initial power.

Chapter 5 .

Non-Coherent Multi-Point Networks

5.1. Introduction

In this chapter, two key challenges in networks with multiple transmission reception points (TRP) are addressed. The asynchronous downlink and imperfect channel state information (CSI) are jointly considered in an information theoretical framework.

The demand for ubiquitous mobile communications has motivated many advanced techniques with distinct ranges of coverage, reliability, and throughput. Such immense diversity has however conveyed to different sorts of inter-cell and intra-cell originated interferences. The multiple transmission reception points (TRP) or the coordinated multipoint (CoMP) is currently under development by 3GPP in fifth generation (5G) mobile communications [75]. In multi-TRP, the key demands for the user equipment (UE) at the cell edge or with unfavorable link conditions are targeted including the enhanced connectivity, increased data throughput, ultra-reliability, and low latency [76].

Traditionally, the uplink and downlink in wireless communications has been based on allocating orthogonal channels to the multiple access and broadcast channels, respectively. However, with the increase in the scale of the networks and the realization of the small cells and heterogeneous networks, the orthogonal multiple access (OMA) schemes may be insufficient in the sense of spectral efficiency and latency. Nonorthogonal multiple access (NOMA) is an alternative approach proposed in 5G new radio (NR). As we have investigated in this thesis, the

resources of frequency, time, space, or code can be shared with multiple TRPs in NOMA, providing sufficient scalability to serve large connectivity in mobile networks. NOMA is vulnerable to asynchronous reception of data, and at least a rough synchronization to reduce the complexity of the receiver is required [9].

The impressive features in multi-TRP networks along with the existing challenges have motivated us in this chapter. We propose a new scheme in mitigating the interference caused by asynchronous reception even with imperfect knowledge of the channel. We adopt the iterative joint detection at the receiver to cooperatively employ the imposed interference instead of cancelling it. The observations from theoretical and simulation perspectives show that despite the asynchronous channel with imperfect CSI, the reliability as well as spectral and power efficiencies would exceed that of the non-cooperative benchmark systems.

In this chapter, we follow our prior research in previous chapter and extend our research in the applications with multiple distributed TRPs who cooperatively transmit the same TB to the target user. Due to the distributed nature of such systems it would be challenging to attain a good trade-off between constructive exploitation of the interference and keep the synchronization and CSI control signaling overhead in a decent extent.

We consider the potential reception of the OFDM data streams with different time delay attributes. We assume delays from TRPs to the target user, in general, may exceed cyclic prefix (CP) length, causing symbol-asynchronous reception at the receiver. Therefore, we have proposed an accurate mathematical model for the asynchronous OFDM-based CoMP, which we have extended to the multiple number of TRPs. The exact expression for the capacity region and outer bound is developed for the sum-rate of multiple TRPs in asynchronous multi-TRP networks. We have derived a low-complexity MMSE-based iterative joint detection and decoding receiver for the asynchronous CoMP, which is generalized to multiple number of TRPs. Moreover, we have considered reasonably complex models in the simulations, reflecting interference scenarios such as imperfect CSI.

Our extensive simulation results show that the reliability and spectral efficiency can exceed that of the non-cooperative transmissions, provided that the proper receiver is employed. We propose our receiver based on iterative joint detection and decoding, by which the performance elevates even as the number of TRPs increases.

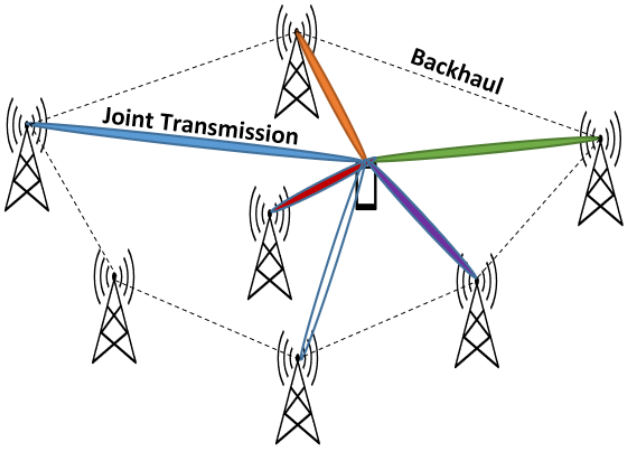

Figure 5.1 Multi-TRP System Model

The first step is deriving the capacity region in non-coherent MTRP systems is to obtain an equivalent channel model based on OFDM symbols. This is accomplished in Section 5.2, where the asynchronous channel parametrized with symbols' cross-correlations is provided. We derive and analyze the capacity region of our proposed scheme in Section 5.3, followed by Section 5.4 where we have proposed our receiver. Simulation results are provided in section 5.5, validating the theoretical findings that are concluded in Section 5.6.

5.2. System Model

In this chapter, a downlink multi-TRP transmission with K single-antenna UEs and N TRPs is considered, where each TRP employs a fixed antenna pattern, see Figure 5.1. The TRPs share the same resource of time and frequency to jointly transmit the same TB to the target user, where TRPs are connected by a mesh of fast backhaul links.

We consider an OFDM-based system with FFT size of N_{FFT} subcarriers, cyclic prefix (CP) comprising of N_{CP} samples, and symbol size of $N_T = N_{FFT} + N_{CP}$. Assuming that the signals from different TRPs are received with different time-delay attributes, the signal received at UE can be written as

$$y_k(m) = \sum_n h_{n,k}(m) \sum_i x_n^i\left(m - \tau_{n,k} - iN_T\right) + w_k(m) \tag{5-1}$$

where the n, k, i are the TRP, UE, and the symbol indices, respectively. The $x_n^i(m)$ is the transmit signal from n-th TRP on the i-th symbol. $\tau_{n,k}$ is the integer time offset implying the delay in samples of the signal received from n-th TRP at the k-th UE. The fractional time offsets have already been investigated in literature causing the inter-carrier interference (ICI). The integer time offsets are considered, as they introduce, in addition to the ICI, inter-block interference (IBI) and inter symbol interference (ISI) [124]. The $h_{n,k}$ correspond to the independent and identically distributed (iid) channel coefficients from the n-th TRP to the k-th UE, that are circularly symmetric complex normal with Rayleigh magnitude and uniformly distributed phase; $w_k(m)$ is the complex AWGN at the k-th UE, denoted as $n \sim N(0, \sigma_k^2)$. It is assumed that users and TRPs are aligned at carrier frequency and there is no carrier frequency offset (CFO) between them [77].

In essence, the cyclic prefix in OFDM is considered to maintain the orthogonality among the subcarriers and to cope with the signals' delay spread by confining the ISI effect of an OFDM symbol on the next symbol. Hence, the data streams received with time-offsets lower than the cyclic prefix can be recovered in OFDM demodulator. In this paper, the special case is considered, where delays in the received signals from different TRPs exceed the length of the cyclic prefix (CP) at the receiver. Therefore, upon the removal of the CP at the receiver, the FFT is taken on the received signal at the k-th UE, i.e. $y_k(m)$, where symbols are overlapped by the preceding or succeeding symbols received from other TRPs [78].

Without loss of generality, it is assumed that the TRPs are ordered based on the received signal delay spread, as such $\tau_{1,k} \leq \tau_{2,k} \leq \cdots \leq \tau_{N,k}$. The time advance (TA) is applied at the k-th UE with regard to the TRP with lowest delay to receive the downlink signal from that TRP at the expected time. The resulting received symbols can be defined in frequency domain based on the overlapping of the symbols,

$$Y_k^i(l) = \sum_n h_{n,k} \left(\sum_{m=0}^{\psi_{n,k}-1} x_n^{i-1}\left(m + N_{FFT} - \psi_{n,k}\right) e^{\frac{-j2\pi lm}{N_{FFT}}} + \sum_{m=\psi_{n,k}}^{N_{FFT}-1} x_n^i\left(m + N_{CP} - \psi_{n,k}\right) e^{\frac{-j2\pi lm}{N_{FFT}}} \right) + W_k^i(l) \quad (5\text{-}2)$$

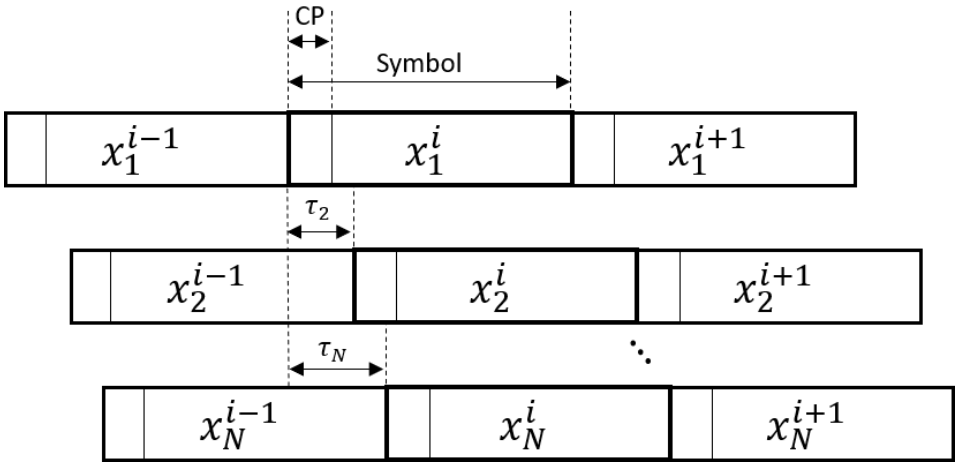

Figure 5.2 Symbol asynchronous Multi-TRP channel for OFDM systems

where, $\psi_{n,k} = \max(\tau_{n,k} - N_{CP}, 0)$ implies the occurrence of the ISI. $W_k^i(l)$ is the l-th sample of the FFT of $w_k(m)$, which are the AWGN samples overlapped with the i-th OFDM symbol at k-th UE [124].

5.2.1. Asynchronous Channel Model

In this section we provide a precise mathematical model for the asynchronous multi-TRP transmission with N TRPs. Due to the asynchronous reception of the OFDM data streams, the timing offsets larger than CP causes each transmitted symbol getting overlapped by two symbols of each of the other TRPs resulting in ISI. Assuming the frame synchronization, the symbol asynchronous channel for the OFDM systems is shown in Figure 5.2. Without loss of generality, it is assumed that UE is synchronous with first TRP, i.e. $\tau_1 = 0$, and TRPs are ordered based on their transmit delay $\tau_1 \leq \tau_2 \leq \cdots \leq \tau_N$.

Considering the signals in the frequency domain, a suitable model is derived in [124] for the interference caused by the overlapping symbols of a SISO OFDM system. The interference is computed per resource element (RE), which represents one subcarrier in frequency domain and an OFDM symbol in time domain.

Using similar procedure in [124], We have expanded the interference for the MTRP system, where the inter-symbol-interference caused by the cross-correlation of the asynchronous signals received from the i-th and j-th TRPs with respect to their time delay difference can be denoted as,

$$\rho_{ij,k} = \frac{1}{N_{FFT}} \Gamma^{i,j,k}(l) e^{\frac{-j2\pi\left(\left|\tau_{j,k}-\tau_{i,k}\right|-N_{CP}\right)}{N_{FFT}}} \tag{5-3}$$

$$\Gamma^{i,j,k}(l) = \begin{cases} \psi_{i,j,k} = \max\left(\left|\tau_{j,k}-\tau_{i,k}\right| - N_{CP}, 0\right), & l = 0 \\ \frac{1-e^{-j2\pi l \psi_{i,j,k}/N_{FFT}}}{1-e^{-j2\pi l/N_{FFT}}}, & l \neq 0 \end{cases} \tag{5-4}$$

Finally, we propose the mathematical model to include the effect of the preceding and following symbols on each resource element (RE), at k-th UE and from all TRPs, that can be defined as

$$\boldsymbol{Y}_k^{i,i+1} = \boldsymbol{R}_{\boldsymbol{A}_k}^{i,i+1}\left(\boldsymbol{H}_k^{i,i+1} \otimes \boldsymbol{X}_k^{i,i+1}\right) + \boldsymbol{W}_k^{i,i+1} \tag{5-5}$$

where, $\otimes$ is the product acting elementwise, $\boldsymbol{Y}_k \in \mathbb{C}^{2N\times 1}$: $\boldsymbol{Y}_k = \left[Y_{k,1}^i, Y_{k,1}^{i+1}, \dots, Y_{k,N}^i, Y_{k,N}^{i+1}\right]^T$, is the received signal, $\boldsymbol{H}_k \in \mathbb{C}^{2N\times 1}$, $\boldsymbol{H}_k = \left[H_{k,1}^i, H_{k,1}^{i+1}, \dots, H_{k,N}^i, H_{k,N}^{i+1}\right]^T$, is the channel coefficients vector, $\boldsymbol{X}_k \in \mathbb{C}^{2N\times 1}$, $\boldsymbol{X}_k = \left[X_{k,1}^i, X_{k,1}^{i+1}, \dots, X_{k,N}^i, X_{k,N}^{i+1}\right]^T$, is the transmitted signal, and $\boldsymbol{W}_k \in \mathbb{C}^{2N\times 1}$ is the added noise. Matrix $\boldsymbol{R}_{\boldsymbol{A}_k} \in \mathbb{C}^{2N\times 2N}$ denotes the cross-correlation impact of the non-coherent received signals from N-TRPs.

The main attribute of the channel in (5-5) is that the noise is correlated due to the channel having memory. Also, each output value depends on $2N-1$ input symbols, while each of these symbols affect two consecutive output vectors. Normally, in a system with N TRPs, the denoted vectors and matrices in (5-5) have an order of N; yet, this is not the case in asynchronous channels. Due to the channel having memory, each symbol at the output corresponds to the vectors of dimension $2N$, to include the channel's memory effect. In other words, the factor 2 is due to the coincidence of each symbol with two symbols of the other data streams. For instance, for a downlink CoMP with two TRPs at a single UE, the system can be presented as

$$\begin{bmatrix} Y_{k,1}^i \\ Y_{k,1}^{i+1} \\ Y_{k,2}^i \\ Y_{k,2}^{i+1} \end{bmatrix} = \boldsymbol{R}_{\boldsymbol{A}_k}^{i,i+1} \begin{bmatrix} H_{k,1}^i X_{k,1}^i \\ H_{k,1}^{i+1} X_{k,1}^{i+1} \\ H_{k,2}^i X_{k,2}^i \\ H_{k,2}^{i+1} X_{k,2}^{i+1} \end{bmatrix} + \begin{bmatrix} W_k^i \\ W_k^{i+1} \\ W_k^i \\ W_k^{i+1} \end{bmatrix} \tag{5-6}$$

We propose the cross-correlation matrix $\boldsymbol{R}_{\boldsymbol{A}_k}^{i,i+1}$ as the asynchronous representation of the channel matrix which includes the asynchronous channels' inter-symbol interference coefficients,

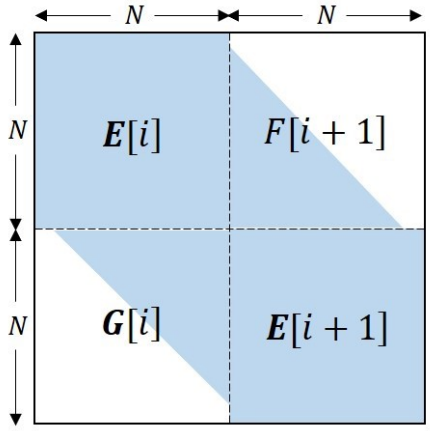

Figure 5.3 Generalized asynchronous multi-TRP channel matrix $\boldsymbol{R}_{\boldsymbol{A}_k}$

see $\rho_{ij,k}$ in (5-3). The matrix $\boldsymbol{R}_{\boldsymbol{A}_k}$ is a $2N \times 2N$ matrix that can be partitioned as shown in Figure 5.3, where the matrices $\boldsymbol{E}, \boldsymbol{F}$, and $\boldsymbol{G}$ have the size $N \times N$.

The matrix $\boldsymbol{E}[i]$ denotes the ISI between the i-th symbol of the received REs from N TRPs as

$$\boldsymbol{E}[i] = \begin{bmatrix} 1 & \rho_{12,k} & \cdots & \rho_{1N,k} \\ \rho_{12,k} & 1 & \cdots & \rho_{2N,k} \\ \vdots & \cdots & \ddots & \vdots \\ \rho_{1N,k} & \rho_{2N,k} & \cdots & 1 \end{bmatrix} \tag{5-7}$$

The matrix $\boldsymbol{F}[i+1]$ is lower-triangular, where only the elements below the diagonal are non-zero, indicating the effect of the succeeding $(i+1)$-th symbols from N TRPs on the i-th symbols,

$$\boldsymbol{F}[i+1] = \begin{bmatrix} 0 & 0 & \cdots & 0 \\ \rho_{21,k} & 0 & \cdots & 0 \\ \vdots & \cdots & \ddots & \vdots \\ \rho_{N1,k} & \rho_{N2,k} & \cdots & 0 \end{bmatrix} \tag{5-8}$$

The matrix $\boldsymbol{G}$ is the transpose of matrix F, as such it is an upper-triangular, where only the elements above the diagonal are non-zero. Matrix $\boldsymbol{G}[i]$ indicates the effect of the preceding symbols on the $i+1$-th symbols

$$\boldsymbol{G}[i] = \begin{bmatrix} 0 & \rho_{21,k} & \cdots & \rho_{N1,k} \\ 0 & 0 & \cdots & \rho_{N2,k} \\ \vdots & \cdots & \ddots & \vdots \\ 0 & 0 & \cdots & 0 \end{bmatrix} \tag{5-9}$$

5.2.2. Imperfect Channel State Information (CSI)

To include the effects of the imperfect CSI, we assume that TRPs could have access to a rough estimate of the CSI. This results in an error on the evaluated CSI given as $\tilde{h}_i(t) = h_i(t) + e_{CSI}$. The channel estimation error has been modeled as a Gaussian distributed random variable in relative literature, such that $e_{CSI} \sim \mathbb{CN}(0, \sigma_{CSI}^2)$ [72][74].

As for the channel estimation error, the variances of $\sigma_{CSI}^2 = 0.001$ and 0.01 are considered in some literature, e.g., [78]. However, our simulations show that considering a trivial variance may not reflect the impact of imperfect CSI. In this chapter, we adopt the work in [72] in assuming $\sigma_{CSI}^2 = 0.1$ which reflects an SINR of 10 dB.

5.3. Capacity Region

In this section, we investigate the information theoretic aspects of our proposed scheme. We compute the capacity region for the multi-TRP asynchronous transmission that can be expressed as in below theorem.

Theorem 1. The outer bound for the capacity region of asynchronous multi-TRP systems is the closure of the convex hull of the rates satisfying

$$(R_1, R_2, \dots, R_N), 0 \le R_i \le \frac{1}{2}\log\left(1 + \frac{|H_{i,k}|^2 S_{i,k}}{{\sigma_k}^2}\right)$$

$$R_1 + R_2 \le \frac{1}{2}\log\left[1 + \frac{|H_{1,k}|^2 S_{1,k} + |H_{2,k}|^2 S_{2,k}}{{\sigma_k}^2} + 2\rho_{ij,k}\sqrt{\frac{|H_{1,k}|^2 S_{1,k}}{{\sigma_k}^2}}\sqrt{\frac{|H_{2,k}|^2 S_{2,k}}{{\sigma_k}^2}}\right]$$

$$R_1 + R_2 + R_3 \le \frac{1}{2}\log\left[1 + \sum_{i=1}^{3}\frac{|H_{i,k}|^2 S_{i,k}}{{\sigma_k}^2} + 2\sum_{\substack{i,j=1 \\ i\neq j}}^{3}\rho_{ij,k}\sqrt{\frac{|H_{i,k}|^2 S_{i,k}}{{\sigma_k}^2}}\sqrt{\frac{|H_{j,k}|^2 S_{j,k}}{{\sigma_k}^2}}\right]$$

$$\vdots$$

$$R_1 + R_2 + \cdots + R_N \le \frac{1}{2}\log\left[1 + \sum_{i=1}^{N}\frac{|H_{i,k}|^2 S_{i,k}}{{\sigma_k}^2} + 2\sum_{\substack{i,j=1 \\ i\neq j}}^{N}\rho_{ij,k}\sqrt{\frac{|H_{i,k}|^2 S_{i,k}}{{\sigma_k}^2}}\sqrt{\frac{|H_{j,k}|^2 S_{j,k}}{{\sigma_k}^2}}\right]$$

(5-10)

Proof. To derive the capacity region of the symbol asynchronous MTRP system, the covariance of $\boldsymbol{Y}_k^i$ is calculated. Index i refers to symbol i as a single resource element and so it is removed for the simplicity. Considering the channel model in (5-5), the covariance matrix of the received signal can be written as

$$\mathrm{cov}(\boldsymbol{Y}_k) = \boldsymbol{R}_N[{\sigma_k}^2\boldsymbol{I}_N + \mathrm{cov}(\boldsymbol{X})\boldsymbol{R}_N] \tag{5-11}$$

where I_N is the identity matrix of size $2N$. Matrix $\boldsymbol{R}_N$ is the $N \times N$ cross-correlation matrix between the i-th received symbols, implying the first N rows and N columns of $\boldsymbol{R}_{\boldsymbol{A}_k}^{i,i+1}$, i.e. matrix $\boldsymbol{E}[i]$ in (5-7). The AWGN noise vector in (s-5) does not have an identity covariance matrix; whereas, it can be identified with zero mean and covariance matrix as $\sigma_k^2\boldsymbol{R}_N$. The $\mathrm{cov}(\boldsymbol{X})$ is the $N \times N$ covariance matrix of transmitted signals from TRPs including the channel coefficients, that can be written as

$$\mathrm{cov}(\boldsymbol{X}_k) = \begin{bmatrix} |H_{1,k}|^2 S_{1,k} & \lambda_{12,k} & \cdots & \lambda_{1N,k} \\ \lambda_{12,k} & |H_{2,k}|^2 S_{2,k} & \cdots & \lambda_{2N,k} \\ \vdots & \vdots & \ddots & \vdots \\ \lambda_{1N,k} & \lambda_{2N,k} & \cdots & |H_{N,k}|^2 S_{N,k} \end{bmatrix} \tag{5-12}$$

where $S_{n,k}$ denotes the transmit power corresponding to signals transmitted from TRP n, and $\lambda_{ij,k}$ are the covariance coefficients between $X_{i,k}$ and $X_{j,k}$. Considering the joint transmission from the TRPs and based on the Cauchy–Schwarz inequality: $\lambda_{ij,k} \leq \sqrt{(|H_{i,k}|^2 S_{i,k}).(|H_{j,k}|^2 S_{j,k})}$.

The entropy of the received vector $\boldsymbol{Y}_k$ as a multivariate normal distribution corresponding to the transmitted signals $\boldsymbol{X}_k$ can be written as

$$h(Y_{1,\mathrm{k}}, Y_{2,\mathrm{k}}, \dots, Y_{N,k}) = \tfrac{1}{2}\log(2\pi e)^2\mathrm{cov}(\boldsymbol{Y}_k) \tag{5-13}$$

Consequently, the mutual information is

$$I(\boldsymbol{X}_k; \boldsymbol{Y}_k) = I(X_{1,k}, \dots, X_{N,k}; Y_{1,k}, \dots, Y_{N,k}) = \tfrac{1}{2}\log\det[\mathrm{cov}(\boldsymbol{Y}_k)] - \tfrac{1}{2}\log\det[{\sigma_k}^2\boldsymbol{R}_N] \tag{5-14}$$

Considering the symmetrical characteristics of the $\mathrm{cov}(\boldsymbol{Y}_k)$ and $\boldsymbol{R}_N$ matrices and singularity of the $\mathrm{cov}(\boldsymbol{X})\boldsymbol{R}_N$ matrix, the mutual information can be expressed as

$$I(\boldsymbol{X}_k;\boldsymbol{Y}_k) = \frac{1}{2}\log\left[1 + \frac{1}{{\sigma_k}^2}\text{trace}(\text{cov}(\boldsymbol{X})\boldsymbol{R}_N)\right] \tag{5-15}$$

Which can be simplified even more to,

$$I(\boldsymbol{X}_k;\boldsymbol{Y}_k) = \frac{1}{2}\log\left[1 + \sum \phi_{ij}\right] \tag{5-16}$$

where, ϕ_{ij} are the elements of matrix $\boldsymbol{\Phi} = \text{cov}(\boldsymbol{X})\otimes\boldsymbol{R}_N$, considering $\otimes$ is the product acting elementwise.

The achievable rates in the capacity region in (5-10) are based on the capacity region of the multiple access channels. Thus, the converse theorem can be based on the fact that the codes for the reliable communication have to satisfy the target bit error rate, no matter which actual channel is in effect [32].

■

As expected, the evaluated capacity region is similar to the capacity region of the MAC, where the extra term in the sum-rate represents the effect of employing the asynchronous channels' cross-correlations as well as the cooperative joint transmission of the TRPs.

As a reminder, the asynchronous MAC capacity region discussed in Section 2.4 did not consider a coordination between the transmitters. Thus, the non-coordinated asynchronous MAC in (2-30) achieves its maximum rate for time offset equal to half the symbol rate, i.e. $\tau = \tau_2 - \tau_1 = 0.5T_s$. This implies that as the asynchronous channels' cross-correlations $\rho_{12,k}$ gets closer to one, the achieved gain in sum-rate capacity reduces.

In practice, the data streams received with time-offsets lower than the cyclic prefix can be recovered in OFDM demodulator. Considering OFDM subcarrier spacing of 15kHz, the cyclic prefix has the length equal to $0.07T_s$ in normal CP configuration [92]. In this chapter, we are interested in schemes in which the time-offsets extend the cyclic prefix; yet they are still in a decent range, i.e. $0.07T_s < \tau \ll 0.5T_s$, $0.5 \ll \rho_{ij,k} < 1$.

In the capacity region in (5-16) the asynchronous channel's cross-correlation, i.e. μ_{ij}, has a linear effect on the sum-rate. As the correlation of the channel increases, the sum-rate escalates closer to the capacity in the coherent channels. Thus, our proposed scheme achieves higher sum-rates for the practical time-offsets compared to non-coordinated approaches.

5.4. Low Complexity IJDD Receiver Implementation

It was shown in previous section that modeling the asynchronous channel as a channel with memory and taking advantage of the channel's cross-correlations, results in spectral efficiencies exceeding that of synchronous reception. This is conditioned on using the proper detection and decoding techniques at the receiver.

The successive interference cancellation (SIC), parallel interference cancellation (PIC), and interference rejection combining (IRC) are some of the baseband processing techniques currently used in the state-of-the-art systems [79][93]. The methodology in the two former receivers in to detect the interference and cancel their contribution from the received signal; whereas, the latter receiver relies on spatial projecting of the desired signals to prevent the interference. The performance of the receivers based on interference cancellation (IC) in multiple-access channels with ISI or specifically asynchronous reception was investigated in Section 2.3. The methodology of interference cancellation at the receiver is based on cancelling and subtracting the interferences from the desired signal. In asynchronous MAC, as the symbols are overlapped by preceding and succeeding symbols of the other sources, the channel changes to a channel with memory. Employing the interference cancellation in asynchronous channels would translate in eliminating the channel's useful cross-correlations, and that is why IC receivers are suboptimal in asynchronous scenarios.

The joint detector is the main block in our receiver which detects the multi-user data based on the aggregate received signal. In previous chapter, we investigated and proved that in asynchronous MAC with cross-correlations between the data streams, the joint detection would lead in harvesting the contribution they have on one another. We proposed that by iterative joint detection and decoding (IJDD) of the data streams, the spectral efficiency gain could be achieved. However, the proposed optimal IJDD has the complexity in order of $O(2^{2N})$, which is not favorable with large number of sources, N.

In this section we propose the low complexity IJDD receiver, that we have adopted from [35] and have promoted it to be used in asynchronous channel models. The proposed detector is based on minimum mean-squared error (MMSE) used iteratively in a joint detection framework. The IJDD is typically shown in Figure 2.8.

Let the MMSE filter at the joint detector in the asynchronous channel be written as

$$\boldsymbol{z}_n(i,i+1) = \boldsymbol{w}_n(i,i+1)^T \boldsymbol{y}_n(i,i+1) \tag{5-17}$$

The $\boldsymbol{y}_n$ is the received signal and the $\boldsymbol{w}_n$ is employed to minimize the mean square error between the estimated code-bits and the output of the detector, denoted as

$$\boldsymbol{w}_n = \arg\min E\{[\boldsymbol{b}_n(i,i+1) - \boldsymbol{w}^T \boldsymbol{y}_n(i,i+1)]^2\} \tag{5-18}$$

where, $\boldsymbol{b}_n \in \mathbb{C}^{2N\times 1}$ is the vector of code-bits that are assumed to be BPSK symbol mapped.

The soft estimate of the code-bits is calculated based on the *a-priori* information from decoders in previous iteration that can be written as

$$\bar{b}_j[i,i+1] = \tanh\left(\frac{1}{2}{\lambda_2}^p\left[b_j(i,i+1)\right]\right) \tag{5-19}$$

The *a-priori* information $\overline{\boldsymbol{b}}_n \in \mathbb{R}^{2N\times 1}$ is further used at the MMSE-based detection module to calculate the Log-Likelihood Ratio (LLR) of each code-bit.

The extrinsic information delivered by the soft instantaneous MMSE filter is

$$\lambda_1[b_n(i)] = \frac{2z_n(i)}{1-\mu_n(i)} \tag{5-20}$$

where,

$$\mu_n(i) = A_n^2\left[\left[\boldsymbol{V}_n(i) + \sigma^2 {\boldsymbol{H}_A}^{-1}\right]^{-1}\right]_{nn} \tag{5-21}$$

$$z_n(i,i+1) = A_n \boldsymbol{e}_n^T\left[\boldsymbol{V}_n(i) + \sigma^2 {\boldsymbol{H}_A}^{-1}\right]^{-1}\left[{\boldsymbol{H}_A}^{-1}\boldsymbol{y}(i,i+1) - \boldsymbol{A}\bar{\boldsymbol{b}}_n(i,i+1)\right] \tag{5-22}$$

Where $\boldsymbol{e}_n$ stands for a $2N$-vector of all zeros, except for the nth element, which is 1. Denote that

$$\boldsymbol{V}_n(i) = \sum_{j\neq n} A_j^2\left[1 - b_j(i)^2\right]\boldsymbol{e}_j\boldsymbol{e}_j^T + A_n^2\boldsymbol{e}_n\boldsymbol{e}_n^T \tag{5-23}$$

5.5. Simulations and Evaluation Results

In this section, we have provided the link-level simulation results to demonstrate the effectiveness of our proposed scheme and confirm the information theoretic findings. We have evaluated the asynchronous channel in scenarios for single TRP, multi-TRP with NOMA, and multi-TRP with cooperative joint transmission. The transmitted signals from TRPs are assumed to be received with equal average transmission power, which is the worst-case scenario as they cause the highest interference on each other. The channel is modeled as an asynchronous Rayleigh-fading multiple access channel. We have used the Monte Carlo method in our simulations. The achievability is simulated so that the channel code guarantees a block error rate (BLER) not exceeding 10^{-5}, which is the target BLER in 3GPP standard for 5G URLLC [24]. The simulation assumptions are briefly provided in Table 5-1.

5.5.1. Asynchronous cooperative and non-cooperative scenarios

We investigate the performance of our proposed system in asynchronous multi-TRP (MTRP) CoMP systems. We have simulated $N = 2, 3, 4$ TRPs, where the data is received asynchronously at the target UE. In the simulations, imperfect CSI with error variance of $\sigma_{CSI}^2 = 0.1$ is assumed.

Table 5-1, Simulation Assumptions

Channel Model	Rayleigh Fading
Modulation Format	BPSK
Error Control Coding	LDPC rate 1/6
Transport Block Size (BPS)	120-Bytes
Time Offsets	$0.07\mathrm{T_s} < \tau \ll 0.5\mathrm{T_s}$
Antenna Configuration	single-antenna receivers
Average Receiver SNR	Equal average SNR
Target BLER	10^{-5}
Receiver Type	IJDD in our proposed scheme SIC for the state-of-the-art systems
Imperfect CSI variance	10 dB SINR

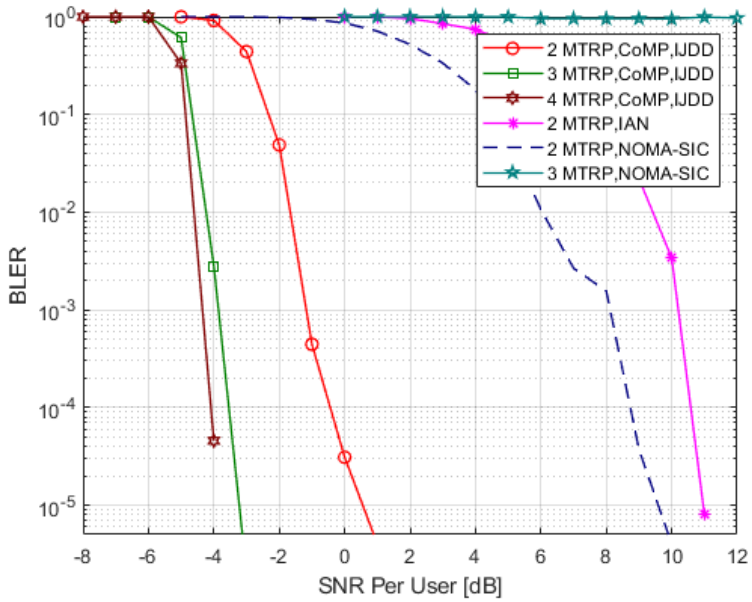

Figure 5.4 Performance of asynchronous multi-TRP in different scenarios

The simulation results are provided for asynchronous receptions with relative delays of 10% of the symbol time, i.e. $\tau_{ij} = |\tau_j - \tau_i| = 0.1T_s$. The result plot is provided in Figure 5.4.

CoMP, IJDD Evaluation. Our proposed IJDD receiver with MMSE-based joint detector is assumed at the receiver side. It is observed that as the number of TRPs increases, the performance elevates, as for 4MTRP, almost 1dB and 4dB performance at $BLER = 10^{-5}$ is achieved in comparison with 3MTRP and 2MTRP, respectively. This is in accordance with the information theoretic findings.

Another interesting observation is on the two-TRP scheme experiencing an error floor at BLER around 10^{-4} which is due to the asynchronous reception of the data streams. The error floor does not exist for higher TRP schemes. This feature points out the performance of our proposed receiver which benefits from the diversity provided by multi-TRP transmission even in the existence of asynchronous reception, and that the performance improves as the number of TRPs increases.

IAN Evaluation. We have also provided the simulation results for the non-cooperative multi-TRP schemes, where the conventional Interference-as-Noise (IAN) signal processing is used. The two-TRP setup is considered, where significant loss in performance is expected due to the severe interference from the other TRP. Based on the simulation results, it is observed that considering

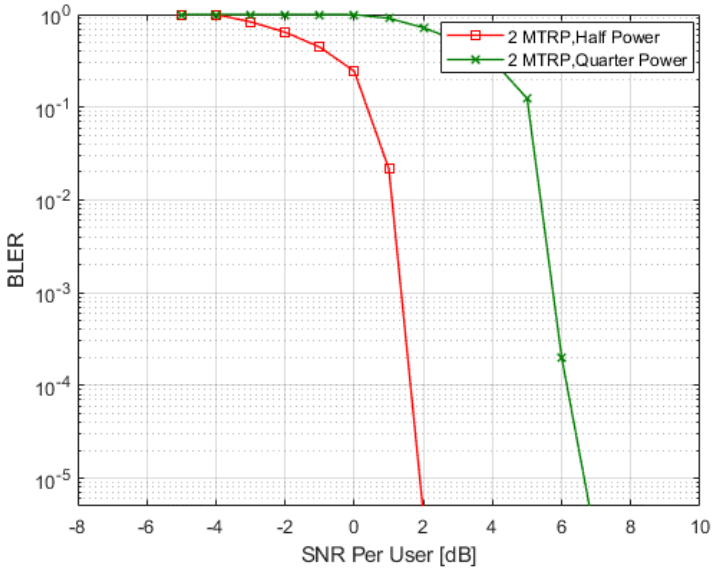

Figure 5.5 Performance in asynchronous CoMP, power reduced to 1/2 & 1/4

IAN degrades the performance for almost 10dB at $BLER = 10^{-5}$, compared to the same setup in CoMP with IJDD at the receiver.

NOMA-SIC Evaluation. We have simulated NOMA for data transmission from two and three asynchronous TRPs. The SIC receiver is considered in NOMA receiver. Employing NOMA improves the performance for about 2dB at $BLER = 10^{-5}$ in 2MTRP compared to the IAN. As the number of TRPs increases, asynchronous NOMA degrades drastically as the BLER does not scale down even for higher SNR in 3MTRP, see Figure 5.4. NOMA is designed in the essence to attain much higher gains for a greater number of TRPs in synchronous platforms. However, it is observed that the asynchronous reception reflects itself in NOMA similar to the interference in IAN. This is in accordance with the information theoretical findings as the ISI caused by asynchronous reception degrades the performance in NOMA with SIC at the receiver.

Discussion. As the number of TRPs increases, the asynchronous channel experiences more correlated time-diversity. This is as extra feed of information to the IJDD resulting in a better performance. However, the extra correlation is dealt as extra interference in the SIC, which degrades the performance. This is confirmed by the simulation results. Furthermore, it is observed that for the 2MTRP scheme, CoMP with IJDD receiver outperforms NOMA with a 9dB gain at BLER=10^{-5}. This shows the advantage of our proposed scheme both in power saving and the

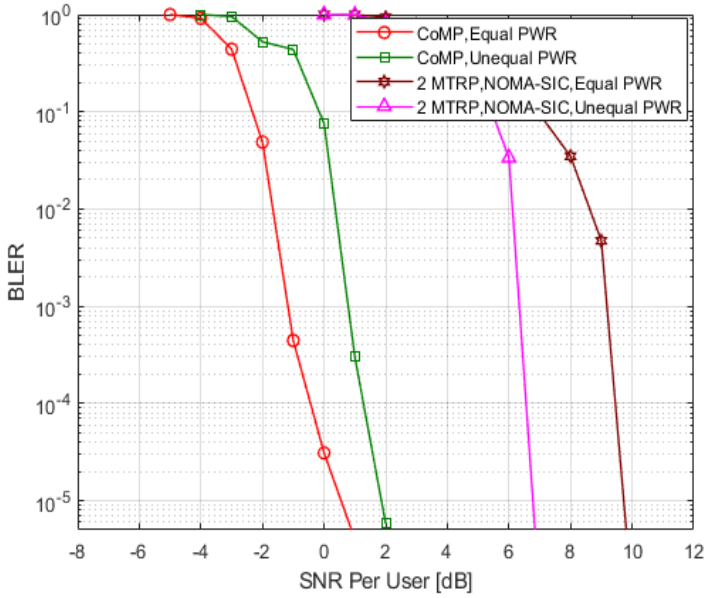

Figure 5.6 Comparing CoMP vs. NOMA for equal power versus unequal power

reliability. Moreover, while NOMA stops functioning, the CoMP with IJDD receiver's performance elevates even as the number of users increases.

5.5.2. Power efficiency

In this section, we evaluate the performance of CoMP with asynchronous transmission where the transmission power is reduced compared to the initial power. In the simulations, imperfect CSI with error variance of $\sigma_{CSI}^2 = 0.1$ is assumed. The simulation results in Figure 5.5 show the two-TRP scenario where the transmission power is reduced to half and one-fourth. It is observed that the performance in CoMP-IJDD is still almost 8dB and 3dB better than the NOMA-SIC, in Figure 5.4, for the power reduced to half and one-fourth of the initial power, respectively.

Moreover, we have evaluated the scenario where the received power from the TRPs are not equal. Two-TRP system is considered where received power from the TRPs are unequal with 3dB difference. The results are provided in Figure 5.6. It is observed that NOMA with unequal power has a performance of 3dB gain compared with equal power NOMA at BLER=10^{-5}. This is due to the fact that the signal from other TRP is considered as interference in NOMA, and so reducing the signal power to half is similar to halving the interference power. However, in case of unequal powers in CoMP, the gain is reduced for about 1dB at BLER=10^{-5}, compared with CoMP with

equal power. This is because the CoMP is based on cooperative recovering of the received signals and if the received power is reduced, so the cooperative effect is reduced as well. It is worth to note that CoMP still outperforms NOMA with 5dB gain even in case of unequal received powers.

5.5.3. Perfect Versus Imperfect CSI

As for the imperfect CSI, Figure 5.7 shows the effect of imperfect CSI on the performance, for two, three, and four TRPs in asynchronous CoMP. The perfect and imperfect CSI are compared,

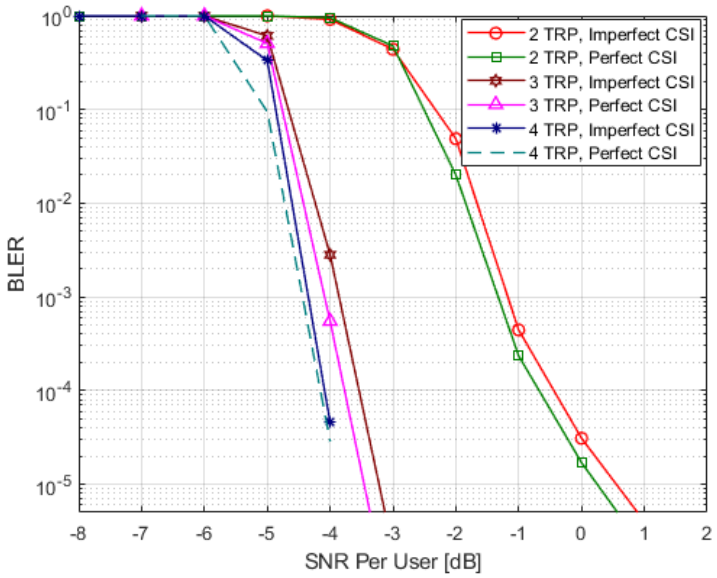

Figure 5.7 Performance in asynchronous CoMP, perfect versus imperfect CSI

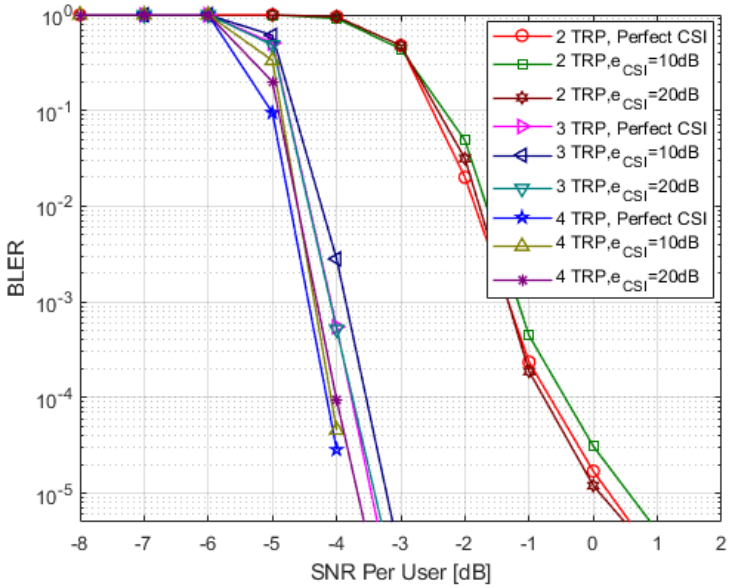

Figure 5.8 Performance in asynchronous CoMP: imperfect CSI 10 vs. 20dB

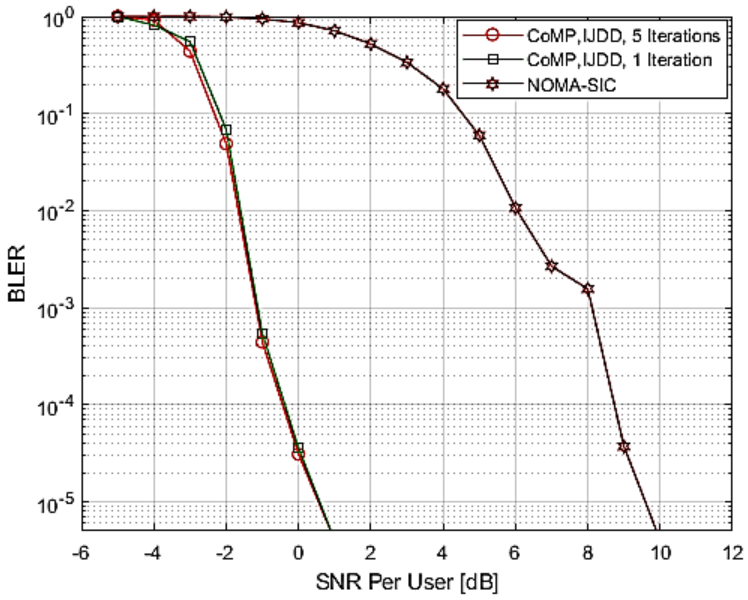

Figure 5.9 Complexity comparison: low-complexity IJDD vs. SIC receiver

where the variance of the error in imperfect CSI is assumed to be $\sigma_{CSI}^2 = 0.1$, reflecting an SINR of 10 dB. It is observed that the channel performance degrades in case of the imperfect knowledge of the channel.

Moreover, we have compared the performance in case of imperfect CSI with different error variances. In Figure 5.8, the e_{CSI}=10dB and 20dB are simulated and compared versus the perfect knowledge of the channel. It is observed that the results for e_{CSI} = 20dB are almost the same as perfect knowledge of the channel. This is to show that e_{CSI}=10dB is the realistic assumption, which we have used in our simulations.

5.5.4. Low Complexity IJDD Receiver

In this section, we have evaluated the number of iterations required in our proposed low-complexity MMSE-based IJDD in asynchronous schemes. Figure 5.9 shows the performance of two-TRP CoMP having IJDD receiver where the number of iterations is limited to single and five iterations. Two-TRP NOMA with SIC receiver is also provided. In NOMA-SIC with N-TRPs, SIC has to perform at least N iterations to recover both data streams [94], which in this case is a minimum of two iterations for the two-TRPs. Based on simulation results, our proposed receiver achieves the BLER=10^{-5} with an average number of 1.00002 iterations for two-TRPs. This implies that the detection module recovers the data streams mostly in the first iteration. It is also

confirmed in Figure 5.9, as IJDD with five iterations outperforms the single iteration system for only 0.1dB at BLER=10^{-5}.

5.6. Discussion

In this chapter, we have investigated the major challenge of the asynchronous reception of data in multi-TRP OFDM-based systems, where the time offsets exceed the length of the cyclic prefix. The accurate mathematical channel model for the asynchronous CoMP is provided and generalized to multiple number of TRPs, which includes both the channel coefficients and the asynchronous channels' cross-correlations. We have developed and generalized the exact expression for the capacity region and outer bound for the sum-rate of multiple TRPs in asynchronous networks. It is shown that while the SIC receiver is suboptimal in asynchronous multiple access channels, significant gain can be realized by taking advantage of the asynchronous channels' cross-correlation, provided that a proper receiver is used. We have proposed the MMSE-based iterative joint detection and decoding (IJDD) receiver, which we have upgraded to be used in asynchronous CoMP channels.

At the presence of CSI estimation error, we have evaluated our proposed scheme through extensive simulations. As one of the benchmarks, we have considered non-orthogonal multiple access (NOMA) where SIC is used at the receiver. It is observed that NOMA-SIC performance degrades severely due to the asynchronous reception, wherein a three-TRP system the block error rate (BLER) would not scale down even for higher SNR.

Simulation results show that our proposed scheme outperforms both single-user and NOMA-SIC in asynchronous channel with imperfect channel knowledge. It is observed that the two, three, and four TRP CoMP with IJDD attain 9, 12, and 13dB gain in comparison to two-TRP NOMA-SIC, respectively. Moreover, the performance elevates with the increase in the number of TRPs, as the error floor in two-TRP BLER does not exist for higher number of TRPs.

As for the complexity, we have compared the number of iterations required in our proposed MMSE-based IJDD versus SIC. The simulation results show that even with bounding the receiver to a single iteration, the performance degrades for only 0.1dB at $BLER = 10^{-5}$ compared to a receiver with five-iterations. Based on simulation results, our proposed receiver achieves the

$BLER = 10^{-5}$ with an average number of 1.00002 iterations for two-TRPs, whereas in a two-user NOMA-SIC, at least two iterations would be required to recover the data.

To conclude, the theoretic findings were confirmed by the simulation results, wherein our proposed scheme the reliability as well as power and spectral efficiency exceed that of the non-cooperative schemes, even as the number of TRPs increases.

Chapter 6 .

Association of the Coordinated Multi-Point Transmission with NOMA

6.1. Introduction

This chapter is the sequel of the previous chapters where the association of the coordinated multi-point (CoMP) and the Non-Orthogonal Multiple Access (NOMA) is investigated. We have proposed our scheme in the next generation of Digital Terrestrial Television (DTT) broadcasting systems, as such the spectral efficiency, coverage, fairness, and reliability are remarkably enhanced.

The demand for the seamless coverage and reliable reception in DTT broadcasting has motivated the state-of-the-art techniques in Advanced Television Systems Committee (ATSC) 3.0 standard. ATSC 3.0 introduces several new features including Layered Division Multiplexing (LDM). The versatile combination of modulation formats and error correcting codes has enabled robust transmissions, while allowing the LDM to extend the spectral efficiency. LDM is a form of power-domain Non-Orthogonal Multiple Access (NOMA), which is based on the constellation superposition technology. In this chapter, we consider the two-layered LDM with different levels of robustness in enhancing the high-quality service coverage and spectral efficiency.

ATSC 3.0 supports the legacy Single Frequency Networks (SFN) where the broadcasters transmit the same multimedia content over the same frequency band. As such, the network can

benefit from improved coverage, spectral efficiency, service quality, and reduced emission power. SFN in the broadcasting networks is a special case of the CoMP network. In SFN DTT, the same multimedia content is transmitted by multiple broadcasters. The SFN DTT mainly aims for improving the coverage and there is no coordination realized from receiver perspective. In other words, receivers are supposed to connect and tune into only one of the broadcasters, while ignoring the signals received from the others. In this chapter, we show that the performance, coverage, as well as spectral and power efficiency could be improved by cooperatively recovering the signals from the coordinating broadcasters.

Due to the nature of the SFN, multiple echoes of the transmitted signals may be received causing the inter-symbol interference (ISI), which may degrade the performance. The conventional broadcasting system is based on interference avoidance and cancellation. In ATSC 3.0 with Orthogonal Frequency Division Multiplexing (OFDM), the effect of ISI is suppressed by employing a guard interval (GI) at the beginning of each OFDM symbol [98]. The GI is set so that it could cover the maximum area between the broadcasters. Considering the distant broadcasting antennas, the GI may span around 400-600 μs, occupying 17-25% of 16k FFT OFDM symbols, in 120-180km distance, respectively.

Moreover, the signals from broadcasters have almost the same power strength at the edge of the DTT coverage areas. Hence, the receivers located in the midway between the broadcasters may experience the two-path zero-dB echo, resulting in a gap in the overlapping areas. In ATSC 3.0, using a directional receiving antenna is the solution to retrieve one of the broadcasted signals [99].

Hence, two of the key challenges in DTT broadcasting networks with ATSC 3.0 are the unfavorable overhead ratio caused by the GI, as well as the need for directional antennas. The impressive features in ATSC 3.0 DTT and multi-TRP networks along with the existing challenges have motivated us in this chapter.

Extending the DTT coverage in single frequency networks with ATSC 3.0 framework, we have considered the LDM at the transmitter to send different multimedia content over the same RF channel. In contrast to the state-of-the-art broadcasting systems that are based on ignoring or cancelling the signals from other transmitters, we propose a cooperative scheme to recover the signals from the coordinating broadcasters.

We consider the potential reception of the transmitted SFN signals with different time delay attributes. The relatively huge GI ratios currently used in ATSC 3.0 to mitigate the impact of the asynchronous reception of the signals could be the bottleneck in achieving the expected spectral efficiency. Therefore, it is very crucial to delve into how the asynchronous reception affects the performance.

While our proposed scheme does not require any guard interval and directional antennas, the coverage is extended throughout the coverage area for both layers in LDM, namely: core-layer and enhanced-layer. Our extensive simulation results show that the reliability and spectral efficiency can exceed that of the non-coordinated reception, provided that the proper receiver is employed.

We propose our receiver based on iterative joint detection and decoding (IJDD), by which the performance elevates even as the number of broadcasters increases. The IJDD receivers proposed in previous chapters were limited to Binary Phase Shift Keying (BPSK) modulation. In this chapter, we have derived an MMSE-based iterative joint detection and decoding receiver for the asynchronous SFN, which is generalized to higher modulation formats.

We have realized the accurate mathematical model for the asynchronous CoMP associated with LDM-NOMA which includes the asynchronous channels' cross-correlations along with the multi-path channel coefficients and the LDM features. Moreover, we have developed the exact expression for the capacity region and inner bound for the sum-rate in asynchronous SFN with embedded LDM. It is based on modeling the channel with memory, where the asynchronous channels' cross-correlations are used as extra sources of information.

Our simulation results show that association of our proposed asynchronous channel's model in iterative joint detection and decoding receiver can outperform the state-of-the-art schemes significantly.

This chapter is organized as follows. In Section 6.2, the system and channel model are provided. We evaluate the capacity region of our proposed CoMP-NOMA scheme in Section 6.3, followed by Section 6.4 where we have proposed the IJDD receiver and have evaluated the receivers computational complexity. Simulation results are provided in section 6.5, validating the theoretical findings that are concluded in Section 6.6.

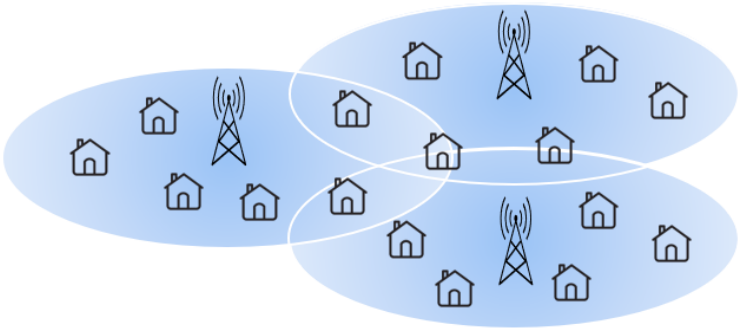

Figure 6.1. Single Frequency Networks

6.2. System Model

Consider an SFN DTT broadcasting system with N broadcasters, where each broadcaster employs a fixed antenna pattern, along with rooftop fixed or portable single-antenna receivers, see Figure 6.1. The broadcasters coordinate to share the same resource of time and frequency to jointly transmit the same multimedia content to the target coverage area.

6.2.1. ATSC 3.0 LDM Model

We have considered the two-layer LDM in the ATSC 3.0 broadcasting system, where the layers are generally named core-layer and enhanced-layer. The two layers have different robustness to target various service qualities. Each layer undergoes a different Bit Interleaved and Coded Modulation (BICM) chain. The layers are combined based on a power injection level (IL) before being transmitted through the channel. At the receiver, the core-layer which is the more robust layer, with lower data rate and stronger modulation, is recovered first. The enhanced layer which usually has higher data rate is then recovered in an interference cancellation procedure.

At each broadcaster, the transmit signal is the multiplex of the core-layer and the enhanced-layer data. The superimposed enhanced layer is multiplied by the injection level before being added to the core layer. The block diagram of the coordinating DTT broadcasters with the embedded LDM in an SFN framework is typically shown in Figure 6.2. The S_C and S_E denote the data streams corresponding to core-layer and enhanced-layer, respectively. At the LDM combiner, α is considered as the injection level, as such the power of the enhanced-layer is reduced in the range of $0dB < \alpha \leq 25dB$ below the associated core layer. The $0 < \beta < 1$ is the power

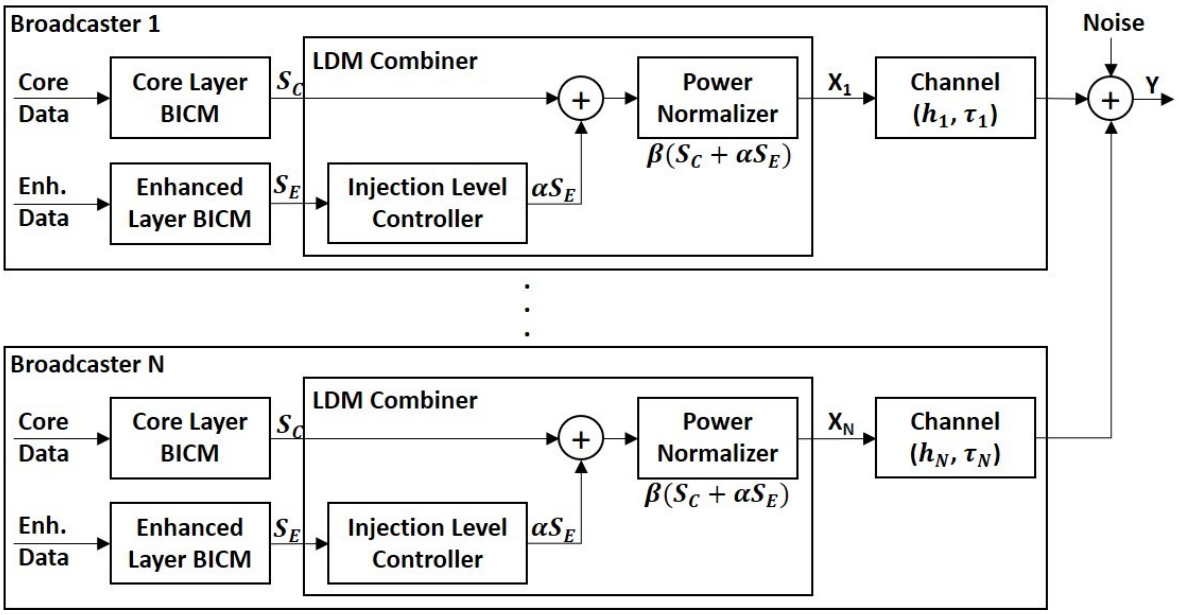

Figure 6.2. Coordinated Multipoint Transmission with Layered-Division Multiplexing

normalizer coefficient to assure the normalized power for the transmit signals. The transmit signal is the superposition of the core and enhanced layers that can be written as

$$x_i(t) = \beta(S_C + \alpha S_E) \tag{6-1}$$

Due to the SFN, the transmit signals include the same content. The transmit signals go through different channels and are received at the receiver with different time delays. The DTT receivers hence receive the summation of the different echoes of the transmit signals plus noise.

The operating parameters in [99] are adopted, where the two-layer LDM with signal to noise ratio (SNR)=0dB for the core-layer and SNR=15dB for the enhanced-layer are referenced. The SNR thresholds are selected such that the core-layer and the enhanced-layer are accessible throughout the coverage area. The core-layer is considered to carry the robust transmission operating at very low SNRs. The enhanced-layer is realized to carry high data rate programs while the robustness and the operating parameters are determined in association with the minimum SNR of 15dB.

6.2.2. Channel Model

We consider a Single-Frequency Network (SFN) applying ATSC 3.0 with OFDM, where the delays from the broadcasters show different time attributes at the receiver. Based on the model considered in Figure 6.2, the received signal at a specific user can be written as

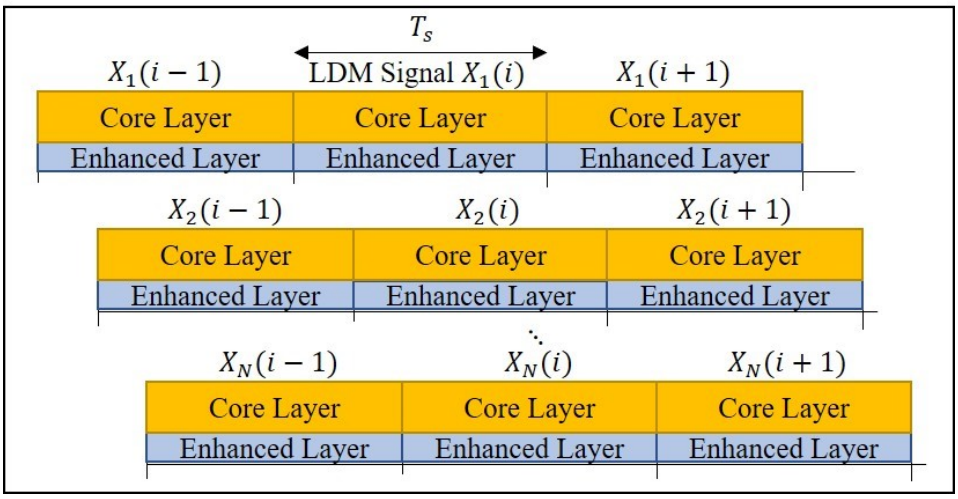

Figure 6.3. Symbol asynchronous CoMP-SFN channel with embedded LDM

$$y(t) = \sum_{i=1}^{N} h_i(t)x_i(t-\tau_i) + n(t) \tag{6-2}$$

Where, x_i is the transmitted data which is the layered-division multiplex of the core-layer and enhanced-layer from broadcaster i, i.e. BR_i. The τ_i denotes the delay, which is an integer multiple of the sample time. The h_i correspond to the independent and identically distributed (iid) channel coefficients from the BR_i to the user, that are circularly symmetric complex normal with Rayleigh magnitude and uniformly distributed phase; $n(t)$ is the complex AWGN, denoted as $n \sim N(0, \sigma_n^2)$. It is assumed that users and broadcasters are aligned at carrier frequency and there is no carrier frequency offset (CFO) between them.

The symbol asynchronous CoMP-SFN channel with embedded LDM can be typically shown in Figure 6.3. It is observed that the core and enhanced layers within each symbol is overlapped with four layers corresponding to the preceding and succeeding symbols of the other broadcasters.

The discrete-time equivalent of the received signal in (6-2) can be written as

$$\boldsymbol{Y}[i, i+1] = \boldsymbol{H}_A[i, i+1]\boldsymbol{X}[i, i+1] + \boldsymbol{N}[i, i+1] \tag{6-3}$$

where $\boldsymbol{Y} \in \mathbb{C}^{2N\times 1}$ is the received signal, $\boldsymbol{H}_A \in \mathbb{C}^{2N\times 2N}$ is the channel matrix, $\boldsymbol{X} \in \mathbb{C}^{2N\times 1}$ is the transmitted signal vector with the embedded LDM, and $\boldsymbol{N} \in \mathbb{C}^{2N\times 1}$ is the added noise. Our proposed asynchronous channel matrix, i.e. $\boldsymbol{H}_A$, includes both the channel coefficients and the asynchronous channels' cross-correlations, which is well investigated in previous chapters.

6.3. Spectral Efficiency Evaluation

In this section, we have evaluated the sum-rate for the LDM-NOMA in the context of the SFN network. Let the single-user spectral efficiency for the core and enhanced-layers be as

$$R_i^l = \frac{1}{4\pi}\int_{-\pi}^{\pi} \log\left(1 + |h(w)|^2 \gamma_i^l(w)\right) dw \tag{6-4}$$

where, $l \in \{CL, EL\}$ denotes the core and enhanced layers, respectively. $h(w)$ is the channel coefficient and $\gamma_i^l(w)$ stands for the signal to interference plus noise ratio (SINR) at a specific receiver and from *i*-th broadcaster per layer l.

The capacity region is calculated in three scenarios as follows.

6.3.1. Interference as Noise (IAN)

Considering the state-of-the-art systems, in this scenario only the signal received from the incumbent broadcaster, i.e. B, is considered and the signals received from other SFN broadcasters are ignored and considered as interference.

Hence, the SINR for the core and enhanced layers at the receiver can be written as

$$\gamma_{B,IAN}^{CL}(w) = \frac{P_{C,B}}{\alpha P_{E,B} + \delta^2 + I_0} \tag{6-5}$$

$$\gamma_{B,IAN}^{EL}(w) = \frac{P_{E,B}}{\delta^2 + I_0} \tag{6-6}$$

Where, $P_{C,B}$ and $P_{E,B}$ are the powers corresponding to the core and enhanced-layer signals, respectively, received from the desired broadcaster B at a specific receiver. The α denotes the linear injection level, I_0 is the interference power from the other broadcasters, and δ^2 is the noise power.

The co-channel interference from other broadcasters exists in both the core and enhanced layers' SINR. Based on the superposition methodology in NOMA, the impact of the enhanced-layer can be seen as the added interference in the SINR of the core-layer. Upon the successful decoding of the core-layer, the enhanced layer SINR is not affected by the core-layer anymore, as it can be seen in (6-6).

6.3.2. Multi-User Detection and Interference Cancellation

The multi-user detection (MUD) and the interference cancellation (IC) is considered as another benchmark scheme. In this scenario only the signal received from the incumbent broadcaster, i.e. B, is considered and the signals received from other SFN broadcasters are detected and cancelled to mitigate their impact as interference.

At a specific receiver, the SINR from the broadcaster B for the core and enhanced layers can be written as

$$\gamma_{B,MUD}^{CL}(w) = \frac{P_{C,B}}{\alpha P_{E,B} + \delta^2} \tag{6-7}$$

$$\gamma_{B,MUD}^{EL}(w) = \frac{P_{E,B}}{\delta^2} \tag{6-8}$$

The co-channel interference from other broadcasters is cancelled in this scenario and so its impact does not exist in either of the core or enhanced layers' SINR. In general, it is expected that the MUD interference mitigation schemes have better performances compared to IAN scheme in the interference-limited SFN systems.

6.3.3. Coordinated Multipoint (CoMP)

In this scenario, we investigate the spectral efficiency in our proposed scheme, where the signals from other broadcasters is neither regarded as noise, nor considered to be ignored or cancelled. Instead, our proposed scheme benefits from the coordinated broadcasters' joint transmission in the context of CoMP and uses the signals received from other SFN broadcasters as extra sources of information. Having multiple transmitters and one receiver, the channel model changes to a multiple-access channel (MAC) instead of the point-to-point channel, where the spectral efficiency is calculated based on the contributions from all broadcasters.

We consider the potential reception of the data streams with different time delay attributes. Considering the symbol asynchronous reception of the transmit signals, the capacity region is adopted from that we calculated in Chapter 5 for the asynchronous CoMP systems. Based on the Equation (5-13), the spectral efficiency can be written as

$$R_1^l + \cdots + R_N^l \leq \frac{1}{4\pi}\int_{-\pi}^{\pi} \log\left[1 + \sum_{i=1}^{N} |h_{ii}(w)|^2 \gamma_i^l(w) + 2\sum_{\substack{i,j=1 \\ i\neq j}}^{N} \left|h_{ij}(w)\right|^2 \left|\mu_{ij}(w)\right| \sqrt{\gamma_i^l(w)}\sqrt{\gamma_j^l(w)}\right] dw \tag{6-9}$$

Where, N is the number of dominant broadcasters that contribute in the SFN close to the target receiver. The terminologies in (6-9) are the same as that discussed in Chapter 5, where the SINR for the data received from i-th broadcaster for the core and the enhanced layers can be written as

$$\gamma_{i,CoMP}^{CL}(w) = \frac{P_{C,i}}{\alpha P_{E,i} + \delta^2} \tag{6-10}$$

$$\gamma_{i,CoMP}^{EL}(w) = \frac{P_{E,i}}{\delta^2} \tag{6-11}$$

In (6-9), the signals received from all N broadcasters are used as sources of information. Also, the extra additive term in (6-9) is achieved due to exploiting the asynchronous channels memory and correlation. As such, the spectral efficiency exceeds that of non-cooperative schemes.

6.4. Receiver Implementation

The iterative joint detection and decoding (IJDD) receiver was proved in previous chapters to be the optimal receiver in a coordinated multipoint (CoMP) scheme with asynchronous reception. The IJDD receiver proposed in previous chapters was based on BPSK modulation format.

In this chapter, the association of CoMP system with NOMA is considered, where the transmit signals include embedded LDM. Due to the different layers of robustness proposed in LDM, the enhanced layer is modulated with higher order modulation formats. In this section, we have first developed the IJDD receiver to accommodate the higher order modulations. We have then used the IJDD block as part of the LDM receiver.

6.4.1. IJDD for Higher Order Modulations

The joint detector is the main block in our receiver which detects the multi-user data based on the aggregate received signal, see Figure 2.8. The optimal IJDD discussed in Chapter 4 has the complexity in order of $O(2^{2N})$, which is not favorable with large number of sources, N. Also, the MMSE-based IJDD proposed in Chapter 5 is based on BPSK modulation.

In this section, we have enhanced the detection module to be used in asynchronous channels with higher order modulation formats. The MMSE filter is modified, where the LLR of code-bits are derived from received symbols. To include the symbols, let the received signal be

$$\boldsymbol{Y}[i, i+1] = \boldsymbol{H}_A[i, i+1]\boldsymbol{A}[i, i+1]\boldsymbol{m}[i, i+1] + \boldsymbol{N}[i, i+1] \tag{6-12}$$

where, $\boldsymbol{m} \in \mathbb{C}^{2N\times 1}$ is the symbols vector and $\boldsymbol{A} \in \mathbb{C}^{2N\times 2N}$ is the diagonal magnitude matrix.

The MMSE filter at the joint detector in the asynchronous channel can be written as

$$\boldsymbol{z}_n(i, i+1) = \boldsymbol{w}_n(i, i+1)^T \mathbf{y}(i, i+1) \tag{6-13}$$

Where, the $\boldsymbol{w}_n$ is employed to minimize the mean square error between the estimated symbol codes and the output of the detector, denoted as

$$\boldsymbol{w}_n(i, i+1) = \arg\min E\{[\boldsymbol{m}_n(i, i+1) - \boldsymbol{w}^T \mathbf{y}(i, i+1)]^2\} \tag{6-14}$$

The soft estimate of the code-bits is calculated based on the *a-priori* information from decoders in previous iteration that can be written as

$$\bar{b}_j(i, i+1) = \tanh\left(\frac{1}{2}{\lambda_2}^p\left[b_j(i, i+1)\right]\right) \tag{6-15}$$

Based on the modulation format, the estimated symbols are calculated, which are denoted as

$$\bar{m}_j(i, i+1) = c\left(\bar{b}_j(i, i+1)\right) \tag{6-16}$$

Where, $c(\boldsymbol{b})$ is the bit to symbol mapping function implying the corresponding complex constellation point.

The extrinsic information delivered by the soft MMSE filter is denoted as

$$z_n(i, i+1) = \{[\boldsymbol{H}_A + \sigma^2\boldsymbol{A}^{-1}]^{-1}\boldsymbol{H}_A\boldsymbol{y}(i, i+1)\} - \bar{\boldsymbol{m}}_n(i, i+1) \tag{6-17}$$

The extrinsic information is then fed to the demodulator to calculate the output of the detection module, i.e. λ_1, in the format of log-likelihood ratio (LLR).

To calculate the LLR for higher modulation formats, we have followed the methods proposed in [103]. In MPSK, all the symbols have the same energy. So, the LLR output can be written as

$$\lambda_{1,MPSK}[b_n(i)] = \ln\left[\frac{\sum_{\boldsymbol{b}:b_n=0}\exp\left(\frac{\langle z_n, c(\boldsymbol{b})\rangle}{\sigma^2}\right)}{\sum_{\boldsymbol{b}:b_n=1}\exp\left(\frac{\langle z_n, c(\boldsymbol{b})\rangle}{\sigma^2}\right)}\right] \tag{6-18}$$

For MQAM, the LLR output is calculated based on squared distance of the constellation points referring to bits equal to one and the ones referring to bits equal to zero [104], denoted as

$$\lambda_{1,MQAM}[b_n(i)] = \ln\left[\frac{\sum_{\boldsymbol{b}:b_n=0}\exp\left(-\frac{\|z_n-c(\boldsymbol{b})\|^2}{2\sigma^2}\right)}{\sum_{\boldsymbol{b}:b_n=1}\exp\left(-\frac{\|z_n-c(\boldsymbol{b})\|^2}{2\sigma^2}\right)}\right] \tag{6-19}$$

6.4.2. IJDD Computational Complexity Analysis

In this section, the order of the computational complexity in our proposed IJDD receiver is investigated. The optimal IJDD was discussed in detail in Section (4.5) with the computation complexity in the order of $O(2^{2N})$, where N is the number of coordinated TRPs [35]. Such order of complexity could not be feasible in practical systems as the number of coordinating multi-points increases.

We evaluate the computational complexity of the IJDD module as it is proposed in this chapter, see Equation (6-17). From the above discussion, it is observed that at each symbol time i, the dominant computation in calculating the soft information delivered by the $z_n(i)$, for $n = 1, \dots, N$, is the $2N$-vector outer product. Thus, in calculating the soft output of the joint detector module, the dominant computation per user per symbol involves a $2N$-vector outer product. Hence, the total computational complexity of the proposed joint detector is in the order of $O(N^2)$. Such order of computational complexity is feasible in practical applications, even as the number of the coordinating TRPs, N, increases.

It is worth to mention that after the first iteration, the performance of the proposed receiver resembles to the performance of a legacy non-iterative receiver, which includes a linear MMSE detector followed by N parallel soft channel decoders.

In the following sections, the simulation results are provided. It can be seen that our proposed receiver with iterative joint detector which is based on our developed asynchronous correlated channel model, outperforms the non-iterative receivers with the interference cancellation procedures. We have also compared the number of iterations required in our proposed IJDD versus MMSE-SIC. The results show that our proposed receiver outperforms the MMSE-SIC with less number of iterations required to recover the data.

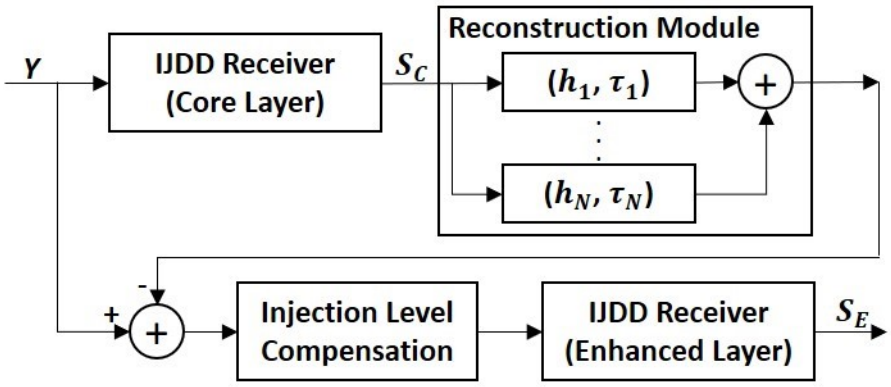

Figure 6.4. Asynchronous CoMP with embedded LDM Receiver

6.4.3. Enhanced Receiver for CoMP with Embedded LDM

The block diagram of the enhanced receiver is provided in Figure 6.4. The CoMP embedded with LDM is considered where the received signals have different time delays. The two-layer LDM is employed, wherein the core-layer is the more robust layer, and the enhanced-layer is the high-rate layer superimposed on the core-layer.

The layered superimposed data streams corresponding to the core and enhanced layer are recovered through a successive procedure. As the first step, the sum of asynchronous received signals enters the IJDD receiver, where the enhanced-layer is considered as the interfering noise. Upon the correct decoding, that could be indicated by parity or cyclic redundancy check (CRC) bits, the core-layer signals corresponding to the coordinated multi-TRPs are reconstructed while reflecting the relative time attributes. The re-constructed core-layer signal is then subtracted from the aggregated received signal. In the second step, the injection level compensation is applied to the signal to recover the enhanced-layer before entering the IJDD receiver.

6.5. Simulation Results

In this section, we have provided the link-level simulation results to demonstrate the effectiveness of our proposed scheme and confirm the information theoretic findings. The simulation assumptions are briefly provided in Table 6-1.

The transmitted signals from broadcasters are assumed to be received with equal average received power, which is the worst-case scenario as they cause the highest interference on each other. The channel is modeled as an asynchronous Rayleigh-fading, where the time offset $\tau =$

Table 6-1, Simulation Assumptions

Channel Model	Rayleigh Fading
Bandwidth	6 MHz
FFT Size	16 k
OFDM Sample Time	0.1447 μs
Antenna Configuration	single-antenna receivers
Average Receiver SNR	Equal average SNR
Target FER	10^{-3}
Symbol Time Offsets	$\tau = 0.2T_s$
Injection Level	19 dB
LDPC Size	64800 bits
Modulation in Core Layer	QPSK
Code Rate in Core Layer	4/15
Modulation in Enhanced Layer	16QAM
Code rate in in Enhanced Layer	10/15

$0.2T_s$ is considered. We have used the Monte Carlo method in our simulations. The achievability is simulated so that the channel code guarantees a frame error rate (FER) not exceeding 10^{-3}. We have evaluated the performance in three scenarios for two-broadcasters model.

Interference as Noise (IAN) Scenario. In the first scenario, interference as noise (IAN) framework is considered with guard-interval of 1024 samples in the 16k FFT size. In the IAN, the interference from the other broadcasters is ignored and considered as noise. This scenario is evaluated as the state-of-the-art system, where the performance degradation is expected due to the severe inter-channel interference.

MMSE-SIC Scenario. In the second scenario, the multiuser detection scheme to mitigate the interference is considered. The legacy minimum mean-square error (MMSE) filter followed by the successive interference cancellation (SIC) receiver is assumed, where no guard interval is considered. This scenario is considered as the benchmark in the multiuser detection schemes. We have shown that SIC receivers are suboptimal in asynchronous channels with ISI in previous chapters. Thus, it is expected to see the effect of ISI in the performance degradation in this scenario.

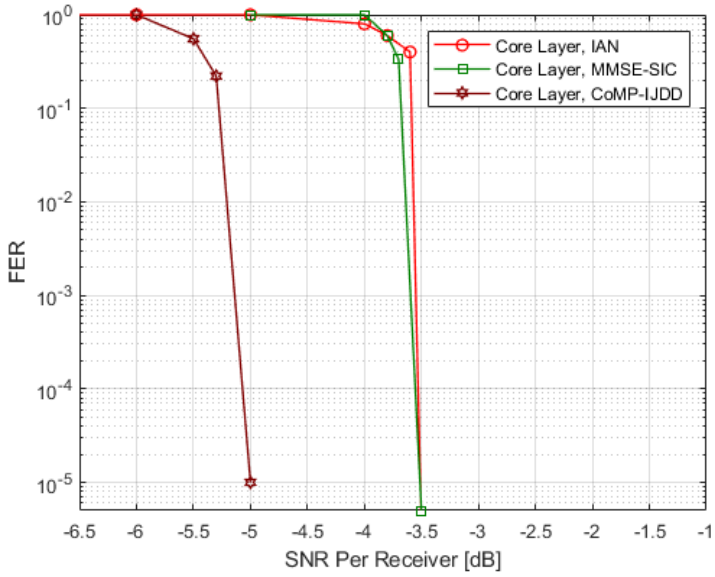

Figure 6.5. Core-Layer Performance Evaluation, Two Broadcasters

CoMP-IJDD Scenario. In the third scenario, we have simulated our proposed MMSE-based iterative joint detection and decoding (IJDD) receiver, considering zero guard interval. Based on the evaluated information theoretic sum-rate, it is expected to achieve enhanced performance compared to the other scenarios.

6.5.1. Performance Evaluation in Core Layer

The core-layer is investigated in Figure 6.5, where the QPSK modulation with LDPC code rate of 4/15 is considered. It is observed that the target $FER = 10^{-3}$ is achieved at $SNR = -3.5dB$ in IAN. The performance in IAN is due to the ultra-robustness of the transmission mode, which is primarily proposed in ATSC 3.0 to enable the receivers to function in very low SNRs.

The MMSE-SIC scheme follows the IAN closely. This is due to MMSE-SIC having the zero-GI, whereas the IAN entails the GI of 1024 samples. Hence, the multiuser detection potential in MMSE-SIC has mitigated the inter-channel interference from the other broadcaster; yet its vulnerability to ISI caused by the asynchronous channel has degraded the performance in zero-guard mode.

As for our proposed scheme based on the CoMP with IJDD receiver, it is observed that the target $FER = 10^{-3}$ is achieved at $SNR = -5.2dB$ for the core-layer. This confirms that IJDD with progressive joint detection and decoding of the data can in fact benefit from the correlation

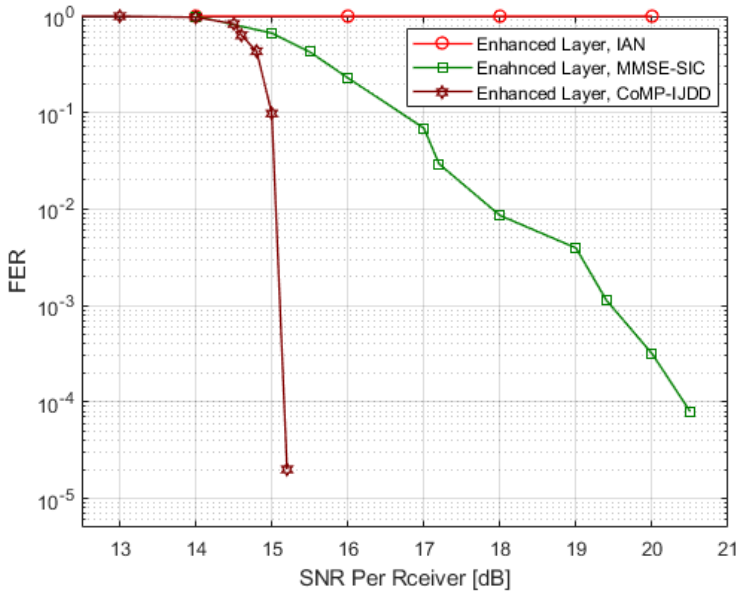

Figure 6.6. Enhanced-Layer Performance Evaluation, Two Broadcasters

in the asynchronous channel. This efficiency is achieved along with improving the reliability in the core layer with more than 1.5dB gain at the target FER compared to the IAN and the MMSE-SIC.

6.5.2. Performance Evaluation in Enhanced Layer

The enhanced-layer is investigated in Figure 6.6, where the 16QAM modulation and 10/15 LDPC code rate is considered. It is observed that the enhanced-layer's performance in IAN scheme degrades drastically as the FER does not scale down even for higher SNR.

As for the MMSE-SIC receiver, the target $FER = 10^{-3}$ is achieved at $SNR = 19.5dB$. In this chapter, we have assumed the operating parameters to enable the access to the enhanced layer throughout the coverage area with minimum SNR of 15dB. So, the implication of zero-GI in enhanced-layer with MMSE-SIC receiver is not feasible in the decent SNR ranges. This was expected, as we have shown that the SIC receivers are suboptimal in channels with ISI. Furthermore, the effect of ISI can be clearly seen in Figure 6.6, as the MMSE-SIC scheme experiences an error floor starting around FER of 10^{-2} which is due to the asynchronous reception of the data streams.

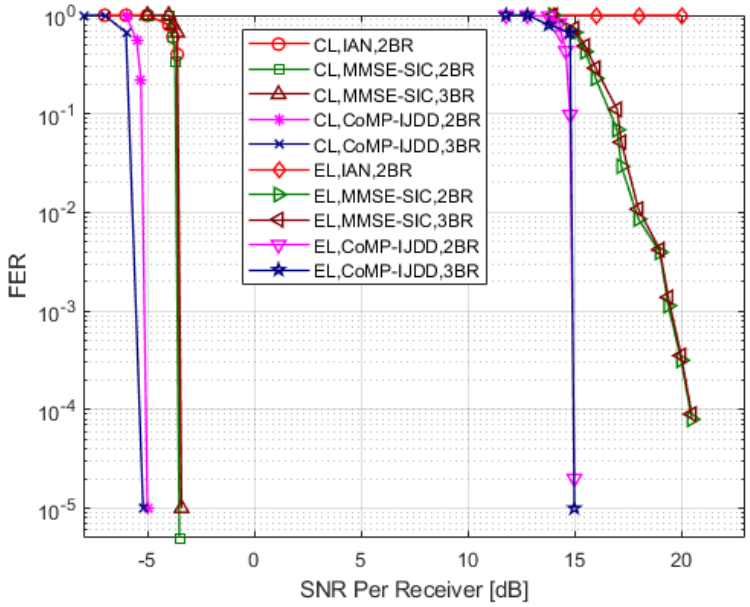

Figure 6.7. Enhanced-Layer and Core-Layer, two and three broadcasters

The result plot shows that our proposed scheme with IJDD receiver achieves the target $FER = 10^{-3}$ at $SNR = 15dB$. The results confirm that our proposed scheme extends the coverage of the enhanced layer throughout the coverage area in addition to improving the reliability with 4.5 dB gain in the enhanced-layer compared to the MMSE-SIC receiver.

6.5.3. Power Efficiency Evaluation

In this section, the power efficiency is investigated. One of the primary advantages in SFN networks is the reduction in the emission power. The FER evaluation of the core-layer (CL) and enhanced-layer (EL) are provided in Figure 6.7. The results show that our proposed scheme with the IJDD outperforms the MMSE-SIC with a gain of 1.5dB and 4.5dB at the target $FER = 10^{-3}$ in the core-layer and enhanced-layer, respectively.

Moreover, the MMSE-SIC and CoMP-IJDD scenarios with two and three broadcasters (BR) are evaluated, where FER of the three broadcasters stays almost in the same range as for the two. This confirms the information theoretic findings and seconds the feasibility of extending the CoMP-SFN to higher number of broadcasters.

6.5.4. Receiver Complexity Evaluation

We have compared the number of iterations required in the MMSE-SIC and CoMP-IJDD as the metric for the complexity of the receivers. In a system with N broadcasters, the successive interference cancellation in MMSE-SIC requires at least N iterations to recover the data streams. However, our simulation results in a CoMP-SFN with two broadcasters show an average of 1.09 iterations in the IJDD at the target $FER = 10^{-3}$. This implies that the data streams received from the two broadcasters have been mostly recovered at the first iteration, which is due to the efficiency of the proposed channel modelling and joint detection scheme.

6.6. Discussion

In this chapter, we have considered the association of the coordinated multi-point (CoMP) transmission with embedded non-orthogonal multiple access (NOMA). We have investigated the major challenge of the asynchronous reception of data in the SFN DTT systems in the context of ATSC 3.0, where zero guard interval and no directional antennas are exercised. The two-layered LDM is considered. In order to realize the different robustness levels proposed in LDM, we have developed the enhanced IJDD receiver for the higher modulation formats.

The performance in the state-of-the-art non-coordinated IAN and MMSE-SIC receivers are evaluated, where the former is equipped with GI and the latter has zero-GI. Simulation results show that in a zero-GI system, the association of our proposed asynchronous channel model with the IJDD receiver outperforms both state-of-the-art schemes significantly. As for the complexity, we have compared the number of iterations required in our proposed IJDD versus MMSE-SIC. The simulation results show that our proposed receiver achieves the $FER = 10^{-3}$ with an average number of 1.09 iterations for two broadcasters, wherein a similar system with MMSE-SIC, at least two iterations are required to recover the data.

To conclude, the theoretic findings were confirmed by the simulation results. While extending the core and enhanced layers' coverage, in our proposed scheme the reliability as well as power and spectral efficiency exceed that of the non-coordinated schemes, even with zero-guard interval and as the number of broadcasters increases.

Chapter 7

Conclusion and Future Work

7.1. Conclusion

In this thesis, we have investigated the coordinated multi-point networks as a means of reusing the limited resources of time and frequency to improve the reliability, as well as the spectral and power efficiency in large-scale networks with massive connectivity. We have addressed two main challenges in coordinated multi-point networks including the time-asynchronous reception of the data streams and imperfect knowledge of the Channel State Information (CSI).

We have realized an accurate mathematical model for the asynchronous channels in coordinated multipoint schemes. The asynchronous received signals from the multi-points are modelled in a channel with memory, where the cross-correlations between the asynchronous channels are included along with the channel coefficients in the extended asynchronous channel matrix. This is succedent of the Salehi, Cover and ElGamal theorem in [38], wherein taking advantage of the partial information of the sources about the others can lead to an error-free transmission. Thus, we employ the unwanted coding provided by the asynchronous channel's cross-correlations as extra information instead of discarding it.

We have developed the exact expression for the capacity region and the bound for the sum-rate in the asynchronous multipoint schemes. It is based on our proposed asynchronous channel model, where the channels' cross-correlations are used as extra sources of information instead of being cancelled. The evaluated capacity is different from memoryless MAC capacity and has a

supplementary term in the sum-rate due to the asynchronous channel's cross-correlation with a linear effect on the sum-rate.

Moreover, we have shown that the Successive Interference Cancellation (SIC) receivers are suboptimal in asynchronous multiple access channels as they either cancel or discard the extra information provided by the asynchronous channel's cross-correlation. Hence, we have provided an improved iterative joint detection and decoding (IJDD) receiver to be used in asynchronous multipoint schemes, which we have further developed in a low-complexity MMSE-based IJDD receiver. Our simulation results show that the association of our proposed asynchronous channel's model in IJDD receiver, can outperform the state-of-the-art non-iterative schemes significantly, even as the number of Transmission and Reception Points (TRPs) increases.

As for the complexity of the proposed joint detection module, we have reduced the receiver's complexity from exponential order to the quadratic. As such, the computational complexity is feasible in practical applications. Finally, we have considered reasonably complex models in the simulations, reflecting interference scenarios such as imperfect CSI.

In Chapter 3, we have investigated the cooperative Non-Orthogonal Multiple Access (NOMA) in a multipoint downlink network. The system model was based on a single-frequency multi-beam satellite system, where the receivers at the border of the beams would experience a severe interference from the adjacent beams. We have proposed that instead of avoiding and fighting the interference, the signal received from the adjacent beam could be used as the extra source of data, as in NOMA. In a system-level analysis, we have provided the optimal user-pairing areas within a cell/beam with two or three cooperative beams. Also, the applicability of the proposed scheme was verified through link-level simulations that showed the gain over the state-of-the-art systems.

In chapter 4, we have investigated the association of the source-coding and multipoint schemes in a jointly cooperative framework. We have addressed the challenges in asynchronous multipoint uplink with the objective to improve the capacity in large networks with low power sensing elements. Considering large-scale networks, the legacy Orthogonal Multiple Access (OMA) schemes could be insufficient. On the other hand, applying NOMA may require huge control overhead to accommodate large number of cooperating nodes. Thus, we have proposed the scheme where the terminals cooperate in sharing and combining their data and jointly transmitting identical content over NOMA channel. The proposed technique takes advantage of the fact that transmitters

are privy to whole data in order to boost the spectral and power efficiency, while increasing the reliability.

In Chapter 5, we have extended our scheme to the downlink of the OFDM-based non-coherent multi-point networks. We have provided our theorem defining the outer bound for the capacity region of asynchronous multi-TRP systems as the closure of the convex hull of the achievable rates. The provided sum-rate is different from memoryless MAC, as it has a supplementary term in the sum-rate depending on the asynchronous channel's cross-correlations. The number of supplementary terms increase with the number of data streams (TRPs) as it denotes the effect of the received signals. In fact, the number of supplementary terms is equal to the combination of two taken from N as the number of TRPs, i.e. $\binom{N}{2}$. This implies that the performance improves as the number of the TRPs increases. Our extensive simulation results have validated the proposed theoretic findings providing a considerable boost in the channel reliability, while enhancing the spectral and power efficiency, even as the number of TRPs increases.

In chapter 6, we have considered the association of the multipoint schemes and NOMA through a symbol asynchronous multipoint channel with embedded Layered-Division Multiplexing (LDM). We have proposed our scheme in the next generation of Digital Terrestrial Television (DTT) broadcasting systems, as such we have addressed the challenges in Single Frequency Network (SFN) DTT including the spectral efficiency, coverage, fairness, and reliability. We have proposed a cooperative scheme with zero-GI and no need for directional antennas to recover the signals from the coordinating broadcasters, instead of ignoring them. We have extended the MMSE-based IJDD receiver for the asynchronous SFN, which is generalized to higher modulation formats. We have also realized the channel model and the channel's capacity for asynchronous CoMP associated with LDM-NOMA. The simulation results confirm that our proposed scheme extends the coverage of both core and enhanced layer throughout the coverage area in addition to improving the reliability, power and spectral efficiency.

7.2. Future Work

The proposed schemes in this thesis to cope the challenges in coordinated multipoint networks can be developed beyond the considered models.

In the asynchronous channel model, one of the schemes that could be investigated further is considering the frame asynchronization in addition to the currently considered symbol asynchronization. The methods on the soft integration of the multiple received data streams as well as the parallel or successive processing could be useful in applications with frame asynchronicity.

Moreover, in this thesis, it was assumed that the transmitters and receivers are aligned at carrier frequency and there is no carrier frequency offset (CFO) between them. Considering the CFO and Doppler effect can be considered as future work to be used specifically in the applications with high-speed attributes.

Furthermore, the performance of the proposed schemes could be evaluated in multi-antenna receivers, as in Multi-Input Multi-Output (MIMO) or Single-Input Multi-Output (SIMO) systems. Thus, the enhanced channel model may be proposed, as such the inter-layer interferences could be considered as well.

As for the measurement of the CSI, the methods on measuring the coefficients of the proposed asynchronous channel can be considered as the future work. The challenges to consider the tradeoff between the payload of the overhead and the conveyed information in the feedback CSI could impressively impact the methodology and system's performance.

Finally, our proposed theorem on the outer bound for the capacity region of asynchronous multi-TRP systems has been investigated and proved for Multiple Access Channels (MAC) and based on the duality between the MAC and the broadcasting channels. An extension of our theorem could be considering the broadcast channels and investigating the corresponding capacity region.

7.3. Publications

The following is the list of the publications that are based on the results investigated in this thesis,

- Nazli Khan Beigi, M.R. Soleymani, "Ultra-Reliable Energy-Efficient Cooperative Scheme in Asynchronous NOMA with Correlated Sources," in IEEE Journal on Internet of Things, April 2019
- Nazli Khan Beigi, M.R, Soleymani, "NOMA-Based Network Coding in IoT Networks with Correlated Sources," in IEEE Annual Consumer Communications & Networking Conference (CCNC), Jan. 2020

- Nazli Khan Beigi, M.R. Soleymani, “Cooperative NOMA in Multi-Content Multimedia Broadcasting Systems,” in ICC Workshop 2018
- Nazli Khan Beigi, M.R. Soleymani, “Interference Management Using Cooperative NOMA in Multi-Beam Satellite Systems,” in ICC 2018
- Nazli Khan Beigi, M.R. Soleymani, “Channel Estimation for Overlay Coding in Multibeam Satellite Systems,” in IEEE VTC, Sept. 2017
- Nazli Khan Beigi, M. R. Soleymani, “Increasing Bandwidth Efficiency in Multibeam Satellite Systems Under Interference Limited Condition Using Overlay Coding”, in IEEE VTC, June 2017

References

[1] M. Bennis, M. Debbah, H. V. Poor, "Ultra-Reliable and Low-Latency Wireless Communication Tail, Risk and Scale," in *IEEE Trans. On Information Theory*, Vol. 106, no. 10, pp.1834-1853, Oct. 2018

[2] C. Mahapatra, *et al.,* "A Reliable & Energy Efficient IoT Data Transmission Scheme for Smart Cities based on Redundant Residue based Error Correction Coding," in *Proc. SECON*, June 2015

[3] Z. Ding, *et al.,* "On the Performance of Non-Orthogonal Multiple Access in 5G Systems with Randomly Deployed Users", in *IEEE Signal Processing Letters*, Vol. 21, no. 12, pp. 1501-1505, Dec. 2014

[4] Z. Ding, M. Peng, H. Vincent Poor, "Cooperative NOMA in 5G systems," in *IEEE Commun. Letters*, Vol.19, no.8, pp. 1462-1465, Aug. 2015

[5] Z. Chen, Z. Ding, X. Dai, and R. Zhang, "An optimization perspective of the superiority of NOMA compared to conventional OMA," in *IEEE Trans. On Signal Processing*, Vol. 65, no. 19, pp. 5191-5202, Oct. 2017

[6] Z. Yang, *et al.,* "A General Power Allocation Scheme to Guarantee Quality of Service in Downlink and Uplink NOMA", *IEEE Trans. On Wireless Commun.*, Vol.15, no. 11, pp. 7244-7257, Nov. 2016.

[7] S.M. Islam, *et al.,* "Power-Domain Non-Orthogonal Multiple Access (NOMA) in 5G Systems: Potentials and Challenges," in *IEEE commun. Surveys & tutorials*, Vol. 19, no. 2, pp. 721-742, 2017

[8] H. Nikopour and H. Baligh, "Sparse code multiple access," in *Proc. PIMRC*, pp. 332-336, Sep. 2013

[9] Z. Yuan, et al., "Multi-user shared access for internet of things," in IEEE Vehicular Tech. Conference, pp. 1-5, May 2016

[10] N.A. Khan Beigi, M.R. Soleymani, "Interference management using cooperative NOMA in multibeam satellite systems," in Proc. ICC, May 2018

[11] A. Haghighat, et al., 'On the performance of IDMA-based NOMA schemes,' in IEEE *Vehicular Tech. Conference*, Sept. 2017

[12] M. Mohammadkarami, M. Ahmad Raza, O.A. Dobre, "Signature-based non-orthogonal massive multiple access for future wireless networks," in *IEEE Vehicular Tech. Magazine*, Vol. 13, no. 4, pp. 40-50, Dec. 2018

[13] A. Avranas, M. Kountouris, P. Ciblat, "Energy-Latency Tradeoff in Ultra-Reliable Low-Latency Communication with Retransmissions," in *IEEE J. on Selected Areas*, Vol. 36, no. 11, pp. 2475-2485, May 2018.

[14] M. Sartipi, F. Fekri, "Distributed source coding using short to moderate length rate-compatible LDPC codes: the entire Slepian-wolf rate region," in *IEEE Trans on Commun.*, Vol. 56, no. 3, pp. 400-411, March 2008

[15] S. S. Pradhan and K. Ramchandran, "Distributed source coding: symmetric rates and applications to sensor networks," in *Proc. IEEE Data Compression Conference*, pp. 363–372, Mar. 2000.

[16] A. D. Murugan, P. K. Gopala, H. El Gamal, "Correlated Sources over wireless channels: cooperative source-channel coding," in *IEEE Journal on selected areas in commun.*, vol. 22, no. 6, pp. 988-998, Aug. 2004

[17] A. E. Mostafa, Y. Zhou, V. Wong, "Connectivity Maximization for narrowband IoT systems with NOMA,' in *Proc. ICC*, May 2017

[18] M. Shirvanimoghaddam, M. Dohler, S. J. Johnson, "Massive Non-Orthogonal Multiple Access for Cellular IoT: Potentials and Limitations," in *IEEE Commun. Magazine*, Vol, 55, no.9, pp. 55-61, Sept 2017

[19] H. Haci, H. Zhu, J. Wang, 'Performance of NOMA with a Novel Asynchronous Interference Cancellation Technique', in *IEEE Trans on Commun.*, Vol. 65, no. 3, pp. 1319-1335, March 2017

[20] M. Yemini, A.S. Baruch, A. Leshem, 'On the multiple access channel with asynchronous cognition,' in *IEEE Trans. on information theory*, Vol. 62, no. 10, pp. 5643-5663, Oct. 2016

[21] J. Cui, *et al.*, 'Asynchronous NOMA for downlink transmission,' in *IEEE Communication letters*, Vol. 21, no.2, pp. 402-405, Feb.2017

[22] X. Wang, F. Labeau, L. Mei, 'Asynchronous uplink NOMA with cyclic prefix', *IEEE wireless commun. & networking conf.*, April 2018

[23] M.Chen, Y. Miao, Y. Hao, K. Hwang, "Narrow band internet of things," in *IEEE Access*, Vol. 5, pp. 20557-20577, Sept. 2017

[24] H. Ji, *et al.*, "URLLC Communications in 5G Downlink: Physical Layer Aspects," in *IEEE Trans on wireless commun*., Vol. 25, no. 3, pp. 124-130, June 2018

[25] T. M. Cover and J. A. Thomas, Elements of Information Theory, 2nd ed. New York, NY, USA: Wiley-Interscience, 1991

[26] Abbas El Gamal and Young-Han Kim, Network Information Theory, Cambridge University Press, 2012

[27] Z. ding, *et al.*, "A survey on NOMA for 5G networks: research challenges and future trends," in *IEEE Journal on Selected Areas in Commun.*, Vol. 35, no. 10, pp. 2181-2195, Oct. 2017

[28] L. Welch, ''Lower bounds on the maximum cross correlation of signals,'' in *IEEE Trans. Inf. Theory*, vol. 20, no. 3, pp. 397-399, May 1974.

[29] D. Slepian, J. Wolf, "Noiseless coding of correlated information sources," in *IEEE Trans. Inform. Theory*, vol. 19, no. 4, pp.471-480, July 1973.

[30] J. Kim, I. Lee, "Capacity analysis of cooperative relaying systems using non-orthogonal multiple access," in *IEEE Commun. Letters*, Vol.19, no.11, pp. 1949-1952, Nov. 2015

[31] S. Luo and K. C. Teh, "Adaptive transmission for cooperative NOMA system with buffer-aided relaying," in *IEEE Commun. Lett.*, vol. 21, no. 4, pp. 937–940, Apr. 2017.

[32] S. Verdu, 'The capacity region of symbol-asynchronous Gaussian multiple-access channel', *IEEE Trans. On Information Theory*, Vol. 35, no. 4, pp.733-751, July 1989

[33] R.S. Cheng, S. Verdu, 'Gaussian multi-access channels with ISI: capacity region and multiuser water-filling', *IEEE Trans. On Information Theory*, Vol. 39, no.3, pp. 773-785, May 1993

[34] C. Zeng, *et al.*, 'Optimal water-filling algorithms for a Gaussian multi-access channel with inter-symbol interference', in *Proc. ICC*, June 2001

[35] X. Wang, H. Vincent Poor, "Iterative (turbo) soft interference cancellation and decoding for coded CDMA," in *IEEE Trans on Commun*, Vol. 47, no. 7, pp. 1046-1061, July 1999

[36] M. Al-Imari, *et al*, "Uplink NOMA for 5G Wireless Networks," in *Proc. ISWCS*, Aug. 2014

[37] A. Benjebbour, *et al*, "NOMA: From Concept to Standardization," in *Proc. CSCN*, Oct. 2015

[38] T. M. Cover, A. El-Gamal, M. Salehi, "Multiple Access Channels with Arbitrarily Correlated Sources", in *IEEE Trans. On Information Theory*, Vol. 26, no.6, pp. 648-657, Nov. 1980

[39] C. Fragouli, et al., "Wireless network coding: opportunities and challenges," in *IEEE Military Commun. Conf.*, Feb. 2008

[40] S. Verdu, Multi-user detection, Cambridge Univ. Press, UK, 1998

[41] Katona, Z., et al., " Performance, cost analysis, and ground segment design of ultra high throughput multi-spot beam satellite networks applying different capacity enhancing techniques," in Int. J. Satellite Communication Network, 2016, vol. 34, pp. 547–573.

[42] M. Angelone, et al., "Performance of a combined dynamic rate adaptation and adaptive coding modulation technique for a DVB-RCS2 system," in Adv. Sat. Multimedia Sys. Conf., Sept. 2012, pp. 124– 131

[43] F. Lombardo, et al. "Throughput distribution analysis of return link multi-gateway interference cancellation strategies for multi-beam broadband satellite systems", in 2012 IEEE Globecom, pp. 95-99.

[44] M. Caus, et al., "An innovative interference mitigation approach for high throughput satellite systems," in IEEE International Workshop of Signal Processing Advances in Wireless Comm., 2015, pp. 515-519

[45] G. Colavolpe, et al., "On the application of multiuser detection in multibeam satellite systems," in IEEE Intern. Conf. Commun., June 15

[46] G. Colavolpe, et al., "Multiuser detection in multibeam satellite systems: Theoretical analysis and practical schemes," in Proc. Inter. Workshop on Signal Proc. Advances for Wireless Commun., June 2015

[47] Z. Ding, L. Dai, H.V. Poor, “MIMO-NOMA design for small packet transmission in the Internet of Things,” in IEEE Access, 2016

[48] Z. Ding, P. Fan, H.V. Poor, “Impact of user pairing on 5G NOMA downlink transmissions,” in IEEE TVT, 2016.

[49] Z. Ding, L. Dai, H.V. Poor, “Relay selection for Cooperative NOMA,” in IEEE Wireless Communication Letters, Vol. 5, no, 4, pp. 416-419, August 2016

[50] M. F. Hanif, Z. Ding, T. Ratnarajah, G. K. Karagiannidis, “A Minorization-Maximization Method for Optimizing Sum Rate in Non-Orthogonal Multiple Access Systems”, IEEE Transactions on signal processing, vol. 64, no. 1, pp. 76-88, Jan. 2016

[51] Z. Ding, F. Adachi and H. V. Poor, “The Application of MIMO to Non-Orthogonal Multiple Access”, IEEE Transactions on signal communications, vol. 15, no. 1, pp. 537-552, Jan. 2016

[52] Z. Ding, L. Dai and H. V. Poor, “MIMO-NOMA Design for Small Packet Transmission in the Internet of Things”, IEEE Access, Vol. 4, pp. 1393-1405, April 2016.

[53] Z. Ding, P. Fan & H. V. Poor, “Random Beamforming in Millimeter-Wave NOMA Networks”, IEEE Access, vol. 5, pp. 7667-7681, 2017.

[54] Y. Liu, Z. Ding, M. Elkashlan & H. V. Poor, “Cooperative Non-Orthogonal Multiple Access with Simultaneous Wireless Information and Power Transfer”, IEEE Journal on Selected Areas in Communication, Vol. 34, no. 4, pp. 938-953, April 2016.

[55] X. Zhu, C. Jiang, L. Kuang, N. Ge, J. Lu, “Non-Orthogonal Multiple Access Based Integrated Terrestrial-Satellite Networks,” in IEEE Journal on Selected Areas in Communication, Vol. 35, no. 10, pp. 2253-2267, July 2017.

[56] H. Chaouech, R. Bouallegue, “Channel estimation and detection for multibeam satellite communications”, in IEEE Asia Pacific Conf. on Circuits and Systems, 2010, pp. 366-369

[57] W. Gappmir, M. Bergmann, B. S. Rechberger, “New results on location aware channel estimation for multibeam satellite links”, in IEEE Communications Letters, vol. 18, No. 8, Aug 2014, pp.1355-1358

[58] L. Xiao, L. Cottatellucci, “Contention resolution and channel estimation in satellite random access channels”, in IEEE Int. Conf. on Communications in China, 2012, pp.562-567

[59] N. Nonaka, A. Benjebbour, K. Higuchi, “System level throughput of NOMA using intra-beam superposition coding and SIC in MIMO downlink when channel estimation error exists”, in IEEE Int. Conf. on Communications Systems, 2014, pp. 202-206

[60] ETSI EN 302 307 v1.2.1, “Digital Video Broadcasting (DVB); Second generation framing structure, channel coding and modulation systems for Broadcasting, Interactive Services, News Gathering and other broadband satellite applications (DVB-S2).”

[61] Yang, Z. Ding, P. Fan, G. Karagiannidis, “On the Performance of Non-Orthogonal Multiple Access Systems with Partial Channel Information”, IEEE Transactions on communications, vol. 64, no. 2, pp. 654-667, Dec. 2015.

[62] N. Jindal, et al., “On the Duality between General Multiple-Access/Broadcast Channels,” in ISIT 2003, June 2003, pp. 313

[63] B.F. Beidas, H. El Gamal, S. Kay, “Iterative interference cancellation for high spectral efficiency satellite communications,” in IEEE Trans on Communications, vol. 50, no. 1, pp. 31-36, Jan 2002.

[64] Z. Ding, et al., “On the performance of NOMA in 5G systems with randomly deployed users,” in IEEE Sig. Proc. Let., Vol 21, No.2, 2014

[65] Z. Ding, M. Peng, H. Vincent Poor, “Cooperative non-orthogonal multiple access in 5G systems,” in IEEE Commun. Letters, Vol.19, No.8, Aug. 2017, pp. 1462-1465

[66] J. Kim, I. Lee, “Capacity analysis of cooperative relaying systems using non-orthogonal multiple access,” in IEEE Commun. Letters, Vol.19, No.11, Nov. 2015, pp. 1949-1952.

[67] M. J. Hagh and M.R. Soleymani, “Raptor coding for non-orthogonal multiple access channels,” in IEEE ICC 2011 proceedings, pp. 1-6.

[68] N. Khanbeigi, M. R. Soleymani, “Increasing Bandwidth Efficiency in Multibeam Satellite Systems Under Interference Limited Condition Using Overlay Coding”, in IEEE Vehicular Tech. Conf., June 2017

[69] N. Khan Beigi, M.R. Soleyamni, “Channel Estimation for Overlay Coding in Multibeam Satellite Systems,” in IEEE VTC, Sept. 2017

[70] Digital Video Broadcasting (DVB), “Implementation guidelines for the second generation system for Broadcasting, Interactive Services, News Gathering and other broadband satellite applications; Part 2 S2 Extensions (DVB-S2X),” DVB Document A171-2, March 2015

[71] P. Kyritsi, A. Valenzuela, D. C. Fox, “Channel and capacity estimation errors”, in IEEE Commun. Letters, Vol. 6, No. 12, Dec. 2002

[72] P. Marsch, G. Fettweis, "Uplink CoMP under a Constrained Backhaul and Imperfect Channel Knowledge," in IEEE Trans. on Wireless Commun., Vol. 10, No. 6, pp. 1730-1742, June 2011

[73] Irmer et al., “CoMP: Concepts, performance, and field trial results,” IEEE Commun. Mag., vol. 49, no. 2, pp. 102–111, Feb. 2011.

[74] Z. Wei, C. Masouros, K Wong, X. Kang, “Multi-Cell Interference Exploitation: Enhancing the Power Efficiency in Cell Coordination,” in IEEE Trans on Wireless Commun, Vol. 19, No. 1, 2020

[75] M. Khoshnevisan et al., “5G Industrial networks with CoMP for URLLC and time sensitive network architecture”, in IEEE Journal of Selected Areas, Vol. 37, No. 4, pp. 947-959, April 2019

[76] X. Yu, Q. Cui, M. Haenggi, “Coherent joint transmission in downlink heteroheneous cellular networks,” in IEEE wireless commun. Letters, Vol. 7, No. 2, pp. 274-277, April 2018

[77] H. Pilaram, M. Kiamari, B. H. Khalaj, “Distributed Synchronization and Beamforming in Uplink Relay Asynchronous OFDMA CoMP Networks,” in IEEE Trans on Wireless Commun, Vol. 14, No. 6, 2015

[78] A. M. Hamza, J.W. Mark, E.A. Sourour, “Interference Analysis and mitigation for time-asynchronous OFDM COMP Systems,” in IEEE Trans. On Wireless Commun., Vol. 17, No. 7, pp. 4780-4791, July 2018

[79] S. Wu, Y. Qi, “Centralized and distributed schedulers for non-coherent joint transmission,” in IEEE Globecom workshops, 2018

[80] R. Tanbourgi, S. Singh, J. G. Andrews, F. K. Jondral, “Analysis of non-coherent joint transmission cooperation in heterogeneous cellular networks,” in IEEE International Conference on Commun.(ICC), 2014

[81] R. Tanbourgi, S. Singh, J. G. Andrews, F. K. Jondral, "A tractable model for noncoherent joint-transmission base station cooperation," in IEEE Trans. On Wireless Commun., Vol. 13, No. 9, pp. 4959-4973, Sept. 2014

[82] M. Shipon Ali, E. Hossain, A. Al-Dweik, D. In Kim, "Downlink power allocation for CoMP-NOMA in multi-cell networks," in IEEE Trans. On Commun., Vol. 66, No. 9, pp. 3982-3998, Sept. 2018

[83] S. Misara, A. Swami, L. Tong, "Cutoff rate optimal binary inputs with imperfect CSI," in IEEE Trans on Wireless Commun, Vol. 5, No. 10, 2006

[84] R1-1903043, "Multi-TRP Enhancement," in 3GPP TSG-RAN WG1, #96, Qualcomm Incorporated, Feb. 2019

[85] N. A. Khan Beigi, M.R. Soleymani, "Ultra-Reliable Energy-Efficient Cooperative Scheme in Asynchronous NOMA with Correlated Sources," in IEEE IoT Journal, Vol. 6, No. 5, April 2019.

[86] M. Medard, "The effect upon channel capacity in wireless communications of perfect and imperfect knowledge of the channel," IEEE Trans. Inf. Theory, vol. 46, no. 3, pp. 933–946, May 2000

[87] T. Yoo and A. Goldsmith, "Capacity and power allocation for fading MIMO channels with channel estimation error," IEEE Trans. Inf. Theory, vol. 52, no. 5, pp. 2203–2214, May 2006

[88] A. Shaverdian and M. R. Nakhai, "Robust distributed beamforming with interference coordination in downlink cellular networks," IEEE Trans. Commun., vol. 62, no. 7, pp. 2411–2421, Jul. 2014.

[89] D. J. Ramirez, M. Koutouris, E. Hardouin, "Coordinated multi-point transmission with imperfect CSI and other-cell interference," in IEEE Trans. On wireless Commun., Vol. 14, No. 4, pp. 1882-1896, April 2015

[90] P. Baracca, F. Boccardi, V. Braun, "A dynamic joint clustering scheduling algorithm for downlink CoMP systems with limited CSI," in International Symp. On Wireless Commun. Systems, Aug. 2012

[91] N. Jindal, S. Vishwanath, A. Goldsmith, “On the duality of Gaussian multiple access and broadcast channels,” in IEEE Trans. on Information Theory, Vol. 50, No. 5, pp. 768-783, May 2004

[92] Erik Dahlman, Stefan Parkvall, Johan Skold, 4G, LTE-Advanced Pro and the Road to 5G, 3rd ed., Elsevier, Academic Press, 2016

[93] F. M. L. Tavares, G. Berardinelli, N. H. Mehmood, T. B. Sorensen, P. Mogensen, “On the Potential of Interference Rejection Combining in B4G Networks,” in IEEE Vehicular Tech. Conf., Fall, 2013

[94] N. Khan Beigi, A. Haghighat, “On Kurtosis of Spreading Sequences for NOMA,” in Consumer Commun. & Netwroking Conf., Jan. 2020

[95] L. Fay, et al., “An overview of the ATSC 3.0 physical layer specification,” in IEEE Trans. On Broadcasting, vol. 62, no.1, pp. 159-171, March 2016

[96] W. Li, et al., “Using LDM to achieve seamless local service insertion and local program coverage in SFN environment,” in IEEE Trans. On Broadcasting, vol. 63, no. 1, pp. 250-259, March 2017

[97] J. L. Carcel, J. J. Gimenez, D. Gomez-Barquero, “Zero-Guard OFDM Performance in SFN with ATSC 3.0 Ultra-Robust Transmission Modes,” in IEEE Int. Symp. On Broadband Multimedia Systems & Broadcasting, June 2017

[98] M. Fuentes, et al., “Physical Layer Performance Evaluation of LTE-Advanced Pro Broadcast and ATSC 3.0 Systems,” in IEEE Trans. On Broadcasting, Vol. 65, no. 3, Sept. 2019

[99] W. Li, et al., “Coverage Study of ATSC 3.0 Under Strong Co-Channel Interference Environments,” in in IEEE Trans. On Broadcasting, Vol. 65, no. 1, March 2019

[100] S. I. Park, et al., “Low Complexity Layered Division Multiplexing for ATSC 3.0,” in IEEE Trans. On Broadcasting, vol. 62, no. 2, Mar. 2016

[101] E. Garro, et al., “Layered Division Multiplexing with distributed multiple-input single-otput schemes” in IEEE Trans. On Broadcasting, vol. 65, no. 1, Mar. 2019

[102] J. Y. Lee, et al., “Layered Division Multiplexing for ATSC 3.0: implementation and memory use aspects,” in IEEE Trans. On Broadcasting, vol. 65, no. 3, Sept. 2019

[103] J. Hamkins, “Performance of low-density parity-check coded modulation,” in Proc. IEEE Aerospace Conf., pp. 1–14, Mar. 2010

[104] X. Cao, Yi Liu, D. Hu, “Simplified LLR algorithm for M-QAM demodulation,” in the Journal of Engineering, vol. 2019, no. 21, pp. 7370-7375, Nov. 2019

[105] J. Aulin, et al., “Terahertz Communication for Vehicular Networks,’ in IEEE Trans on Veh. Tech.., Vol. 66, no. 7, pp. 5617-5625, July 2017

[106] K. M. S. Huq, et al., “Terahertz-Enabled Wireless System for Beyond-5G Ultra-Fast Networks: A Brief Survey,” in IEEE Network, Vol. 33, no. 4, pp. 89-95, July/August 2019

[107] H. Zhang, L. Song, Z. Han, H.V. Poor, “Cooperation techniques for a cellular internet of unmanned aerial vehicles,” in IEEE Wireless Commun. Vol. 26, No. 5, pp.167–173, October 2019

[108] M. Elsaadany, A. Ali, W. Hamouda, “Cellular LTE-A technologies for the future IoT: Physical layer features and challenges,” in IEEE commun. Surveys & Tutorials, Vol. 19, No. 4, 4th quarter 2017.

[109] Y. Zeng, Q. Wu, Rui Zhang, “Accessing from the sky: a tutorial on UAV communications for 5G and beyond,” in Proceedings of the IEEE, Vol. 107, No. 12, pp. 2327-2357, Dec. 2019

[110] M. Y. Arafat, S. Moh, “Localization and clustering based on swarm intelligence in UAV networks for emergency communications”, in IEEE IoT Journal, Vol. 6, No. 5, pp. 8958-8976, Oct. 2019.

[111] Z. Wei, Z. Feng, H. Zhou, L. Wang, H. Wu, “Capacity and delay of unmanned aerial vehicle networks with mobility” in IEEE IoT Journal, Vol. 6, No. 2, pp. 1640-1653, April 2019 (store-carry-and-forward (SCF)

[112] L. Xie, J. Xu, R. Zhang, “Throughput maximization for UAV-enabled wireless powered communication networks,” in IEEE IoT Journal, Vol. 6, No. 2, pp. 1690-1703, April 2019 (hover and fly)

[113] S. Zhang, H. Zhang, B. Di, L. Song, “Cellular cooperative unmanned aerial vehicle networks with sense-and-send protocol,” in IEEE IoT Journal, Vol. 6, No. 2, pp. 1754-1767, April 2019

[114] Y. Chen, N. Zhao, Z. Ding, M.S. Alouini, “Multiple UAVs as Relays: Multi-Hop Single Link Versus Multiple Dual-Hop Links,” IEEE Trans. Wireless Commun., vol. 17, no. 9, pp. 6348–59, Sept. 2018

[115] Z. Li, J. Xu, Q. Guo, “Information fusion algorithm based on Intelligent Algorithm for multiple UAVs information interaction deception,” in IEEE Inter. Conf. on Cloud Computing & Intell. Systems, Nov. 2018

[116] C. Teuliere, E. Marchand, L. Eck, “3D model-based tracking for UAV indoor localization,” in IEEE Trans. On Cybernetics, Vol. 45, No. 5, pp. 869-879, May 2015.

[117] M. Elloumi, et al., “Monitoring Road Traffic with a UAV-based System,” in IEEE Wireless Commun. & Networking Conf., April 2018.

[118] H. Niu, N. Gonzalez-Prelcic, R. W. Heath, “A UAV-based Traffic Monitoring System,” in IEEE Vehicular Tech. Conf., June 2018.

[119] M. Hossain, Md. A. Hossain, F. A. Sunny, “A UAV-Based Traffic Monitoring System for Smart Cities,” in Intern. Conf. on Sustainable Technologies for Industry 4.0, Dec. 2019

[120] J. Luo, K. R. Pattipati, P. K. Willet, “A Sliding Window PDA for Asynchronous CDMA, and a Proposal for Deliberate Asynchronicity” in IEEE Trans. On Communications, Vol. 51, No.12, pp.1970-1974, Dec. 2003

[121] M. Al-Imari, P. Xiao, M. A. Imran, “Receiver and Resource Allocation Optimization for Uplink NOMA in 5G Wireless Networks” in Int. Symposium On Wireless Communication Systems, Aug. 2015

[122] M.Y. Tsai, S. Yousefi, “Improved Iterative Joint Detection and Decoding of Coded V-BLAST Systems,” in IEEE Communications Letters, Vol. 13, No.1, pp. 19-21, Jan. 2009

[123] Y. Zhang, R. S. Blum, “Iterative Multiuser Detection for Turbo-Coded Synchronous CDMA in Gaussian and Non-Gaussian Impulsive Noise” in IEEE Trans. On Communications, Vol. 49, No.3, pp. 397-400, March 2001

[124] A. M. Hamza and J. W. Mark, “Closed-form expressions for the BER/SER of OFDM systems with an integer time offset,” IEEE Trans. Commun., vol. 63, no. 11, pp. 4461–4473, Nov. 2015.